

CRYOPRESERVATION OF REPRODUCTIVE CELLS AND TISSUES

A Thesis

Submitted to the Graduate Faculty of the
Louisiana State University and
Agriculture and Mechanical College
in partial fulfillment of the
Requirement for the degree of
Master of Science in Mechanical Engineering

in

The Department of Mechanical Engineering

By

Guanglei Li

B.S., University of Science and Technology of China, 1999

December 2005

Acknowledgements

It is a great pleasure to thank many people who made this thesis possible. First I want to thank my advisor, Dr. Ram V. Devireddy for all his valuable teaching and guiding. His insight and wide knowledge inspired and motivated me a lot throughout this work while his excellent personality made me always felt happy working on all the projects. Next, I am grateful to my committee members, Dr. Charalampopoulos and Dr. Wong who have been helpful and generous with their time and expertise to evaluate my thesis. I learnt a lot from Dr. Wong's two courses as well.

I also thank all the members of Bioengineering Laboratory, for providing me with an environment and support for my work.

I am thankful to all my friends and well wishers, especially Guanyuan Fu, for their support and help. I want to give my special thanks to Mingyuan Huang for his constant support and getting through all the difficulties along with me.

My final acknowledgement is due to my parents and family back in China, who has always behind me with their love. Without them, I have not have been here.

This work has been funded by a Biomedical Engineering Research Grant from the Whitaker Foundation. The LSU veterinary school also helped with providing and processing of the ovarian tissue samples.

Table of Contents

ACKNOWLEDGEMENTS.....	ii
LIST OF TABLES.....	v
LIST OF FIGURES.....	vi
NOMENCLATUR.....	viii
ABSTRACT.....	ix
CHAPTER 1. INTRODUCTION.....	1
1.1 Cryobiology.....	1
1.2 Water Transport Model.....	4
1.3 Differential Scanning Calorimeter.....	7
1.4 Biology of Reproductive Tissues.....	11
1.4.1 Sperm Biology.....	12
1.4.2 Ovary Biology.....	14
CHAPTER 2. EFFECT OF GLYCEROL AND CHOLESTEROL-LOADED CYCLODEXTRIN ON FREEZING INDUCED WATER LOSS IN BOVINE SPERMATOZOA.....	17
2.1 Introduction.....	17
2.2 Materials and Methods.....	18
2.2.1 Semen Collection.....	18
2.2.2 Preparation of Cholesterol-loaded Cyclodextrin.....	19
2.2.3 Loading of Glycerol and CLC.....	20
2.2.4 DSC Experiments.....	20
2.2.5 Translation of Heat Release to Cell Volume Data.....	21
2.2.6 Water Transport Model.....	22
2.2.7 Numerical Methods.....	23
2.2.8 Theoretical Prediction of Optimal Rates of Cooling.....	23
2.3 Results.....	24
2.3.1 Semen Collection.....	24
2.3.2 Dynamic Cooling Response and Water Transport Parameters.....	24
2.3.3 Optimal Rates of Cooling Bovine Spermatozoa.....	28
2.4 Discussion.....	29
2.4.1 Water Transport Parameters in the Absence of Extracellular Ice.....	29
2.4.2 Convergence of Theoretical and Experimental Optimal Rates of Freezing Bovine Sperm.....	30
2.4.3 Effect of Extracellular Ice on Bovine Sperm Membrane Transport Properties.....	31
2.4.4 Effect of Glycerol and CLC on Bovine Sperm Membrane Properties.....	32
2.5 Summary and Conclusion.....	33

CHAPTER3. SUPRAZERO COOLING CONDITIONS SIGNIFICANTLY INFLUENCE SUBZERO PERMEABILITY PARAMETERS OF EQUINE OVARIAN TISSUE.....	34
3.1 Introduction.....	34
3.2 Theoretical Background.....	36
3.3 Materials and Methods.....	39
3.3.1 Tissue Collection and Isolation.....	39
3.3.2 Calorimetric Experiments.....	40
3.3.3 Numerical Methods and Simulations.....	42
3.3.4 Theoretical Prediction of Optimal Cooling Rates.....	43
3.4 Results.....	43
3.5 Discussion.....	50
3.6 Conclusion.....	54
CHAPTER4. SUBZERO WATER TRANSPORT CHARACTERISTICS AND OPTIMAL RATES OF FREEZING MACACA MULATTA (RHESUS MONKEY) OVARIAN TISSUE.....	55
4.1 Introduction.....	55
4.2Materials and Methods.....	56
4.2.1 Tissue Collection and Isolation.....	56
4.2.2 Water Transport Experiments.....	57
4.2.3 Numerical Methods and Optimal Cooling Rates.....	59
4.3 Results.....	59
4.4 Discussion.....	71
CHAPTER 5. CONCLUSION AND FUTURE WORK.....	75
REFERENCES.....	77
VITA.....	91

List of Tables

Table 2.1 Water transport parameters for bovine sperm in the absence of CPAs, with glycerol and with cholesterol-loaded cyclodextrin (CLC) at a cooling rate of 20 °C/min.....	25
Table 3.1 Description of variables used in Eqn. (4.1) and (4.2).....	37
Table 3.2 Membrane Permeability Parameters for Mare Ovarian Tissue ($V_b = 0.5V_o$)....	44
Table 3.3 Membrane Permeability Parameters for Mare Ovarian Tissue (in the absence of CPAs).....	49
Table 4.1 Membrane Permeability Parameters for Rhesus Monkey Ovarian Tissue ($V_b = 0.2V_o$).....	66
Table 4.2 Membrane Permeability Parameters for Rhesus Monkey Ovarian Tissue ($V_b = 0.4V_o$).....	67
Table 4.3 Membrane Permeability Parameters for Rhesus Monkey Ovarian Tissue ($V_b = 0.1V_o$).....	68

List of Figures

Figure 1.1 Cell survival percentage against cooling rate.....	2
Figure 1.2 Typical heat flux curve of differential scanning calorimeter.....	7
Figure 1.3 Diagram of a heat flux differential scanning calorimeter.....	8
Figure 1.4 Diagram of a power compensated differential scanning calorimeter.....	9
Figure 1.5 Heat Flow curve of differential scanning calorimeter.....	10
Figure 1.6 Heat Flow curve of differential scanning calorimeter at temperature T.....	11
Figure 1.7 Structures of a sperm.....	12
Figure 1.8 Major Components of an Ovary.....	15
Figure 2.1 Volumetric response of bovine sperm as a function of subzero temperatures obtained using the DSC technique at 20 °C/min.....	26
Figure 2.2 Contour plots of the goodness of fit parameter R^2 (= 0.98) for the parametric space of bovine sperm cooled in the absence of CPAs, with glycerol and with CLC.....	27
Figure 2.3 Volumetric response of bovine spermatozoa at various cooling rates as a function of subzero temperatures using the “best-fit” water transport parameters.....	29
Figure 3.1 Schematic drawing of the Krogh cylinder, a representation of a mare ovarian tissue unit.....	39
Figure 3.2 Volumetric response of the ovarian tissue as a function of subzero temperatures using the DSC technique at a freezing rate of 5 °C/min.....	45
Figure 3.3 Krogh model: Volumetric response of the ovarian tissue at various freezing rates as a function of subzero temperatures using the best fit membrane permeability parameters.....	46
Figure 3.4 Krogh model: Volumetric response of the ovarian tissue at various freezing rates using the best fit membrane permeability parameters.....	47
Figure 3.5 Contour plots of the goodness of fit parameter R^2 (= 0.98) for the parametric space in ovarian tissue that is cooled at either 0.5 °C/min or at 40 °C/min from 25 ° to 4 °C in the absence of CPAs (assuming $V_b = 0.5V_o$).....	50

Figure 4.1 Volumetric response of ovarian tissue as a function of subzero temperatures using the DSC technique, at a freezing rate of 5°C/min and in the absence of CPAs.....	60
Figure 4.2 Volumetric response of the ovarian tissue as a function of subzero temperatures using the DSC technique at 5 °C/min in the presence of 0.85 M DMSO (2A), 0.85 M glycerol (2B) or 0.85 M EG (2C).....	61
Figure 4.3 Krogh model: Volumetric response of the ovarian tissue at various freezing rates as a function of subzero temperatures using the best fit membrane permeability parameters.....	64
Figure 4.4 Krogh model: Volumetric response of the ovarian tissue at various freezing rates using the best fit membrane permeability parameters.....	65
Figure 4.5 A contour plot of the goodness of fit parameter R^2 (= 0.96) for the parametric space in ovarian tissue that is cooled at 0.5°C/min between 25° and 4°C or at 40°C/min between 25° and 4°C in the absence of CPAs ($V_b = 0.2V_0$).....	69
Figure 4.6 A contour plot of the goodness of fit parameter R^2 (= 0.96) for the parametric space in ovarian tissue that is cooled at 0.5°C/min between 25° and 4°C or at 40°C/min between 25° and 4°C in the presence of 0.85 M DMSO (Fig. 6A), Glycerol (Fig. 6B) and EG (Fig. 6C).....	70

Nomenclature

L_{pg}	Membrane permeability in the absence of CPA ($\mu\text{m}/\text{min}\cdot\text{atm}$)
$L_{pg}[cpa]$	Membrane permeability in the presence of CPA ($\mu\text{m}/\text{min}\cdot\text{atm}$)
E_{LP}	Apparent activation energy in the absence of CPA (kJ/mol)
$E_{LP}[cpa]$	Apparent activation energy in the presence of CPA (kJ/mol)
V	Cell volume (m^3)
A_C	Effective membrane surface area for water transport
R	Universal gas constant
B	Constant cooling rate (K/min)
C_i	Concentration of intracellular solutes
C_o	Concentration of extracellular solutions
V_b	Osmotically inactive cell volume
n_{cpa}	Number of moles of CPAs
v_{cpa}	Molar volume of CPA ($\mu\text{m}^3/\text{mol}$)
v_w	Molar volume of water ($18 \times 10^{12} \mu\text{m}^3/\text{mol}$)
φ_s	Disassociation constant for salt
n_s	Number of moles of salt
ΔH_f	Latent heat of fusion of water (335 mJ/mg)
ρ	Density of water ($1000 \text{ kg}/\text{m}^3$)
T	Temperature
T_R	Reference temperature
r_{vo}	Radius of the extracellular space
X	Distance between the microvascular channels
L	Axial length of the Krogh cylinder
V	Cellular space with volume

Abstract

Cryopreservation of reproductive cells and tissues is a useful technique to deliver an intact genome and maximize the distribution of favorable genes. It is widely applied to many fields such as biology, medicine, ecology and agriculture. To optimize the procedure, the biophysical responses of reproductive biological systems at different cooling conditions and in different mediums need to be clearly understood. In the present study we studied the biophysical response during freezing of: 1) bovine sperm frozen at a cooling rate of 20 °C/min in three media: without cryopreservation agents (CPAs), with 0.7 M glycerol, and with 0.7 M glycerol along with 1.5 mg/ml of cholesterol-loaded cyclodextrin (CLC); 2) equine ovarian tissue cooled either at 40°C/min or at 0.5°C/min from 25° to 4°C, and then cooled to subzero temperatures at 5 °C/min in the presence and absence of 0.85 M glycerol and 0.85 M dimethylsulfoxide; and 3) *Macaca mulatta* (rhesus monkey) ovarian tissue cooled at 0.5°C/min or 40°C/min from 25° to 4°C, and then cooled to subzero temperatures at 5 °C/min in the absence and presence of 0.85 M glycerol, 0.85 M dimethylsulfoxide and 0.85 Methylene glycol. For all the three reproductive systems, a shape-independent Differential Scanning Calorimeter (DSC) technique was used to measure the volumetric shrinkage during freezing. A model of water transport was then fitted to the experimentally obtained volumetric shrinkage data and the best fit membrane permeability parameters (L_{pg} and E_{Lp}) was yielded. For bovine sperm, L_{pg} ranged from 0.02 to 0.036 $\mu\text{m}/\text{min-atm}$ and E_{Lp} ranged from 26.4 to 42.1 kcal/mol. The subzero water transport parameters of bovine sperm are significantly different from those reported in literature. The experimentally determined optimal rate of freezing bovine spermatozoa agrees quite closely with the theoretically calculated range, from 45 to 60 °C/min. For equine tissue, L_{pg} ranged from 0.06 to 0.73 $\mu\text{m}/\text{min-atm}$ and E_{Lp} ranged from 6.1 to 54.2 kcal/mol. For rhesus ovarian tissue L_{pg} ranged from 0.7 to 0.15 $\mu\text{m}/\text{min-atm}$ and E_{Lp} ranged from 22.1 to 32.1 kcal/mol. Calculation of equine and macaque ovarian tissue data suggest the optimal cryopreservation rates are significantly dependent upon suprazero cooling conditions and cryoprotective agents.

Chapter 1

Introduction

1.1 Cryobiology

The effect of low temperatures on living organisms is complex in that it affects the physical structures and biophysical processes of organisms in a highly coupled manner. Living cells may be cooled to extreme low temperature either to destroy them selectively or to store them for long periods. According to these two different effects of freezing, there are two major applications of cryobiology: cryopreservation of biological systems and cryosurgery.

Cryopreservation is a technique used to preserve and genetically stabilizing cells at cryogenic temperatures. Storage of living systems in low temperatures as been successfully applied to various mammalian systems including erythrocytes, lymphocytes, gametes, embryos, hepatocytes, bone marrow stem cells, cornea, skin and pancreatic tissues (Mazur, 1984; McGrath, 1985). Cryopreservation technology is currently available for many biological systems such as mammalian oocytes (Bernard and Fuller, 1996), stem cells (Hubel, 1997), rat and human liver slices (Day et al., 1999) and engineered tissues (Oegema et al., 1999). Its other applications extend in a variety of fields such as food science, plant and animal cold hardiness, ecology and agriculture.

Cryopreservation protocol usually includes several necessary steps: a) extension and addition of CPAs b) extracellular ice nucleation c) freezing at an optimal cooling rate to $-196^{\circ}C$ (liquid nitrogen temperature) d) store at liquid nitrogen temperature for a period of time e) thawing and removal of CPAs. The range of temperature lethal to cell and tissues is reported to be about -15 to $-60^{\circ}C$ (Mazur, 1984). So the cells experience most destructive effects during step c. Clearly, minimizing this destructive effect is essential for the cryopreservation protocol. This goal could be achieved by quantitative knowledge of the biophysical response during freezing of biological system.

The cryopreservation process involves complex biophysical responses of cells and tissues which are still not fully understood. The factors that affect the cell survival rate after cooling and thawing process includes: cooling rate, phase change temperature, holding time at each

step, substance transport and ice formation. However, the two major cellular responses during freezing is water loss of cell and intracellular ice formation (IIF). During slow cooling, freezing occurs outside the cell before intracellular ice begins to form (Farrant, 1980). As extracellular ice forms, water is removed from the extracellular environment and an osmotic imbalance occurs across the cell membrane leading to water migration out of the cell. This phenomenon is known as the solute concentration effects and this increase in solute concentration outside and inside the cell can be detrimental to cell survival. Rapid cooling minimizes the solute concentration effects as ice forms uniformly, but leads to more intracellular ice formation. Mazur postulated that ice crystal formation and the solution effect both impact cell inactivation, and that an optimum cooling rate should minimize the effect of both (Mazur et al., 1972). The curve of cell survival percentage against cooling rate has a reserve U shape as shown in figure 1.1. Figure 1.1 is from the master's thesis of Sreedar Thirumala, May 2004, page 15. At The maximal point, the injury effect is the least and cooling rate is optimal. However, the optimal cooling rate is not the same for different cell types. The rate of water loss is found to be affected by cell permeability; more permeable cells are able to tolerate rapid cooling better than less permeable cells (Nei, 1969). The optimal cooling rate is also found to be related to the surface area of the membrane and the surface to volume ration of the cell.

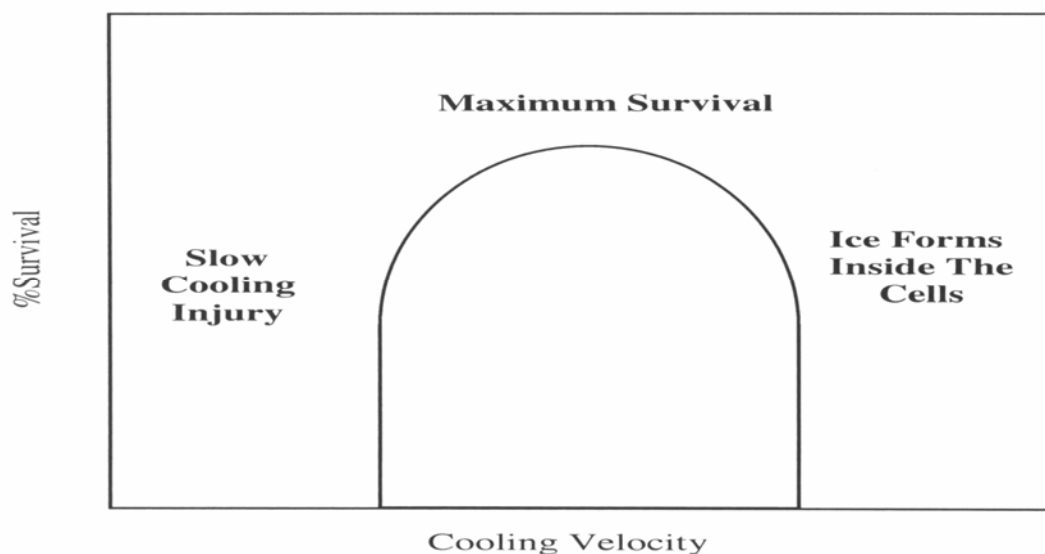


Figure 1.1 Cell survival percentage against cooling rate

Cryosurgery is another important application of cryobiology, defined as a technique to kill abnormal biological systems by freezing to low temperature. Low temperature is first used for the treatment of malignant tumors by James Arnott in the 1950s. In his experiment, iced saline solutions were applied to ulcerating cancers and afterwards a reduction in size, odor, discharge and pain was observed. The first cryosurgical device capable of freezing the tumor region in vivo by liquid nitrogen and producing a cryolesion in the liver of cat is developed by Cooper and Lee (Cooper and Lee, 1961). Currently cryosurgery has been performed in a variety of organs such as the rectum, breast, skin, lung, brain, prostate, uterus, oral cavity, pancreas and liver (Gage, 1992; Gage and Baust, 1998). The objective of cryosurgery is completely killing abnormal cells without injuring normal cells. However, the widely use of cryosurgery is hampered by lack of effective methods to monitor the freezing process in organs. The introduction of intra-operative ultrasound (Onik et al., 1984) and magnetic resonance imaging (MRI) as a method of guiding the cryoprobe and monitoring the iceball has led to a renewed interest in the use of cryosurgery. Besides, various numerical simulation methods are developed and the results are used to monitor and optimize the process. According to the location of tumors, the protocol is different. For external tumor and cancer, abnormal cells are on the skin thus liquid nitrogen is applied directly to the site with cotton swabs or spraying devices. For tumors inside the body, a hollow instrument called cryoprobe is placed in contact with the tumor and liquid nitrogen or argon gas is circulated through the cryoprobe to cool the system. After cryosurgery, the frozen tissue thaws and is either naturally absorbed by the body (for internal tumors), or it dissolves and forms a scab (for external tumors).

During cryopreservation and cryosurgery, chemicals additives including cryopreservative agents (CPAs), antifreeze protein (AFP), and cryosurgery adjuvants, are often added to improve the survival of cells. With the addition of these chemicals, the composition and properties of the solution will be changed and the phase relationships of the system will be complex. Since equilibrium conditions are frequently not attained, the solid-liquid state diagrams are adopted to obtain the thermophysical properties of solution. Among these additives, the most commonly used one is cryopreservative agents (CPAs), which includes sugars, serum, solvents and their combinations. During the freezing process, cryoprotective agents can serve several functions: lowering the freezing point, binding water to prevent it

freezing at zero degree, and decreasing membrane damages(Farrant, 1980).According to their ability to transport through cell membrane, CPAs are classified as penetrating (glycerol and DMSO) and nonpenetrating ones (lactose and trehalose). Both types can osmotically induce water egress and cause a dehydration of cells, but their ability to enter the cell and reside in cytoplasm and membranes is different.

The choice of cryoprotective agents (CPAs) depends on the characteristics of the cryopreserved substances. Currently, The most commonly used CPAs are glycerol and Dimethyl Sulphoxide(DMSO) and they has proved to be most effective for many substances. However, glycerol with the concentration higher than 3-4M is biochemically toxic to kidney (denature some enzymes) and DMSO is more likely to have a dissolving effect for membrane. Other kinds of CPAs like ethylene glycol and methoxylated compound are also used in specific cases. For example, human sperm membrane is 4 times more permeable to ethylene glycol than to glycerol. And the membrane transport of ethylene glycol is less affected by temperature than is glycerol (Gilmore et al., 1997). Prior to being added to the cell suspension, CPAs should be diluted to the desired concentration in fresh growth mediums. This procedure will minimize the potentially negative effects of chemical reactions on CPAs and reduce the potential toxic effects. Generally, DMSO and glycerol are used in concentrations ranging from 5-10% (v/v).

The mechanism of cell injuries is frequently studied but is not yet clearly understood. According to Wolfe (2001), survival of freezing cells involves combination of intracellular ice formation, dehydration, freezing point depression, supercooling and intracellular vitrification. Dilution shock is also referred to be crucial in freezing process (Farrant, 1977)this is the damage to cells induced during the dilution that occurs both as ice melts during rewarming and when any cryoprotective additives are removed after thawing Damage due to high concentrations of solutes and formation of intracellular ice(Mazur, 1963).

A useful experimental apparatus, cryomicroscope, can be used to study the freezing and thawing processes in living cells and to determine the conditions requisite for intracellular freezing in human erythrocytes.

1.2 Water Transport Model

According to Mazur's two factor hypothesis, biological systems during freezing experience either water loss at low cooling rates or intracellular ice formation at high cooling rates. In

cryopreservation an optimal cooling rate is used so that cooling occurs slowly enough to avoid intracellular ice formation yet fast enough to avoid cellular hydration. In cryosurgery most cells in the iceball experience low cooling rate (≤ 10 K/min) with varying boundary conditions, hold times and thawing rate (Bischof, 1997). Cell injury is likely to be caused by extensive cellular hydration and exposure to high concentration of electrolytes. Clearly, cell volume changes during freezing and thawing is a critical factor determining whether the cells survive.

In response to the changes in environment, the volume of cell varies several times as the function of substances movement across the membrane. The first volume adjustment of cells occurs when CPAs are added to cells in isotonic Media (Roy et al., 1990). Associated with osmotically driven egress of intracellular water, the component of cells shrink fast, and then as the penetrating CPAs enters the volume slowly return to the original value. The second volume adjustment occurs in the process of extracellular water freezing, water move out of cells in response to high concentrations of extracellular salts. Thawing yields analogous but opposite volume changes. Excellent examples of measured changes in the size of embryos and ova during passage through a freezing and thawing cycle are provided by Schneider (1986). However, a more precise description of the cell volume changes needs a quantitative understanding of the water transport during the freezing process.

Kedem and Katchalsky (1958) first proposed a model for water and solute transport across a cell membrane during freezing. In their model the water and CPA flux across the membrane was described by two differential equations. If the flux of CPAs is negligible compared to the water flux during freezing (McCaa et al., 1991; Gilmore et al., 1995), the Kedem-Katchalsky model reduces to a model only including water transport, as proposed by Mazur (1984) and later modified by Levin et al. (1976). In suspended single-cell biological systems, ice tends to form first extracellularly in the freezing process. A chemical difference across the cell membrane is induced by the extracellular ice and thus intracellular water tends to move out of cell membrane. Consequently, the cellular volume will decrease. This volumetric shrinkage response of cells during freezing is incorporated in the modified water transport model of as follows:

$$\frac{dV}{dT} = -\frac{L_p A_c R T}{B v_w} \times \left[\ln \frac{(V_0 - V_b - n_{cpa} v_{cpa}) / v_w}{(V_0 - V_b - n_{cpa} v_{cpa}) / v_w + (\phi_s n_s + n_{cpa})} - \frac{\Delta H_f v_w \rho}{R} \left(\frac{1}{T_R} - \frac{1}{T} \right) \right] \quad (1.1)$$

$$L_p = L_{pg}[cpa] \exp\left[-\frac{E_{Lp}[cpa]}{R} \left(\frac{1}{T} - \frac{1}{T_R} \right)\right] \quad (1.2)$$

Here L_{pg} is the reference membrane permeability of CPAs, defined by Levin et al. (1976); E_{Lp} is the apparent activation energy of CPAs (kJ/mol); V is the sperm volume at temperature T (K); A_c is the effective membrane surface area for water transport; and V_0 and V_b are the isotonic and osmotically inactive sperm volumes. R is the universal gas constant (8.314 J/mol K); B is the constant cooling rate (K/min); n_{cpa} is the number of moles of CPA; v_{cpa} is the molar volume of CPA ($\mu\text{m}^3/\text{mol}$); v_w is the molar volume of water ($18 \times 10^{12} \mu\text{m}^3/\text{mol}$); ϕ_s is the disassociation constant for salt (McGrath, 1988); n_s is the number of moles of salt; ΔH_f is the latent heat of fusion of water (335 mJ/mg); and ρ is the density of water (1000 kg/m^3).

The value of geometric parameters depends on the geometry model of cells. Several different models have been reported. According to Devireddy (2002c), the sperm cell is assumed as a long cylinder. The parameters of cells in the model system can be obtained by microscopy. The initial cell volume (V_b) is normally determined based on the composition of the CPA medium. According to Devireddy (1998), the osmotically inactive cell volume can be predicted by extrapolating the figures of equilibrium volume of water in the cells at different subzero temperatures to infinite osmolalities. In the absence of CPAs the osmotically inactive cell volume, V_b is assumed to be $0.6 V_0$, a value within the range reported for a variety of mammalian sperm (Gilmore et al., 1995; Gravance et al., 1996). On the other hand, in the presence of permeating CPAs, V_b is different dependent on the kind of CPAs. In the case of glycerol, V_b is reported to be $0.623 V_0$ (Smith et al., 1998). The two membrane permeability parameters of the model, either L_{pg} and E_{Lp} or $L_{pg}[cpa]$ and $E_{Lp}[cpa]$, were determined by curve-fitting the water transport model to experimentally obtained volumetric shrinkage data during freezing.

With this water transport model, the volume changes of cells during the whole process could be monitored and used for further dynamic analysis of the biophysical process occurred

during freezing and thawing.

1.3. Differential Scanning Calorimetry

Differential scanning calorimetry (DSC) is a thermoanalytical technique in which the difference in the amount of heat required to increase the temperature of a sample and reference are measured as a function of temperature. A differential scanning calorimeter consists of two sealed pans: a sample pan and a reference pan (an empty sample pan). These pans are often composed of aluminum, which has a very high thermal conductivity and acts as a radiation shield. Cell suspension with weight from 0.1 to 100 mg is added to the sample pan. The two pans are then heated, or cooled, uniformly while the heat flow difference between the two is monitored in a temperature scanning process. The temperature scanning can be done isothermally or by changing the temperature at a constant rate. The differences in the heat flow between the sample and reference during this process is sent to a computer, and a plot of the differential heat flow between the reference and sample cell as a function of temperature is produced by the computer. A process without thermodynamic chemical reactions will result in a flat or very shallow base line on the plot. However, an exothermic or endothermic process within the sample results in a significant deviation in the difference between the two heat flows and thus there is a peak in the DSC curve. Exothermic processes will show as positive peaks (above the baseline) while peaks resulting from endothermic processes are negative (below the baseline). A typical example of the DSC heat flow curve is shown in Figure 1.2.

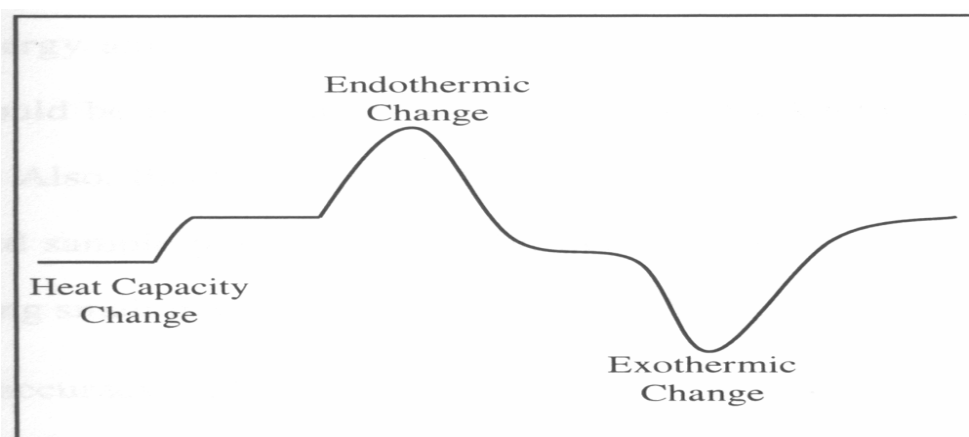


Figure 1.2 Typical heat flux curve of differential scanning calorimeter

Subtracting the sample heat flow from the reference heat flow in the curve, we can obtain the differential heat flow. The enthalpy of transition can be expressed using the following equation: $\Delta H = KA$ and could be obtained by integrating the peak corresponding to a given transition. Here ΔH is the enthalpy of transition, K is the calorimetric constant, and A is the area under the curve. The calorimetric constant will vary instrument to instrument, and can be determined by analyzing a well-characterized sample with known enthalpies of transition. Figure 1.2 is from the master's thesis of Sreedar Thirumala, May 2004, page 7.

There are two main types of differential scanning calorimeters: heat flux DSC and power compensation DSC. In a heat flux calorimeter, the sample and reference are placed on raised platform on a constantan disk through which heat is transferred to them. The heat transported to the sample and reference is controlled while some chromel-alumel thermocouples monitor the temperature difference between the two. Under each of these platforms there is a chromel wafer. The junction between these two alloys forms a chromel-constantan thermocouple. The signal from these sensors is the used to measure the differential heat flow. The components of heat flux DSC are shown in Figure 1.3. Source of Figure1.3:<http://www.answers.com/topic/differential-scanning-calorimeter>, last time visit time: 11/08/2005.

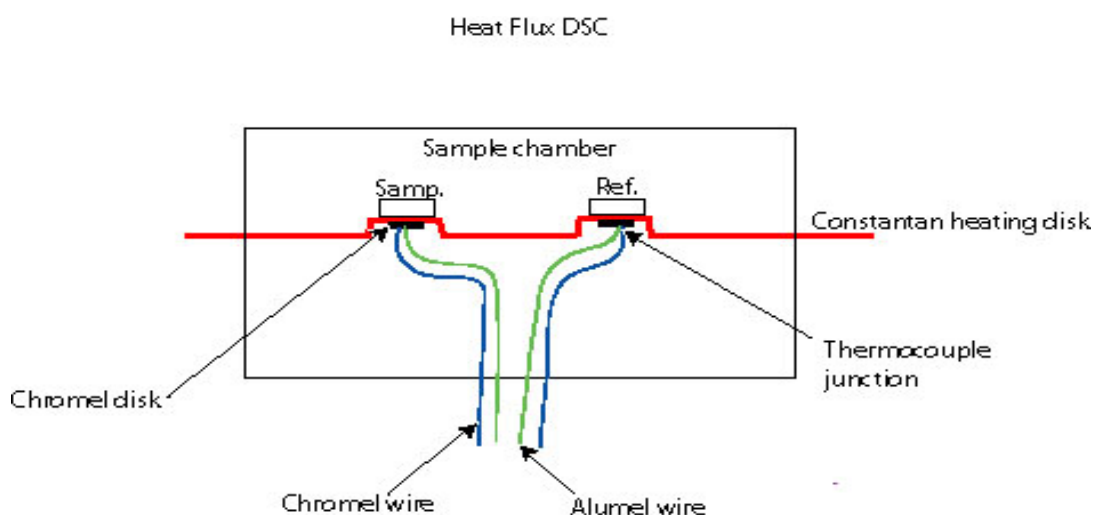


Figure1.3 Diagram of a heat flux differential scanning calorimeter

In power compensated calorimeters, separate heaters beneath the sample and reference are used. Both the sample and reference are maintained at the same temperature while the electrical power used by their heaters is monitored. The heating elements are small (about 1 gram) to

reduce the delay of heating, cooling, and thermal equilibration processes. The temperatures are monitored using electronic temperature beneath the samples. Generally platinum resistance thermometers are used due to their high melting point. The components of power compensated DSC are shown in Figure 1.4. Source of Figure 1.4: <http://www.answers.com/topic/differential-scanning-calorimeter>, last time visit time: 11/08/2005.

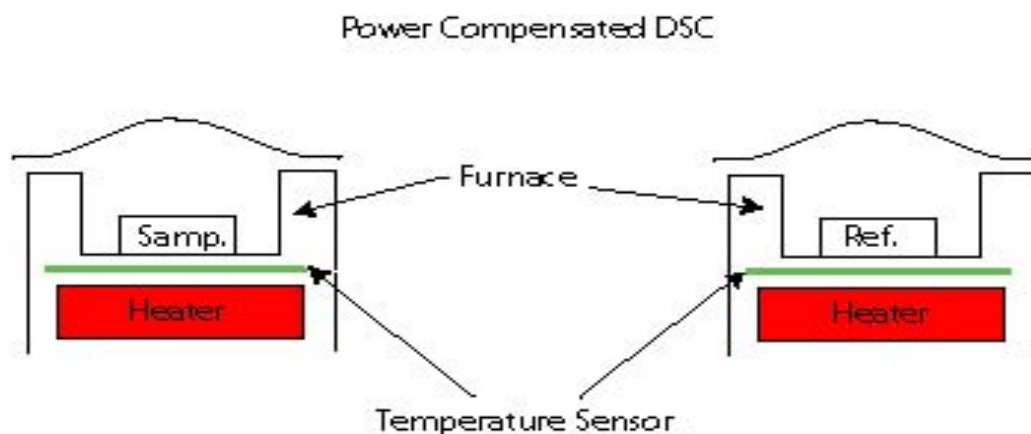


Figure 1.4 Diagram of a power compensated differential scanning calorimeter

The DSC used in our study is Perkin-Elmer DSC 7, a power compensation one and can run from -170 to 725 °C. The basis of DSC measurement is the fact that different substances will release or adsorb different amount of heat during the same freezing process. The common procedure of DSC technique is as follows: measure the heat release of an osmotically active cellular suspension during a designed freezing process; kill all the cells through a freezing and thawing process, measure the heat release of the osmotically inactive or lysed cell suspension in the same freezing procedure as that for the osmotically active sample; compare the heat releases of the two cellular suspension and converse the difference between heat release into cell volume. According to Devireddy (1998), the heat release between osmotically active and inactive cellular suspension is determined by latent heat of freezing of pure water and the fractions of cells, salts and nonionic solutes in the suspension. The heat release can be related to the cell volume as following (Devireddy, 1999; Bevington, 1992):

$$\frac{V_i - V(T)}{V_i - V_b} = \frac{\Delta q(T)_{dsc}}{\Delta q_{dsc}} \quad (1.3)$$

Rearrange the above equation, we get

$$V(T) = V_i - \frac{\Delta q(T)_{dsc}}{\Delta q_{dsc}} (V_i - V_b) \quad (1.4)$$

Here V_i is the initial or the isotonic cell volume, assumed to be V_0 in the absence of CPAs and V_b is the final or the osmotically inactive cell volume.

A typical heat release curve of DSC is shown in Figure 1.5 and the heat release data can be converted to cell volume responses using the water transport model.

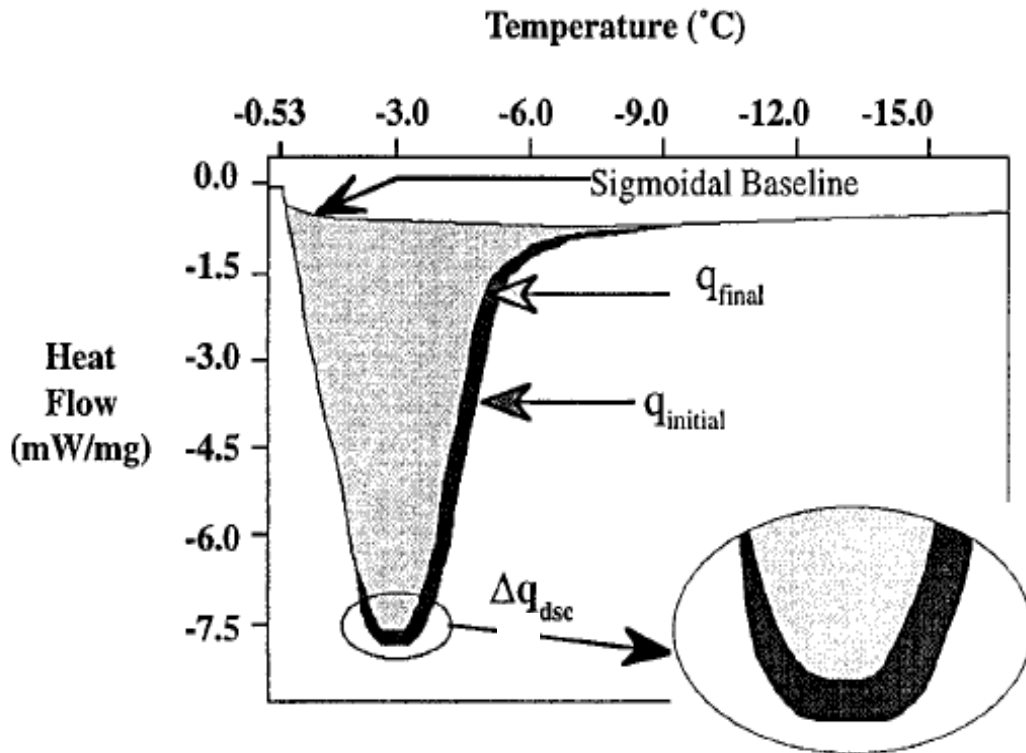


Figure 1.5 Heat Flow curve of differential scanning calorimeter

Here $q_{initial}$ is the heat release of live or osmotically active cells in the whole freezing process and q_{final} is heat release of dead or osmotically inactive cells in the whole freezing process while $\Delta q(T)_{dsc}$ is the heat release of cells from the initial time of freezing to the state with temperature T. The $\Delta q(T)_{dsc}$ term could be used in equation (1.4) to calculate the cell volume at temperature T. With the cell volume at all different times, we can get the

volume change of cells during the whole process and further study the biophysical responses of cells during freezing process.

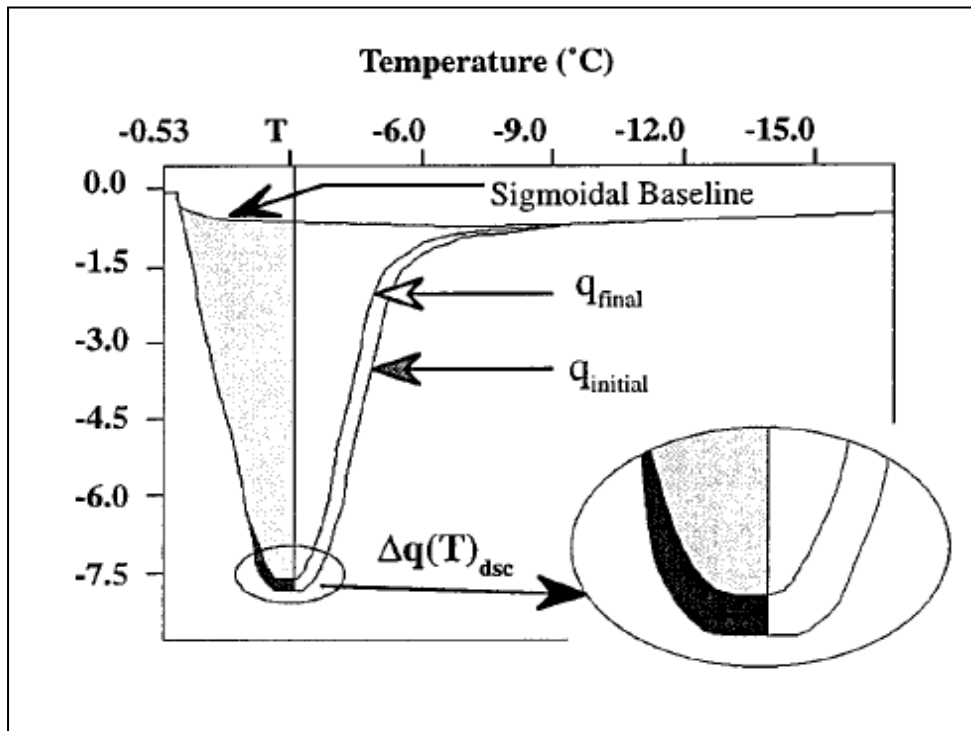


Figure 1.6 Heat Flow curve of differential scanning calorimeter at temperature T

With the above relationship and heat release data, the experiment data of DSC experiments could be converted to the volume change of cells during freezing and thawing process. Coupled with the water transport model, the volume change history of cells can be used to further study the cellular biophysical response including water and solute transport through the membrane.

1.4 Biology of Reproductive Tissues

Reproduction and fertility is one of the most important activities of all species. However, in modern society numerous people suffer from or are at the risk of losing ability of fertility due to many kinds of diseases. Besides, some other valuable species like endangered animals and economically raised animals also met this problem. An effective way to solve this problem is to cryopreserve reproductive cells and tissues and later transplant them to the species in need of these tissues at a proper time. Sperm and ovary are two critical types of cells in the reproductive systems so they are chosen to be studied in current work.

1.4.1 Sperm Biology

Sperm are defined as the male reproductive cells produced by the testicles. They are carried in fluid called semen, capable of fertilizing an egg cell to form a zygote. A zygote can grow into a new organism, such as a human. Sperm cells contain half of the genetic information needed to create life. Generally, the sex of the offspring is determined by the sperm cells, through the chromosomal pair "XX" (for a female) or "XY" (for a male). Sperm cells were first observed by Antoni van Leeuwenhoek in 1679. Spermatozoa are differentiated cells, normally composed of a head, basal body, and tail. The head contains some cytoplasm and the nuclear material for fertilization. The basal body has a high concentration of mitochondria which provides the energy for sperm motility through the production of ATP. The tail is usually a flagellum served for propulsion. The detailed structure of sperm is showed in Figure 1.7. Parts 1-5 represent acrosome, cell membrane, nucleus, mitochondria, tail respectively. .Source of Figure 1.7 http://www.answers.com/main/ntquery;=7418 js210?method=4&dsid=2222&dekey=Sperm&gwp=8&curtab=2222_1&sbid=lc04a&linktext=spermatozoa. Last visit date is 11/07/2005.

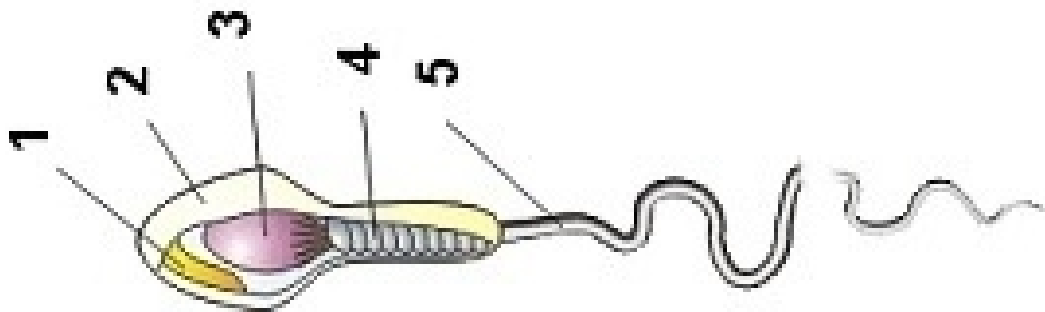


Figure 1.7 Structure of a Sperm

Cryopreservation of spermatozoa and spermatogenic cells for intracytoplasmic sperm injection has been developed primarily to deliver an intact genome. Artificial insemination (AI) has been an important tool to achieve genetic improvement and disease control for important species (Bailey et al., 2000). Sperms from genetically superior males could be used to impregnate multiple females to maximize the distribution of favorable genes. AI also eliminates the need of physical contact between different animals and thus prevents the spread of diseases. This is especially useful in agri-food industry. However, the widely use of AI over natural breeding depends on the success cryopreservation of sperms.

Cryopreservation makes it possible to store sperm in a long term and transport over distances. Sperm cryopreservation of agriculturally important species, like cattle, has been an established industry worldwide (Bailey et al., 200). Genome banking will also benefit those endangered and valuable transgenic species. Another important application of sperm cryopreservation is to freeze human sperm and make pregnancy following intrauterine insemination possible, though there may be arguable ethics issues.

The application of cryopreservation to bull sperm has been successful but application to other species is problematic. The major reason for this is our inadequate understanding of the mechanism of subcellular components injury and an absence of cellular models. During freezing the cells encounter membrane phase state change, ice formation and increased concentration of all other solutes and they must respond to these changes within the finite time allowed by cryopreservation protocol (Mazur and Cole, 1989; Schneider and Mazur, 1984). With all these considerations, an appropriate protocol for maximizing cell survival is required. Schneider and Mazur (1984) derived some equations to describe the cooling rate and some other variables. However, applications of these concepts are impossible without the understanding of cellular response to solvent and solute movements. Water and solute transport has been studied in various biological systems (de Gier, 1989; Verkman and Mazur, 1988). It is shown that the rate of water transport is affected by composition and phase preference of individual lipids (de Gier, 1989) as well as structure of membrane (Verkman and Mazur, 1988).

Theoretically, sperms should recover fertilizing ability and remain membrane integrity after freezing and thawing. However, ultra-structure damages to plasma membrane, acrosome and flagella of sperm have been observed after cryopreservation (Barthelemy et al., 1990), and the causes are reported to be membrane swelling, acrosome swelling, acrosome loss, and pulling back of the mitochondrial sheath (Royere1 et al., 1996). Species differences in female tract anatomy, sperm transport mechanisms, ability to time inseminations and deliver spermatozoa are also determinants of fertility with cryopreserved spermatozoa (Holt, 2001).

Cryopreservation of bull sperm is a useful technique. It is widely used in agriculture food science. Although it has been quite successful compared with sperm cryopreservation of other species (Hammerstedt et al., 1998), the current procedure is determined empirically.

Improvement of this technique depends on a better understanding of the biophysical characteristics of bull sperm. Cryopreservation has induced many stresses on bull sperm, like phase transformation of the cell membrane (Purdy and Graham, 2003). Some of these harmful stresses could be decreased by adding lipids to the sperm prior to cooling and thawing. Especially, the phase transformation could be eliminated by adding sufficient of cholesterol to the sample. According to Purdy and Graham, bull sperm treated with proper amount of cholesterol-loaded cyclodextrin has an increased viability and motility after cryopreservation. In this study, cryopreservation experiments of bull sperms treated with proper amount of cholesterol-loaded cyclodextrin were performed using differential scanning calorimeter (DSC). The water transport model of cells is then adopted to study the biophysical response of cells, especially water transport through membrane, during freezing.

1.4.2 Ovary Biology

During treatment of malignant or autoimmune diseases, women may be at the risk of premature ovarian failure due to chemotherapy, radiotherapy or radical reproductive surgery. There are three possible ways for preserving these women's fertility: cryopreservation of their oocytes, embryos, and ovarian tissue. Cryopreservation of mature oocytes, although successful in the mouse (Carroll et al., 1993; Carroll and Gosden, 1993; Bos-Mikich, 1995), is difficult to applied to other species including man (Parks and Ruffing, 1992; Trounson and Bongso, 1996). Cryopreservation of embryos is reasonably successful (Wang, 1994; Kaufman et al., 1995) but it has associated problems, source of oocytes for fertilization and related ethical problems preventing the operation of method. Ovarian tissue cryopreservation is a viable alternative to cryopreservation of oocytes or embryos.

Ovary is defined as the paired female or hermaphroditic reproductive organ which produces ova and, in vertebrates, estrogen and progesterone. Normally, a female have two ovaries, each performing different functions: producing eggs and secreting hormones. For human beings, the two ovaries are held in place on each side of the uterus by a membrane and each ovary is about the size of an almond. The interaction between the gonadotropic hormones from the pituitary gland and the sex hormones from the ovary controls the monthly cycle of women's ovulation and menstruation. After its release from the ovary, the ovum passes into the oviduct and into the uterus. If the ovum is fertilized by the sperm, pregnancy

ensues. The ovary, both a cytogenic and an endocrine organ, consist of cortex, medulla, germinal epithelium, stroma, follicles and tunica albuginea. Follicles can be further divided into four kinds: primordial, primary, secondary and atretic follicle. Figure 1.8 shows the major components of an ovary. Source of Figure 1.8: <http://devcell.bio.uci.edu/images/ovary%20structure%20and%20ova%20production.gif>.

The last visit date of the website is 11/07/200.

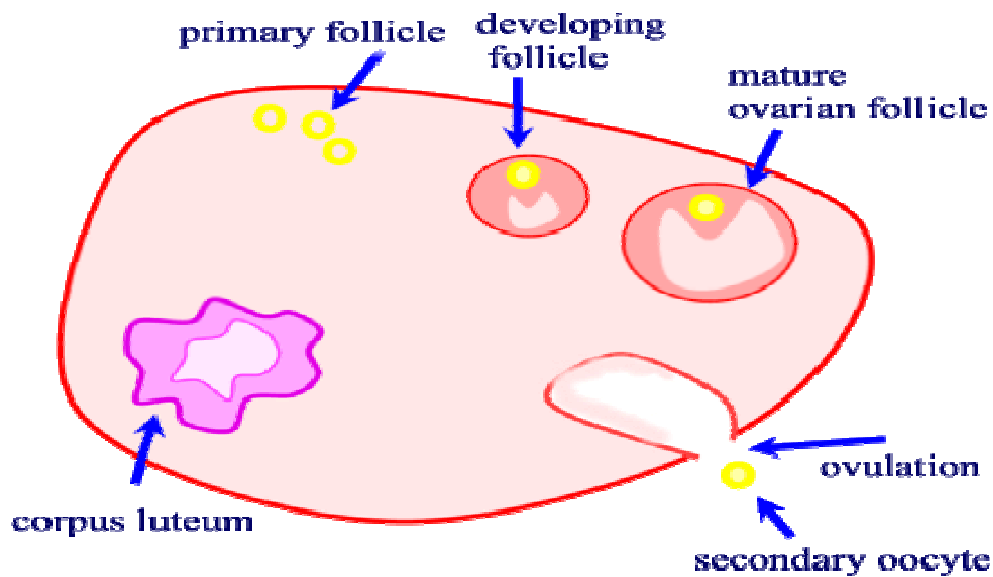


Figure 1.8 Major Components of an Ovary

Live young have been obtained from fresh and frozen ovarian tissue grafts in mice (Carroll and Gosden, 1993; Parrott, 1960) and sheep (Gosden et al., 1994) although it still has some difficulty applied to human beings. The technique of ovarian cryopreservation is promising and with the improvement of this technique, many women will benefit from it. Its application could also be extended to other species like horse, bull, monkey and some endangered animals and many fields such as agriculture, food science and ecology would correspondingly advance. In this technique, wedges of ovarian tissue for cryopreservation were collected by laparoscopy from each ovary at any stage of the menstrual cycle without compromising a female individual's health or fertility and then frozen to low temperature with liquid nitrogen. When needed, they are thawed and autotransplanted to the same female individual. The viability and fertility of ovaries after cryopreservation is greatly affected by the freezing and thawing

procedure. To achieve the best effect of cryopreservation, the biophysical responses of ovarian cell and tissues during freezing should be clearly understood. In this study, the Differential scanning Calorimeter (DSC) technique is used to monitor the volume changes of ovarian cells during freezing. The cellular volume data is then coupled with the water transport model to get the permeability parameters of the cell membranes. These data can be further used to predict the optimal freezing and thawing procedure of ovarian tissues. Here equine ovarian tissues are chosen because of ready accessibility of ovaries from mares that were to be euthanized for other research projects at the Louisiana School of Veterinary Medicine. And the *Macaca mulatta* (rhesus monkey) ovarian tissues are used for their close relationship with human. They are both primates and are genetically similar in many aspects. Our ultimate goal is to find out an optimum procedure to cryopreservation the ovarian tissues for human and other valuable species.

Chapter 2

Effect of Glycerol and Cholesterol-Loaded Cyclodextrin on Freezing Induced Water Loss in Bovine Spermatozoa

2.1 Introduction

Soon after the serendipitous observation by Polge and colleagues (Polge et al., 1949) that sperm cells survived freezing stress in the presence of glycerol than in its absence, the first calf was produced using cryopreserved spermatozoa in 1951 (Stewart, 1951). Today the modern cattle industry worldwide is based on the use of artificial insemination and frozen semen and cryopreservation has allowed exploitation of superior sires and achieved rapid, large-scale genetic improvement in cattle stocks coupled with a reduction in disease transmission (Foote, 1999). This impact would not have been possible without successful freezing of bull spermatozoa (Parkinson and Whitfield, 1987; Foote and Parks, 1993; Woelders, 1997; Vishwanath and Shannon, 2000; also see Foot 2002 for a historical review on artificial insemination).

The process of cryopreservation represents an artificial interruption of the progress of the spermatozoon towards post-ejaculation capacitation and fertilization (Graham, 1978; Hammerstedt et al., 1990). One of the initial steps in sperm capacitation is a loss of cholesterol from the plasma membrane (Langlais and Roberts, 1985; Ehrenwald et al., 1988) and when sufficient cholesterol is removed, the membrane becomes unstable, enhancing its ability to fuse with the outer acrosomal membrane, resulting in the acrosome reaction (Nolan et al., 1992). Adding cholesterol to the incubation medium results in an inhibition of the acrosome reaction (Visconti et al., 1999; Khorasani et al., 2000; de Jonge, 2005). Altering the lipid composition of sperm plasma membranes not only affects the ability of sperm to capacitate and acrosome react, it also affects the way sperm respond to cryopreservation (He et al., 2001; Awad and Graham, 2002; Purdy and Graham, 2004a; Moore et al., 2005). However, Purdy and Graham (2004a) found that when cyclodextrins are preloaded with cholesterol (CLC) and then incubated with bull sperm before cryopreservation, higher percentages of motile and viable cells are recovered after freezing and thawing, compared with control sperm. This added cholesterol most likely benefits cells by eliminating or at least lowering the temperature at which the sperm plasma membranes undergo the lipid phase

transition from the fluid to the gel state as the cells are cooled (Blok et al., 1976; Watson, 1981; Steponkus, 1984; Caffrey 1987; Drobnis et al., 1993). More importantly, Purdy and Graham (2004b) also showed that after freezing and thawing, CLC-treated bovine sperm do indeed undergo capacitation and the acrosome reaction at rates similar to control sperm, and fertilize oocytes *in vitro* and *in vivo* similarly well. Therefore, adding cholesterol to sperm membranes using CLC technology has been proven to be very useful in enhancing the cryosurvival of bovine sperm (Awad and Graham, 2002; Purdy and Graham, 2004a; Purdy and Graham, 2004b) and recently in equine sperm, as well (Moore et al., 2005). The purpose of the present study is to measure, if any, the changes in the bovine sperm membrane permeability to water during freezing with and without the CLC-treatment.

The unique morphology and small size of mammalian spermatozoa limit the applicability of standard cryomicroscopy techniques to measure the biophysical responses (water transport and intracellular ice formation) of spermatozoa during freezing. However, a novel method using a differential scanning calorimeter (DSC) has enabled the measurement of the water transport response during freezing of spermatozoa of several species, including those of the mouse (Devireddy et al., 1999), human (Devireddy et al., 2000), horse (Devireddy et al., 2002a; Devireddy et al., 2002b), canine (Thirumala et al., 2003), pacific oyster (He et al., 2004), boar (Devireddy et al., 2004), green swordtail (Thirumala et al., 2005) and southern platyfish (Pinisetty et al., 2005). This DSC technique was used in this study to measure the membrane permeability parameters of bovine spermatozoa at a cooling rate of 20 °C/min in three different media: i) in the absence of any cryoprotective agents or CPAs, ii) in the presence of 0.7 M glycerol and iii) in the presence of 1.5 mg/ml CLC and 0.7 M glycerol. The experimentally determined membrane permeability parameters were then used to calculate the optimal rates of freezing bovine sperm cells in the presence and absence of glycerol and CLC.

2.2 Materials and Methods

2.2.1 Semen Collection

In this study, semen was collected over a 2-month interval from mature, healthy fertile Angus (n = 3) and Senepol (n = 5) bulls that were housed in temperature-controlled paddocks

at the Genex Custom Collection Service near the Louisiana State University campus. The bulls ranged from 2 to 7 years in age (means = 3.5 years for the Angus bulls and 3.4 years for the Senepol bulls), were in good body condition and had body weights that ranged from 603 to 1,250 kg at the onset of semen collection. Semen was collected once or twice a week, with never less than 3 days between semen collections from one week to the next. Each bull was in semen production and thus, accustomed to the standard semen collection procedures at the bull stud facilities. Males were randomly selected from the bull group on the day of semen collection.

All bulls were collected by the same experienced technicians across the duration of the study. Briefly, two false mounts were made by the bulls before actual semen collection from a trained teaser steer. A total of nine separate semen ejaculates (collection days = 9) from eight bulls were randomly allotted as replicates across this experiment. One Angus bull (#AN179) was collected twice during the collection interval. Semen was harvested using a 15-ml sterile glass tube, extended in a standard bovine egg yolk based diluent and then placed into a 37°C water bath for equilibration prior to evaluating progressive motility. Sperm concentration was calculated using a standard curve from a spectrophotometer following standard commercial bull stud procedures. The semen sample was then transported in a 15 ml glass conical tube, held in a 50 ml water bath (37°C) in a standard Styrofoam container to the LSU Bioengineering Laboratory (~10 minutes) for Differential Scanning Calorimetry (DSC) experiments. Ejaculates from bulls were used randomly across the replicates of the DSC experiments and all experiments were completed within 3 to 6 hours of collection.

2.2.2 Preparation of Cholesterol-Loaded Cyclodextrin (CLC)

Methyl- β -cyclodextrin (Sigma Aldrich, St. Louis, MO) was loaded with cholesterol as described previously by Purdy and Graham (2004a; 2004b). Briefly, 200 mg of cholesterol was dissolved in 1 ml of chloroform. In a second tube, 1 g of Methyl- β -cyclodextrin was dissolved in 2 ml of methanol and 0.45 ml of the cholesterol solution added. The combined cyclodextrin/cholesterol solution was thoroughly mixed, and the solvents then removed using a stream of nitrogen gas. The resulting crystals were stored at 22 °C until use. To add cholesterol to sperm, a solution of 1.5 mg/ml of CLC was made by adding 50 mg of CLC to 1

ml TALP (Nolan et al., 1992) at 37°C and mixing vigorously using a vortex mixer, as described by Purdy and Graham (2004a).

2.2.3 Loading of Glycerol and CLC

For DSC experiments in the absence of CPAs, spermatozoa were concentrated by gentle centrifugation (300 g, ~25 °C) for 5 min and resuspended in residual supernatant. Similarly DSC experiments on bovine spermatozoa were also conducted in the presence of a permeating cryoprotective agent or CPA (0.7 M glycerol or 6% v/v glycerol). We chose to study membrane transport in the presence of glycerol, since bull sperm is routinely cryopreserved in the presence of 4% v/v to 8% v/v glycerol (Rodriguez et al., 1975; Robbins et al., 1976; for a review on various bovine sperm preservation media see Vishwanath and Shannon, 2000). Stepwise addition of CPAs was performed at 25 °C to minimize the osmotic injury and to lessen the volumetric excursions of bovine spermatozoa during the CPA loading process (Liu and Foote, 1998; Devireddy et al., 1999; Devireddy et al., 2000). At room temperature (25 °C), a stock of 1.4 M of CPA was added to the sperm cells in 5 equal volume steps at 5 min intervals such that the final concentration of the CPA was 0.7 M. The equilibration time and the number of steps were chosen based on the equations developed by Kedem and Katchalsky (1958). After the addition of glycerol, the samples were concentrated by gentle centrifugation (as described earlier). For DSC experiments in the presence of CLC, the cells after equilibration with glycerol were incubated at room temperature (25 °C) for 10 minutes with 1.5 mg/ml CLC; a value shown to be optimal for bovine sperm by Purdy and Graham (2004a) and Purdy and Graham (2004b). As before the spermatozoa were concentrated by gentle centrifugation (300 g, ~25 °C) for 5 min and resuspended in residual supernatant, in preparation for the DSC experiments.

2.2.4 DSC Experiments

DSC dynamic cooling experiments were performed on concentrated bovine sperm samples in standard aluminum sample pans (Perkin Elmer Corporation, Norwalk, CT) in the presence of *P. syringae* (ATCC, Rockville, MD), a natural ice nucleator. Briefly, 1 ml of semen was concentrated by centrifugation (300 g) for 5 minutes, at either room temperature or at 4 °C, and resuspended in ~25 µl of residual supernatant. Approximately 10 µl of this

sperm suspension was loaded in a DSC sample pan with ~0.1 mg *P. syringae*. The DSC dynamic cooling protocol used to measure the water transport during freezing of bovine sperm is the same as reported in earlier studies on mammalian and aquatic sperm cells (Devireddy et al., 1998; Devireddy et al., 2000; Thirumala et al., 2003; Devireddy et al., 2004; He et al., 2004; Pinisetty et al., 2005; Thirumala et al., 2005). Briefly, in the DSC technique, two heat releases from the same cell suspension (or tissue system) are measured: (i) during freezing of osmotically active (live) cells in medium (at which the intracellular water is being transported across the cell membrane to freeze in the extracellular space) and; (ii) during freezing of osmotically inactive (dead) cells in medium. The difference in the measured heat release between the two cooling runs is correlated to water transport. To ensure the accuracy and repeatability of the experimental data, a set of calibration and control experiments were performed as detailed previously for a DSC-7 (Perkin Elmer Corporation) machine (Devireddy et al., 1998).

2.2.5 Translation of Heat Release to Cell Volume Data for Dynamic Cooling

The heat release measurements of interest are Δq_{dsc} and $\Delta q(T)_{dsc}$ and are the total and fractional difference between the heat releases measured by integration of the heat flows during freezing of osmotically active (live) cells in medium and during freezing of osmotically inactive (dead) cells in medium. This difference in heat release has been shown to be related to cell volume changes in several biological systems (Devireddy et al., 1998; Devireddy et al., 1999; Devireddy et al., 2002a; Thirumala et al., 2003; Devireddy et al., 2004; Pinisetty et al., 2005) as,

$$V(T) = V_o - \frac{\Delta q(T)_{dsc}}{\Delta q_{dsc}} \cdot (V_o - V_b). \quad (2.1)$$

Note that the heat release readings $\Delta q(T)_{dsc}$ and Δq_{dsc} are obtained separately at a cooling rate of 20 °C/min in the three freezing media studied, i.e., with no CPAs, with glycerol, and with glycerol and CLC. The unknowns needed in Equation (2.1) apart from the DSC heat release readings are V_o (the initial or the isotonic cell volume) and V_b (the osmotically inactive cell volume) and were taken from the literature (van Duijn, 1960; van Duijn and van Voorst, 1971; Drevius 1972; Hammerstedt et al. 1978; Cummins and Woodall,

1985; Révay et al. 2004).

2.2.6 Water Transport Model

The reduction in cellular volume that occurs during freezing has been modeled thermodynamically (Mazur, 1963; Levin et al., 1976) and is described by the following relationship,

$$\frac{dV}{dT} = -\frac{L_p A_c R T}{B} [C_i - C_o] \quad (2.2)$$

With L_p , the plasma membrane permeability to water defined as,

$$L_p = L_{pg}[cpa] \exp\left(-\frac{E_{Lp}[cpa]}{R} \left(\frac{1}{T} - \frac{1}{T_R}\right)\right) \quad (2.3)$$

where, L_{pg} or $L_{pg}[cpa]$ is the reference membrane permeability ($\mu\text{m}/\text{min}\cdot\text{atm}$) at a reference temperature, T_R ($= 273.15$ K) in the absence and presence of CPA; E_{Lp} or $E_{Lp}[cpa]$ is the apparent activation energy (kJ/mol) or the temperature dependence of the cell membrane permeability in the absence and presence of CPA; V is the sperm volume at temperature, T (K); A_c is the effective membrane surface area for water transport, assumed to be constant during the freezing process; R is the universal gas constant; B is the constant cooling rate (K/min); finally C_i and C_o represent the concentrations of the intracellular and extracellular (unfrozen) solutions.

In the present study, we modeled the bovine sperm cell as a long cylinder with length (L) $39.8 \mu\text{m}$ and a radius (r_0) of $0.4 \mu\text{m}$ which translates to an initial (or isotonic) cell volume $V_0 \sim 20 \mu\text{m}^3$ and $A_c \sim 100 \mu\text{m}^2$ (Cummins and Woodall, 1985). The osmotically inactive cell volume, V_b , was taken to be $0.61V_0$, a value reported earlier for bovine spermatozoa by Guthrie et al., (2002). The various assumptions made in the development of Mazur's model of water transport are discussed in detail elsewhere (Mazur, 1963; Levin et al., 1976; Toner, 1993). The two unknown water transport parameters of the model, either $L_{pg}[cpa]$ and $E_{Lp}[cpa]$ in the presence of CPA or L_{pg} and E_{Lp} in the absence of CPA, are determined by

curve-fitting the water transport model to experimentally obtained volumetric shrinkage data during freezing.

2.2.7 Numerical Methods

A nonlinear least squares curve fitting technique was implemented using a computer program to calculate the water transport parameters that best-fit the volumetric shrinkage data as previously described by Bevington and Robinson (1992). The optimal fit of Equation (2.3) to the experimental data was obtained by selecting a set of parameters which minimized the residual variance (χ^2) and maximized a goodness of fit parameter (R^2) (Smith et al., 1998). All the curve fitting results presented have an R^2 value greater than or equal to 0.98 indicating that there was a good agreement between the experimental data points and the fit calculated using the estimated water transport parameters.

2.2.8 Theoretical Prediction of Optimal Rates of Cooling

Thirumala and Devireddy (2005) reported that for a variety of biological systems a comparison of the published experimentally determined values of B_{opt} (in °C/min) agreed quite closely with the value obtained using a Generic Optimal Cooling Rate Equation (GOCRE) that defines:

$$B_{opt} = 1009.5 \cdot \exp^{(-0.0546 \cdot E_{Lp})} \cdot (L_{pg}) \cdot \left(\frac{SA}{WV}\right) \quad (2.4)$$

In this equation, L_{pg} and E_{Lp} represent the membrane permeability parameters (in $\mu\text{m}/\text{min}\cdot\text{atm}$ and kcal/mol , respectively), while the term SA/WV (in μm^{-1}) represents the ratio of the available surface area for water transport ($SA = A_c$) to the initial volume of intracellular water ($WV = V_o - V_b$). Based on the assumed values of V_b and cell dimensions, the ratio of SA to WV for bovine sperm is $12.5\mu\text{m}^{-1}$. The use of Eqn. [4] greatly simplifies the prediction of optimal freezing rates and is based on the assumption that the optimal rate of cryopreservation of any cellular system can be defined as the freezing rate at which 5% of the initial water volume is trapped inside the cells at -15°C (Thirumala and Devireddy, 2005). Once L_{pg} and E_{Lp} are determined using the fitting procedure described

above, we propose to utilize Eqn. (4) to predict the optimal rates of freezing bovine spermatozoa.

2.3 Results

2.3.1 Semen Collection

The mean semen volume per ejaculate and sperm concentration per ml were 7.9 ml (range = 2 to 11.5 ml) and 0.563×10^9 (range 1.2 to 0.127×10^9) for the Angus bulls and 6.9 ml (range = 2.5 to 10 ml) and 0.473×10^9 (range = 0.302 to 0.689×10^9) for the Senepol bulls, respectively. No bull had more than the accepted range for percent abnormal sperm for all bulls in the commercial stud (abnormal sperm <30%). During the semen collection interval in this study there was no statistical difference in semen volume per ejaculate and in sperm concentration per ml between the two bull breed types. The overall mean semen volume (\pm SE) was 7.3 ± 1.1 ml per ejaculate with a concentration of 0.530×10^9 (± 0.105) sperm per ml for all bulls used in the experiment. The mean sperm concentration after extending was 0.301×10^9 (± 0.043) sperm per ml.

The mean percent progressive motility and the percent live sperm per ejaculate were 55% (range = 50 to 65%) and 67% (range 60 to 80%) for the Angus bulls and 58% (range = 50 to 65%) and 76% (range = 65 to 85%) for the Senepol bulls. Also, there was no statistical difference detected for percent progressive motility and percent live sperm between bull breed types. The overall mean percent progressive motility was 57% and the percent live sperm per ejaculate was 73% for all bulls used in the study.

2.3.2 Dynamic Cooling Response and Water Transport Parameters

Fig. 2.1 shows a comparison of the water transport data at a cooling rate of 20 °C/min for samples cooled without CPAs (Fig. 2.1A), with glycerol (Fig. 2.1B) and with CLC (Fig. 2.1C). The best fit parameters for L_{pg} and E_{Lp} are shown in Table 2.1. The volumetric responses generated by these parameters in Equation (2.2) are shown in Fig. 1 as solid lines (——). The model simulated equilibrium cooling response is also shown in Figs. 1A, 1B and 1C and is generated by setting the left hand side (LHS) of Equation (2.2) = 0 and balancing the intracellular and extracellular unfrozen chemical activity of water on the right hand side (RHS) at a particular subzero temperature. Equilibrium is achieved at each

temperature when the internal and external osmotic pressures are equal (i.e., $\pi_i = \pi_o$).

Table 2.1 Water transport parameters for bovine sperm in the absence of CPAs, with glycerol and with cholesterol-loaded cyclodextrin (CLC) at a cooling rate of 20 °C/min.

FREEZING MEDIA	L_{pg} or L_{pg} [cpa] μm/min-atm	E_{Lp} or E_{Lp} [cpa] Kcal/mol	Optimal Cooling Rate ^a °C/min
No CPAs	0.036	42.1	45
Glycerol	0.025	30.9	58
CLC Treated	0.02	26.4	60

^aobtained using Equation (2.4); see “Materials and Methods” for a more detailed description.

The water transport parameters between sperm that were cooled in the absence of CPAs (Fig. 2.1A) and in the presence of glycerol (Fig. 2.1B) or CLC (Fig. 2.1C) were statistically significantly different from each other ($P < 0.01$), using Student's t-test, over the entire temperature range of interest (-0.53 °C to -25 °C). Additionally, the differences in the water transport parameters between sperm that were cooled in the presence of glycerol and in the presence of CLC were statistically significant, albeit at a lower confidence level ($P < 0.05$). Thus, the addition of either glycerol or CLC alters the bovine sperm membrane permeability to water during freezing. And finally, the differences in the measured water transport response among bulls was found to be statistically not significant ($P < 0.99$) or the differences among bulls were statistically significant with $P < 0.01$.

Figs. 2.1A, 2.1B and 2.1C show water transport data for bovine sperm with no CPAs, for bovine sperm that were loaded with glycerol and for bovine sperm that were treated with CLC, respectively. The model simulated equilibrium cooling response obtained is shown as a dotted line (-----) in all the figures. The model simulated dynamic cooling response is shown as a solid line (——) and was obtained by using the 'best fit' membrane permeability parameters (L_{pg} and E_{Lp}) shown in Table 2.1, in the water transport equation (Eqns. [2.2] and [2.3]). The nondimensional volume is plotted along the y-axis and the subzero temperatures are shown along the x-axis. The error bars represent the standard

deviations in the data.

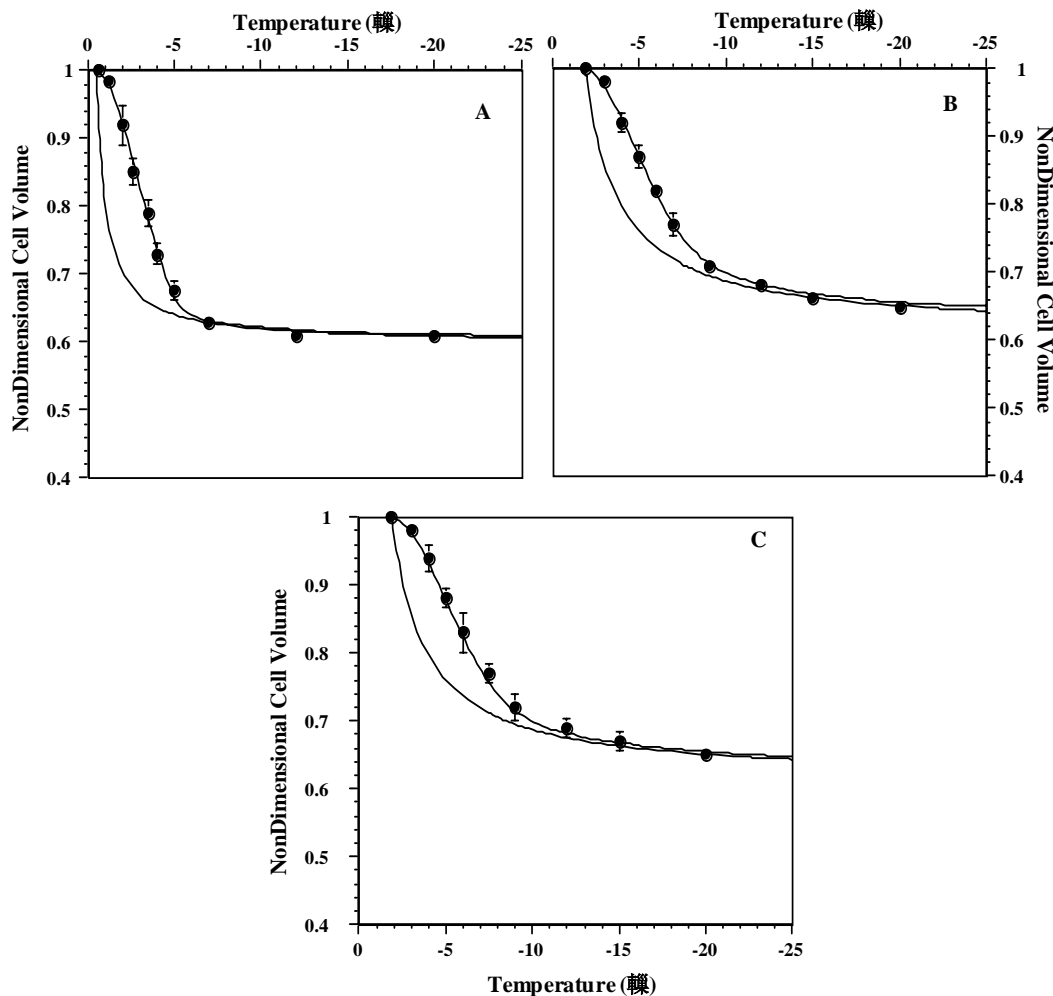


Figure 2.1 Volumetric response of bovine sperm (\bullet) as a function of subzero temperatures obtained using the DSC technique at 20 °C/min.

Figure 2.2 shows the contour plots of the goodness of fit parameter ($R^2 = 0.98$) in the L_{pg} and E_{Lp} (or $L_{pg}[cpa]$ and $E_{Lp}[cpa]$) space that “fit” the volumetric shrinkage data at 20 °C/min without CPAs, with glycerol and with CLC. Any combination of L_{pg} and E_{Lp} (or $L_{pg}[cpa]$ and $E_{Lp}[cpa]$) shown to be within the contour will “fit” the volumetric shrinkage data in that media with an R^2 value > 0.98 . The common region within all the three contours represent the combination of L_{pg} and E_{Lp} (or $L_{pg}[cpa]$ and $E_{Lp}[cpa]$) that will fit the measured water transport data concurrently in the three media investigated. An

examination of the contours suggests that the parametric space corresponding to the CLC treated bovine sperm samples is almost completely enclosed within the corresponding contour obtained for bovine spermatozoa in the presence of glycerol. This suggests that the membrane transport properties obtained for CLC treated samples can predict the water transport response of bovine spermatozoa in the presence of glycerol while the converse is not necessarily true. Also, the contour space corresponding to bovine spermatozoa in the absence of CPAs is significantly larger than that obtained in the presence of glycerol or in the presence of CLC.

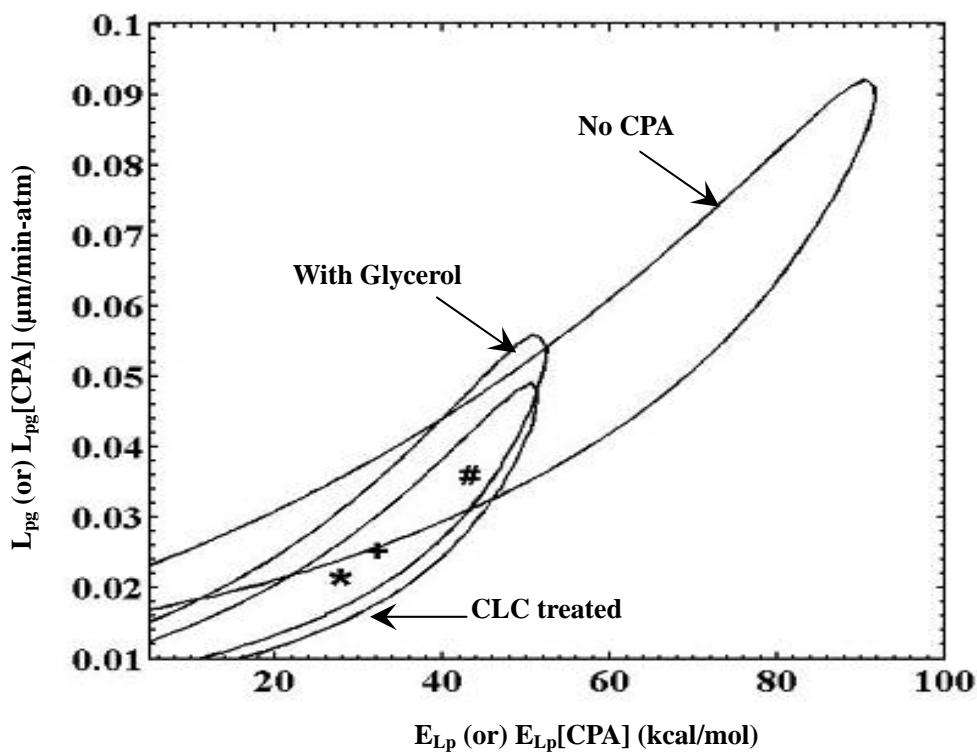


Figure 2.2 Contour plots of the goodness of fit parameter R^2 ($= 0.98$) for the parametric space of bovine sperm cooled in the absence of CPAs, with glycerol and with CLC.

The predicted best fit parameters for the three media are shown as (#) for media with no CPA, as (+) for media with glycerol and as (*) for media with CLC and glycerol, within their respective contours (see Table 2.1 for the numerical values). The membrane permeability at 0 °C, L_{pg} ($\mu\text{m}/\text{min}\cdot\text{atm}$) is plotted on the y-axis while the apparent activation energy of the membrane, E_{Lp} (kcal/mol) is plotted on the x-axis.

2.3.3 Optimal Rates of Cooling Bovine Spermatozoa

By incorporating the best fit parameters of water transport (Table 2.1) into (2.4), the theoretically predicted optimal rates of freezing bovine sperm cell suspensions were obtained and are also listed in Table 2.1. To independently verify the predicted rates of optimal freezing bovine spermatozoa, additional numerical simulations were also performed at various cooling rates (5 to 100 °C/min) using Equations 2.2 and 2.3 and the best fit parameters. The results from the numerical simulations for cells that were frozen in the absence of CPAs, in the presence of glycerol and in presence of CLC are shown in Figs. 2.3A, 2.3B and 2.3C, respectively. As an illustrative example, an examination of the model simulations in Fig. 2.3C shows that bovine sperm cells cooled in the presence of CLC are essentially dehydrated for cooling rates < 60 °C/min. At cooling rates > 60 °C/min, the amount of water trapped inside the tissue cells increases rapidly with increasing cooling rate. A more detailed analysis of the water transport simulations was also performed as described in earlier studies, including Devireddy et al., (1999), Devireddy et al., (2000), Thirumala et al., (2003), and Devireddy et al., (2004), to determine the optimal rate of freezing bovine sperm in the three freezing media investigated. Briefly, we found that the predicted optimal rates of freezing obtained by analyzing the water transport simulations are within 5% of the values obtained using Equation (2.4) and shown in Table 2.1. Thus, the predicted rates of optimally freezing bovine sperm obtained using Equation (2.4) or by a detailed analysis of the water transport simulations (shown in Figure 2.3) are essentially in agreement and show that the theoretically predicted optimal rate of freezing bovine sperm range from 45 to 60 °C/min.

In Figure 2.3, the changes in the normalized cell volume (V/V_0) as a function of temperature for different cooling rates are shown in the absence of CPAs (Figure 3A), with glycerol (Figure 3B) and with CLC (Figure 3C), respectively. The water transport curves (——) plotted in Figure 3 represent the model simulated response for different cooling rates (from left to right: 5, 20, 40, 60, 80 and 100 °C/min) using the “best-fit” parameters shown in Table 1. The model simulated equilibrium cooling response is also shown in all the figures as a dotted line (-----). The subzero temperatures are shown along the x-axis

while the nondimensional volume is plotted along the y-axis.

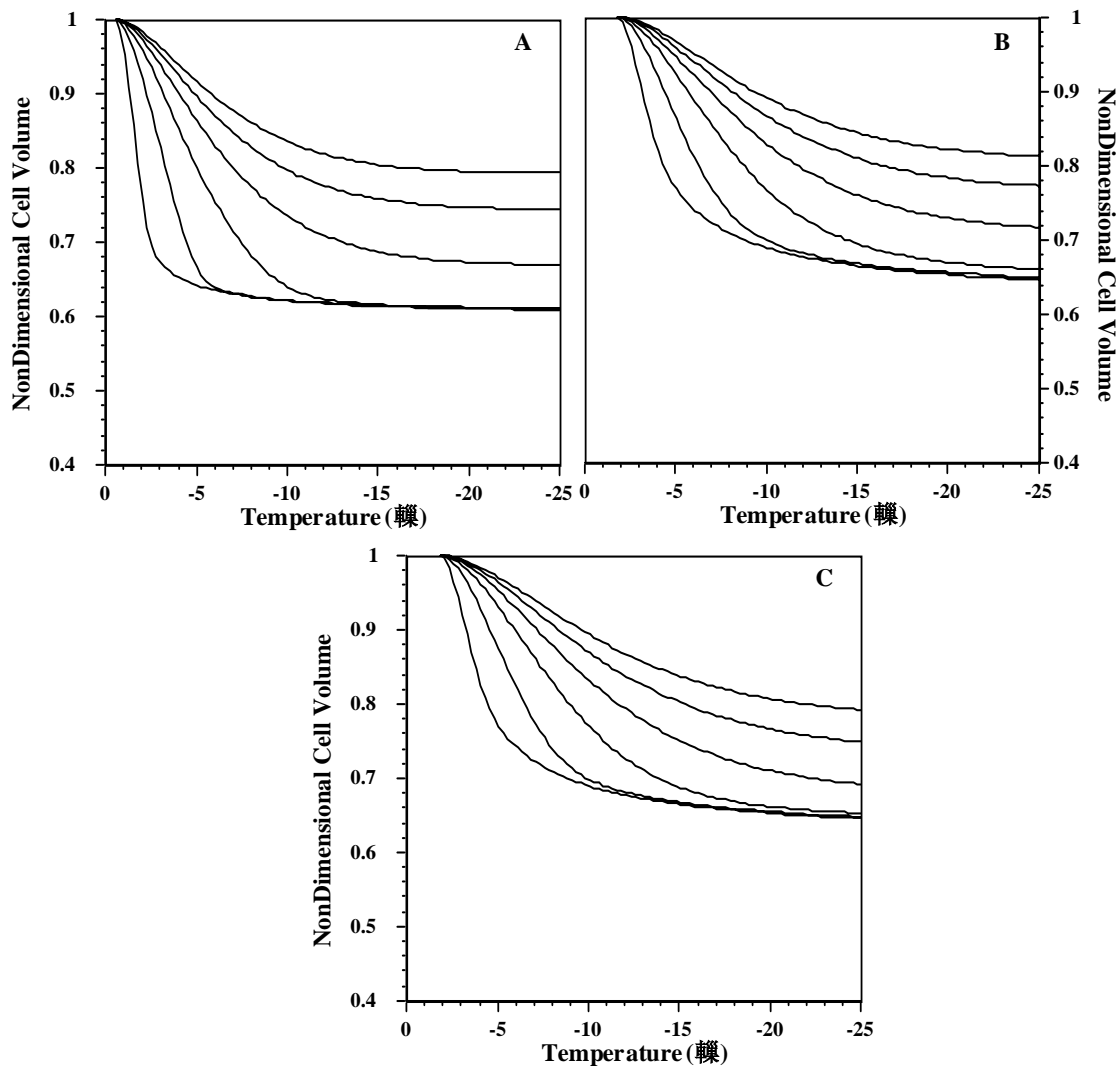


Figure 2.3 Volumetric response of bovine spermatozoa at various cooling subzero temperatures using the “best-fit” water transport parameters (shown in Table 1).

2.4 Discussion

2.4.1 Water Transport Parameters in the Absence of Extracellular Ice

As mentioned earlier, there are currently no experimental techniques, with the exception of the DSC technique, that yield data on how spermatozoa either dehydrate or form intracellular ice during freezing in the presence of extracellular ice. However, there exist a few techniques like the *Time to Lysis* method (Drevius, 1971; Watson et al., 1992), a *Coulter Counter* technique (Gilmore et al., 1998) and a stopped-flow method based on the self-quenching of an entrapped fluorophore (Curry et al., 2000; Chaveiro, 2004) to measure the volumetric response of spermatozoa to external changes in osmolality, at suprazero

temperatures. The parameters obtained using these techniques are essentially in agreement: suprazero water transport permeability parameter, $L_p \sim 0.3$ to $10 \mu\text{m}/\text{min-atm}$ and activation energy at suprazero temperatures, $E_a \sim 3$ to 14 kcal/mol (Curry, 2000). More specifically, Drevius (1971) and Watson et al. (1992) using the *Time to Lysis* method have reported a L_p value for bovine spermatozoa of $\sim 10 \mu\text{m}/\text{min-atm}$ and an activation energy of $\sim 3 \text{ kcal/mol}$. Recently, Chaveiro et al. (2004) using a stopped-flow method have reported a L_p value for bovine spermatozoa of $\sim 0.68 \mu\text{m}/\text{min-atm}$ in the absence of CPAs and values of L_p ranging from ~ 0.91 to $0.29 \mu\text{m}/\text{min-atm}$ in the presence of various CPAs, including glycerol. This serves to provide a good understanding of suprazero water (and CPA) transport response for spermatozoa of various mammals, including those of the human, ram, bull, rabbit and mouse (Holt, 2000).

2.4.2 Convergence of Theoretical and Experimental Optimal Rates of Freezing Bovine Sperm

Unfortunately, the suprazero permeability parameters obtained in the absence of extracellular ice using the techniques described above cannot predict the experimentally determined optimal rate of freezing bovine sperm or other mammalian sperm (Ravie and Lake, 1982; Duncan and Watson, 1992; Curry et al., 1994). For example, an L_p value of $0.5 \mu\text{m}/\text{min-atm}$ and an activation energy of 3 kcal/mol results in a theoretically predicted optimal rate of freezing bovine sperm as $\sim 5,000 \text{ }^\circ\text{C}/\text{min}$. When in fact experiments show that the “optimal cooling rate” for bovine spermatozoa is 30 to $100 \text{ }^\circ\text{C}/\text{min}$, with a major decrease in viability after cooling at $300 \text{ }^\circ\text{C}/\text{min}$ (Rodriguez et al., 1975; Robbins et al., 1976; Foote and Parks, 1993; Woelders et al. 1997; Woelders 1997; Woelders and Malva, 1998; Kumar et al., 2003)¹. One way to reconcile this discrepancy is that the values of water transport parameters at subzero temperatures in the presence of extracellular ice are markedly

¹Although there is reasonable agreement in the experimentally determined cooling rates for optimal freezing of bull sperm, there is some variation in the reported values. For example, Woelders (1997) and Woelders and Malva (1998) show an optimum cooling rate of $100 \text{ }^\circ\text{C}/\text{min}$, and this is greater than the optimum of $26\text{--}52 \text{ }^\circ\text{C}/\text{min}$ suggested earlier for bovine spermatozoa by Robbins et al., (1976) and an optimum of $30 \text{ }^\circ\text{C}/\text{min}$ in a controlled rate freezer by Kumar et al., (2003).

different than those reported in literature at suprazero temperatures. In particular, if L_{pg} at subzero temperatures is lower by two orders of magnitude than L_p at suprazero temperatures and E_{Lp} at subzero temperatures is higher by a factor of five than the corresponding E_a at suprazero temperatures, then the discrepancy between numerical simulations and experimental data can be reconciled (Curry et al., 1994; Devireddy et al., 1999; Devireddy et al., 2004). The best-fit parameters obtained in this study using the DSC water transport data (shown in Table 2.1) during freezing of bovine spermatozoa confirm that this is indeed the case; $L_{pg} = 0.02$ to $0.036 \mu\text{m}/\text{min}\cdot\text{atm}$ and $E_{Lp} = 26.4$ to $42.1 \text{ kcal}/\text{mol}$. The predicted optimal rates of freezing bovine sperm utilizing these subzero values range from 45 to $60^\circ\text{C}/\text{min}$ and are within the range of experimentally determined values. This represents a significant advance in our ability to predict the freezing behavior of bovine sperm cells.

2.4.3 Effect of Extracellular Ice on Bovine Sperm Membrane Transport Properties

The water transport parameters obtained in this study using the DSC technique during freezing of bovine spermatozoa are significantly lower than the reported suprazero permeability values for other mammalian species (Curry, 2000). A similar dissimilarity between the suprazero and subzero water transport parameters was also found for mouse (Devireddy et al., 1999), human (Devireddy et al., 2000), horse (Devireddy et al., 2002a; Devireddy et al. 2002b), canine (Thirumala et al., 2003) and boar (Devireddy et al., 2004) sperm cells. This discrepancy between the membrane permeabilities may be associated with possible changes in the sperm cell plasma membrane during suprazero cooling, including a lipid phase transition between 0 and 4°C (Noiles et al., 1995) and/or a cold shock damage or “chilling” injury during cooling (Blok et al., 1976; Watson, 1981; Steponkus, 1984). These changes in membrane transport properties might also be associated with solidification in the extracellular medium (phase change) phenomena, including changes in the membrane fluidity (Drobnis et al., 1993) and lyotropic (i.e., independent of cooling rate) membrane phase changes and corresponding alterations of water transport (Caffrey 1987; Noiles et al., 1995). The presence of extracellular ice has also been shown to alter the cell membrane transport properties (McGrath, 1988).

2.4.4 Effect of Glycerol and CLC on Bovine Sperm Membrane Transport Properties

As stated earlier, we have measured the effect of adding glycerol and CLC to the subzero water transport response of bovine spermatozoa. As shown in Table 2.1, addition of glycerol leads to a reduction in both the measured value of reference membrane permeability and the activation energy of bovine spermatozoa. This trend is consistent with results reported in previous studies on membrane permeability parameters of other mammalian sperm cells (Thirumala et al., 2003; Devireddy et al., 2004) and in isolated rat hepatocytes (Smith et al. 1998). Also, the addition of CLC further reduces the bovine sperm membrane water transport parameters, although the predicted rates of optimal freezing with CLC are within 10% of those obtained in the presence of glycerol² (Table 2.1). This result is intriguing and suggests that the beneficial effect of incubating bovine sperm with CLC prior to freezing is some what dependent on its ability to mediate membrane transport across the cell membrane; so far as it relates to the rate of intracellular water loss during an imposed freezing stress. Although several studies, including Grahams and Foote (1987), Parks and Lynch (1992), De Leeuw et al., (1993), White (1993), Zeron et al., (2002) and Amirat et al. (2005), have detailed the beneficial effects of adding lipids/cholesterol/fatty acids to biomembranes prior to cooling, we are unaware of any previous studies that report the effect of adding CLC or other fatty acids to subzero water transport properties of cells. Although, it seems reasonable to expect “alterations” in the bovine sperm membrane transport properties in the presence of CLC, a recent study by Purdy et al., (2005) found CLC treatment did not significantly alter membrane fluidity of bovine sperm after suprazero temperature changes. Clearly, further studies are needed. It is also as yet unclear, if varying the concentration of CLC from 1.5 mg/ml used in the present study will result in corresponding changes to the measured subzero water transport response of bovine sperm. We propose to conduct, in future, similar experiments with bovine, equine and porcine spermatozoa to further delineate the effect of CLC treatment on the subzero water transport response of mammalian spermatozoa.

²As shown in Equation (4) a decrease in the value of L_{pg} lowers the predicted optimal cooling rate. However, decreasing E_{Lp} has the opposite effect. Thus, their decrease in the presence of CLC does not significantly alter the predicted optimal rate of freezing CLC treated bull sperm when compared with the optimal rate of freezing in the presence of glycerol.

2.5 Summary and Conclusion

In conclusion, water transport (volumetric shrinkage) data for bovine spermatozoa in the presence of extracellular ice, a CPA (glycerol), and cholesterol-loaded cyclodextrin (CLC) during freezing were obtained using a DSC technique at 20 °C/min. The DSC volumetric data were curve fitted to a model of water transport (Equations 2.2 and 2.3) to predict the water transport parameters (L_{pg} and E_{Lp} (or $L_{pg}[cpa]$ and $E_{Lp}[cpa]$). We modeled the bovine spermatozoa as a cylinder of length 39.8 μm and radius 0.4 μm with an osmotically inactive cell volume of $0.61V_0$. The “best-fit” parameters of water transport for bovine spermatozoa in the absence of CPAs are: $L_{pg} = 0.0036 \mu\text{m}/\text{min-atm}$ and $E_{Lp} = 42.1 \text{ kcal/mol}$ (goodness of fit, $R^2 = 0.99$); the corresponding parameters in the presence of 0.7 M glycerol are: $L_{pg} = 0.025 \mu\text{m}/\text{min-atm}$ and $E_{Lp} = 30.9 \text{ kcal/mol}$ ($R^2 = 0.99$); and in the presence of 1.5 mg/ml of CLC and 0.7 M glycerol are: $L_{pg} = 0.02 \mu\text{m}/\text{min-atm}$ and $E_{Lp} = 26.4 \text{ kcal/mol}$ ($R^2 = 0.99$). The parameters obtained in this study are significantly different from the water transport parameters reported in literature for bovine and other mammalian spermatozoa obtained in the absence of extracellular ice at suprazero (and subzero) temperatures. The new parameters obtained in this study help to explain the discrepancy between the predicted optimal cooling rates based on suprazero permeability parameters (on the order of thousands of degree C per min) and the experimentally determined optimal cooling rates (on the order of tens of degree C per min). In addition, we also report that the addition of CLC alters the bovine sperm subzero water transport properties. The experimentally determined water transport data and modeling presented here may lead to a rational way of optimizing freezing procedures for bovine sperm.

Chapter 3

Suprazero Cooling Conditions Significantly Influence Subzero Permeability Parameters of Equine Ovarian Tissue

3.1 Introduction

Numerous studies have been conducted to derive methods to cryopreserve cells and tissues based on measurements of their biophysical properties, especially the permeability to water and the activation energy of this permeability. These properties dictate to a large extent how tissues respond when they are cooled to subzero temperatures and ice forms around the tissue (Mazur et al., 1972; Leibo, 1980). As examples of such efforts, we have measured subzero water transport parameters (reference membrane water permeability or L_{pg} and activation energy or E_{Lp}) during freezing of several types of mammalian tissues (Devireddy and Bischof, 1998; Devireddy et al., 1999; Devireddy et al, 2001). Using the data of Newton et al. (1998), we have recently determined the suprazero permeability coefficients of human ovarian tissues to various cryoprotective additives or CPAs (Devireddy, 2005). Preliminary evidence suggested to us that the rate at which cells or tissues are cooled at temperatures above 0°C, i.e. suprazero temperatures, might influence the response of cells when they are cooled at a specific freezing rate at subzero temperatures. This in turn might affect the calculated values of L_p and E_{Lp} . [For convenience and brevity, throughout this paper, we have denoted temperature changes above 0°C as “cooling rate” and temperature changes after ice forms below 0°C as the “freezing rate.”] To test our proposition, we have measured and report here the water transport responses and the membrane permeability parameters, L_{pg} and E_{Lp} , of equine ovarian tissue cells cooled at either 40°C/min or 0.5°C/min from 25°C to 4 °C before being cooled to low subzero temperatures at a freezing rate of 5°C/min. We also determined the effect of suprazero cooling rates on the subzero water transport responses of ovarian tissue cooled at a freezing rate of 5°C/min in the presence of two commonly used CPAs, 0.85 M glycerol or 0.85 M dimethylsulfoxide (DMSO). Equine tissue was chosen as a model for ovarian tissue of other species because of the ready accessibility of ovaries from mares that were to be euthanized for other research projects at the Louisiana School of

Veterinary Medicine.

There is now considerable interest in cryopreservation of human ovarian tissue as an adjunct to its transplantation to restore fertility of female cancer survivors (Tulandi and Gosden 2004; Picton et al., 2002). The first attempts to freeze ovarian tissue were conducted with rodents (Parrott, 1960). Since then, numerous studies of ovarian tissue of many species have been performed, including those of mice (Carroll et al., 1990; Carroll and Gosden, 1993; Harp et al., 1994), rats (Yin et al., 2003), sheep (Gosden et al., 1994; Baird et al. 1999), monkeys (Schnorr 2002), cattle (Paynter et al. 1999), and humans (Chen, 1986; Newton et al., 1996; Picton et al., 2002; Kim et al., 2002; Practice Committee, 2004; Donnez et al., 2004; Lee et al. 2004; Gosden 2004; Oktay et al., 2004; Silber 2005; Lobo 2005; Donnez et al., 2005).

When ice forms within vascular spaces of tissue during freezing, water flows out of the cells of the tissue, i.e. the cells undergo dehydration. If the cells do not dehydrate sufficiently, then at some subzero temperature, intracellular ice forms within the cells themselves. These biophysical responses of cell dehydration and intracellular ice formation (IIF) are directly coupled to cellular injury as described by Mazur's two factor hypothesis (Mazur et al., 1972). According to this hypothesis, the following factors operate. Factor 1: At low freezing rates, cells may be injured because they are exposed to solutions the properties of which have been drastically altered by the decreasing unfrozen fraction of the vascular/extracellular space. Factor 2: At high freezing rates, injury may result from IIF (Mazur et al., 1972). But since the words "low" and "high" are relative terms, the specific freezing rates are characteristic of a given cell type and need to be experimentally determined. These biophysical events during freezing were first elucidated in single cells by cryomicroscopy (Molisch, 1897; Leibo et al., 1978; McGrath, 1987; Cosman et al., 1989; Toner, 1993; Smith et al., 1998; Diller, 2005). Recently, analogous experimental data in whole tissues are emerging. Water transport studies in tissue sections at suprazero temperatures were performed by Newton et al. (1998) and Devireddy (2005), and measurements of water transport at subzero temperatures have been performed on rat liver (Pazhayannur and Bischof, 1997; Devireddy and Bischof, 1998), on rat prostate tumor (Devireddy et al., 1999a) and on uterine fibroid tumor (Devireddy et al., 2001). Subzero permeability measurements have been made using a combination of low temperature

microscopy and calorimetric techniques (Bischof, 2000).

In the present study, the calorimetric technique was used to measure the efflux of water from equine ovarian tissue cells that were cooled from 25°C to 4°C at either 40°C/min or 0.5°C/min and then frozen to low subzero temperatures in the presence or absence of either of two cryoprotective agents. By fitting a model of water transport to the experimentally measured volumetric shrinkage response of the cells, it was possible to calculate the membrane water permeability or L_{pg} and activation energy or E_{Lp} of ovarian tissue cells that had been frozen at 5°C/min. The experimentally determined membrane permeability parameters were then used to calculate the theoretical optimum rates of freezing mammalian ovarian tissue cells.

3.2 Theoretical Background

During freezing of tissues, ice tends to form first in the vascular/extracellular space of whole tissues (Love, 1966; Rubinsky et al., 1987). The presence of vascular/extracellular ice creates a small highly concentrated unfrozen saline fraction that induces a chemical potential difference across the tissue cell membrane. In response to this gradient, intracellular water flows out of the cell into the vascular/extracellular space. Water transport across the membrane of a spherical cell during freezing in the presence of extracellular ice has been modeled by Mazur (1963); this model was later modified by Levin et al. (1976) and Karlsson et al. (1994). The corresponding reduction in tissue cellular volume was modeled using a Krogh cylinder by Rubinsky and Pegg (1988), Pazhayannur and Bischof (1997), Devireddy et al., (1999):

$$\frac{dV}{dT} = - \frac{L_p A_c R T}{B v_w} \left[\ln \frac{(V_o - V_b - n_{cpa} v_{cpa}) / v_w}{(V_o - V_b - n_{cpa} v_{cpa}) / v_w + (\varphi_s n_s + n_{cpa})} - \frac{\Delta H_f v_w \rho}{R} \left(\frac{1}{T_R} - \frac{1}{T} \right) \right] \quad (3.1)$$

with L_p , the tissue cell membrane permeability to water defined by Levin et al. (1976) as,

$$L_p = L_{pg} [cpa] \exp \left(- \frac{E_{Lp} [cpa]}{R} \left(\frac{1}{T} - \frac{1}{T_R} \right) \right). \quad (3.2)$$

Table 3.1 Description of variables used in Eqn. (3.1) and (3.2)

Variable	Description	Value (units)
L_{pg}	Reference membrane permeability at T_R	($\mu\text{m}/\text{min}\cdot\text{atm}$)
$L_{pg} [cpa]$	Reference membrane permeability in the presence of CPAs at T_R	($\mu\text{m}/\text{min}\cdot\text{atm}$)
T_R	Reference temperature	273.15 (K)
E_{Lp}	Activation energy	(Kcal/mole)
$E_{Lp} [cpa]$	Activation energy in the presence of CPAs	(Kcal/mole)
R	Universal gas constant	8.314 (J/molK)
B	Cooling rate	($^{\circ}\text{C}/\text{min}$)
n_{cpa}	Number of moles of salt	(moles)
v_w	Molar volume of water	18×10^{12} ($\mu\text{m}^3/\text{mole}$)
φ_s	Dissociation constant for salt	2
C_i	Initial cell osmolality	0.285 (moles)
V_o	Isotonic (initial) cell volume	(μm^3)
V_b	Osmotically inactive cell volume	(μm^3)
n_s	Number of moles of salt	$C_i \cdot (V_o - V_b)$
ΔH_f	Latent heat of fusion of water	335 (mJ/mg)
ρ	Density of water	1000 (kg/m^3)
V	Tissue cell volume	(μm^3)
T	Temperature	(K)
A_c	Effective membrane surface area	(μm^2)

The variables used in Eqns. (3.1) and (3.2) are shown in Table 3.1.

Fig. 3.1 shows the Krogh cylinder model used in this study and the corresponding

dimensions including the radius of the extracellular space (r_{v0}), the distance between the microvascular channels (ΔX) and the axial length of the Krogh cylinder (L). In the Krogh cylinder model, the cellular space with volume V is modeled as the box surrounding the cylinder ($V = L \Delta X^2 - \Delta r_{v0}^2 \pi L$), i.e. the extracellular volume including the interstitial and vascular spaces is modeled as the cylinder of volume $\pi \Delta r_{v0}^2 L$ and the effective membrane surface area available for water transport (mass transfer) during the freezing process, $A_c = 2 \pi \Delta r_{v0} L$. Note that the length of the Krogh cylinder, L , is not important in the Krogh model, i.e. under conditions of uniform temperature throughout the Krogh unit, the water transport simulations obtained using Eqns. (3.1) and (3.2) are identical with different values of L . This is because the ratio of cellular volume, V , and the available membrane surface area, A_c , is independent of the length of the Krogh unit, L . The use of the Krogh model necessitates the use of several other assumptions (Rubinsky et al., 1987; Rubinsky and Pegg, 1988; Pazhayannur and Bischof, 1997). These are: (a) the tissue is composed of a number of identical Krogh units all experiencing the same thermal history, (b) axial flow of blood in the vasculature is neglected, (c) a single lumped permeability for water transport between the intracellular and vascular/extracellular spaces and (d) the cell volume (V) is equal to the isotonic cell volume (V_0) at temperature T_{ph} , the phase change temperature of the extracellular medium. Thus, a theoretically determined temperature-volume history of a cell during freezing can then be predicted by integrating Eqns. (3.1) and (3.2). The two unknown membrane permeability parameters of the model either $L_{pg}[cpa]$ and $E_{Lp}[cpa]$ in the presence of CPA or L_{pg} and E_{Lp} in the absence of CPA, are determined by curve-fitting the water transport model to experimentally obtained volumetric shrinkage data during freezing. The various assumptions made in the development of Mazur's model of water transport are discussed in detail elsewhere (Mazur, 1963; Rubinsky and Pegg, 1988; Toner, 1993; Pazhayannur and Bischof, 1997; Smith et al., 1998).

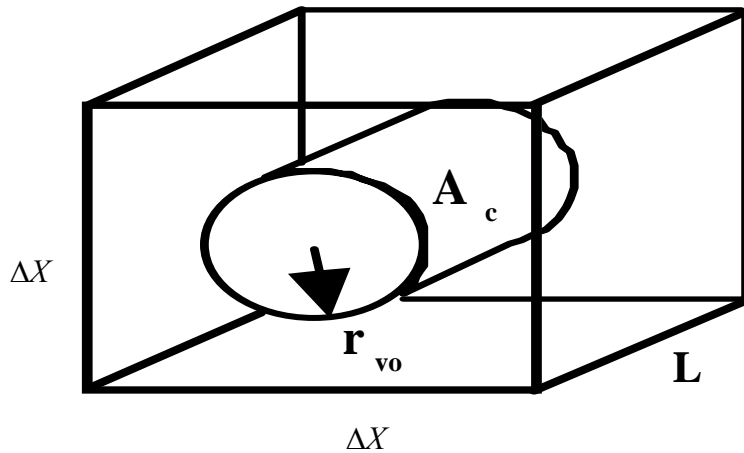


Figure 3.1 Schematic drawing of the Krogh cylinder, a representation of a mare ovarian tissue unit.

The Krogh cylinder dimensions for the mare ovarian tissue are: ΔX , the distance between the microvascular channels = $18.4\mu\text{m}$, r_{vo} , the initial radius of the extracellular space = $5.4\mu\text{m}$, and L , the axial length of the Krogh cylinder = $26.2\mu\text{m}$.

3.3 Materials and Methods

3.3.1 Tissue Collection and Isolation

All ovarian tissue samples were excised from euthanized mares by trained veterinary surgeons. The mares were euthanized at the LSU Veterinary School for unrelated experiments or for humanitarian purposes; and all protocols were approved by Institutional Animal Care and Use Committee (IACUC) at LSU. The age of the seven euthanized mares ranged from 3 to 23 years. All the samples were collected outside of the normal breeding season (Nov 2004 to Feb 2005) and hence, were hormonally inactive. After being excised, the ovarian tissue was placed in a plastic bag with D-PBS solution (GIBCO BRL, Rockville, MD) and transported from the LSU Veterinary School to the LSU Bioengineering Laboratory (a distance of less than a mile). Upon arrival at the LSU Bioengineering Laboratory, the samples were sectioned and equilibrated with two cryoprotective agents or CPAs (dimethylsulfoxide or DMSO and glycerol) at a concentration of 0.85 M (Hovatta et al., 1996; Newton et al., 1998). Stepwise addition of CPAs was performed at $25\text{ }^{\circ}\text{C}$ to minimize the osmotic injury and to lessen the volumetric excursions of the ovarian tissue cells during the CPA loading process (Schneider and Mazur, 1984; Newton et al., 1998; Paynter et al., 2005). At room temperature, a stock of 1.7 M of CPA was added to ovarian tissue cells in 5 equal

volume steps at 5 min intervals such that the final concentration of the CPA was 0.85 M. The equilibration time and the number of steps were chosen based on the equations developed by Kedem and Katchalsky (1958) and described elsewhere (Devireddy, 2005). To prevent ischemic damage, all experiments were completed within 3 to 5 hours after excision.

3.3.2 Calorimetric Experiments

Calorimetric experiments were performed on excised ovarian tissue slices using a Differential Scanning Calorimeter (DSC) (DSC-7, Perkin Elmer Corp, Norwalk, CT). The tissue was cut into small pieces (1-1.5 mm³) using a razor blade. The tissue slices were then patted externally using a blotting paper and their weight was measured (1-1.5 mg). The samples were then placed in standard DSC aluminum sample pans (kit #0219-0062, Perkin Elmer Corp, Norwalk, CT) and a small drop (< 8 μ l) of the freezing medium was added to keep the tissue slice hydrated. A natural ice nucleator *Pseudomonas syringae* (ATCC, Rockville, MD) was sprinkled (~0.1 mg) onto the sample before the pans were sealed and reweighed. The ice nucleating agent *P. syringae* always nucleated the vascular/extracellular space at temperatures $\geq -4^{\circ}\text{C}$ to avoid damaging intracellular ice formation, which occurs predominantly at temperatures below -5°C in most cell systems (Toner, 1993). The total sample weight was always kept ≤ 10 mg.

The calorimetric protocol used to measure water transport out of ovarian tissue cells is the same as the one previously described for rat liver (Devireddy and Bischof, 1998), for prostate tumor (Devireddy et al., 1999), and for uterine fibroid tumor (Devireddy et al., 2001). The DSC experiments were conducted at a freezing rate of 5 $^{\circ}\text{C}/\text{min}$. Since the DSC cannot distinguish between the heat released due to dehydration (water transport) and intracellular ice formation (IIF), additional experiments were not performed at higher freezing rates ($> 5^{\circ}\text{C}/\text{min}$), at which there is a strong likelihood of IIF. To ensure the accuracy and repeatability of the experimental data, a set of calibration and control experiments were also performed (Devireddy and Bischof, 1998). A brief description of the DSC cooling protocol is given below:

Step 1: The sample (tissue slices + isotonic PBS) + 0.1 mg of *P. syringae* bacteria were cooled from 25 $^{\circ}$ to 4 $^{\circ}\text{C}$ at either 40 $^{\circ}\text{C}/\text{min}$ or at 0.5 $^{\circ}\text{C}/\text{min}$. The sample was allowed to

equilibrate at 4°C for ~3 minutes and then cooled at 5°C/min until the vascular/extracellular ice nucleated (usually around -3.5 °C).

Step 2: At the time of nucleation, the sample was manually triggered to thaw at a warming rate (10°C/min) such that the phase change temperature of the freezing medium, T_{ph} (~ -0.53°C in the absence of CPAs and ~ -2.1°C in the presence of CPAs) was reached (but not overshoot) and ice remained in the extracellular solution.

Step 3: The sample was then frozen to -50°C at 5°C/min and the initial heat release due to the medium mixed with live cells was measured ($q_{initial} = \sim 124$ mJ/mg of tissue).

Step 4: The sample was allowed to equilibrate again at T_{ph} by thawing it at 50°C/min.

Step 5: To differentiate between the heat released by the medium and the intracellular fluid in Step 3, the tissue cell membranes were compromised by freezing the sample at a “high” freezing rate (200°C/min) down to -150°C.

Step 6: Step 4 was repeated.

Step 7: The sample was then frozen to -50°C at 5°C/min to measure the final heat release due to lysed or osmotically inactive cells mixed with medium ($q_{final} = \sim 116.5$ mJ/mg of tissue).

To confirm that the fast freezing run in Step 5 (200°C/min to -150°C) damaged the membrane integrity of all the ovarian tissue cells in the sample, Steps 6 and 7 were repeated. No further decrease in the measured heat release (q_{final}) was found. A separate control experiment was also performed using ovarian tissue stored at +4°C for a week and whose cells had all lysed. Calorimetric experiments were performed using these lysed tissue slices as described above and $\Delta q_{dsc} (= q_{initial} - q_{final})$ was measured and found to be zero and the measured heat release was further found to be equal to q_{final} obtained in Step 7 of the DSC cooling protocol (± 0.3 mJ/mg of tissue). This small variation in the final heat release, q_{final} (~0.3 mJ/mg of tissue), was neglected as it represents < 4% of the measurement of interest in a typical DSC experiment, Δq_{dsc} (~7.5 mJ/mg of tissue). These results confirm the

assumption that the fast freezing in Step 5 (200°C/min to -150°C) lysed the membranes of all the cells in the sample.

The heat release measurements of interest are Δq_{dsc} and $\Delta q(T)_{dsc}$ that are the total and fractional difference between the heat releases measured by integration of the heat flows during freezing of osmotically active (live) cells in medium and during freezing of osmotically inactive (dead) cells in medium. This difference in heat release was related to cell volume changes by equation (2.1).

Note that the heat release readings of $\Delta q(T)_{dsc}$ and Δq_{dsc} are obtained separately at a freezing rate of 5°C/min for ovarian tissue cells that were cooled from 25° and 4°C at either 40°C/min or at 0.5°C/min in the three freezing media that were studied. The unknowns needed in Equation (3.3) apart from the DSC heat release readings are V_O (the initial or the isotonic cell volume) and V_b (the osmotically inactive cell volume). The Krogh model dimensions (see Fig. 3.1) or V_O were taken from previously published results for mammalian ovarian tissues (Rubin and Sutton, 1993; Stevens and Lowe, 1996) while the value of V_b was assumed to be $0.5V_O$. The effect of different assumed values of V_b was also studied, as described in the results.

3.3.3 Numerical Methods and Simulations

A nonlinear least squares curve fitting technique was implemented in a computer program to calculate the membrane permeability parameters (L_{pg} and E_{Lp}) that best fit the volumetric shrinkage data obtained from the DSC and the low temperature microscopy experiments as previously described (Bevington and Robinson, 1992). The computer program used a fourth order Runge-Kutta method to calculate the volume as a function of temperature (based on selected parameters and cooling conditions) and then compared the simulated water transport volumes to experimental data (Smith et al., 1998). The optimal fit of Eqn. (3.1) to the experimental data was obtained by selecting a set of parameters that minimized the residual variance, χ^2 , and maximized a goodness of fit parameter, R^2 (Smith

et al., 1998). All the curve fitting results presented have the goodness of fit parameter, R^2 , value being greater than or equal to 0.96 indicating that there was a good agreement between the experimental data points and the fit calculated using the estimated membrane permeability parameters. Note that an R^2 value of 1.0 indicates a perfect fit between the model and the data.

To simulate biophysical responses of tissue cooled at various rates, the best fit parameters were substituted in Eqn. (3.2) and the water transport equation (Eqns. 3.1 and 3.2) was numerically solved using a 4th order Runge-Kutta method with a temperature step of 0.1 °C using a FORTRAN code on a Powerbook G4 (Apple Computers, Cupertino, CA) workstation (He et al., 2004; Thirumala et al., 2005). The sensitivity of the model solution was tested by decreasing the temperature step to 0.01 °C and the simulation was repeated. This test had no effect on the results, thus confirming the convergence of our solution.

3.3.4 Theoretical Prediction of Optimal Cooling Rates

Once L_{pg} and E_{Lp} are determined using the fitting procedure described above, the optimal rates of freezing mare ovarian tissue cells could be obtained by Eqn. (2.4).

3.4 Results

The water transport data and simulation for ovarian tissue cells cooled at 5 °C/min are shown in Fig. 3.2. The filled (•) and open (o) circles represent the dynamic DSC water transport data for cells that were cooled from 25° to 4°C at 0.5°C/min or at 40°C/min, respectively. The dynamic portion of the cooling curve is between -0.53 °C to ~-8 °C in the absence of CPAs (Fig. 3.2A) and between -2.1°C and -12°C in the presence of glycerol (Fig. 3.2B) and in the presence of DMSO (Fig. 3.2C). The differences in the water transport response obtained for cells that were cooled from 25° to 4°C at 0.5°C/min or at 40°C/min are statistically significant (confidence level > 99% using Student's t-test) in the medium containing no CPA (Fig. 3.2A) and in the medium containing DMSO (Fig. 3.2C) while the differences are only significant at a lower confidence level of 95% in the medium containing glycerol (Fig. 3.2B). No differences were found among the measured water transport responses of ovarian tissue from seven mares (confidence level > 99%). The best fit

parameters of water transport for ovarian tissue sections in the absence and presence of CPAs are listed in Table 3.2. The volumetric responses generated by these parameters in Eqn. (3.1) are shown in Fig. 3.2 as solid lines (——). The volumetric response of cells cooled infinitely slowly (equilibrium cooling) is also shown for reference as a dashed line (- - - -) in all the figures.

Table 3.2 Membrane Permeability Parameters for Mare Ovarian Tissue ($V_b = 0.5V_0$): A tabulated comparison of the membrane permeability parameters obtained using the DSC water transport data at 5 °C/min in the presence and absence of CPAs.

<i>Freezing Media</i>	<i>Cooling Rate Between 25 °C and 4 °C (°C/min)</i>	$L_{pg}[cpa]$ ($\mu\text{m}/\text{min-atm}$)	$E_{Lp}[cpa]$ (Kcal/mole)	B_{opt}^{**} (°C/min)
No CPA	0.5	0.73	20.5	65.0
	40	0.61	53.2	8.2
0.85 M Glycerol	0.5	0.06	6.1	11.9
	40	0.05	8.2	8.8
0.85 M DMSO	0.5	0.07	9.1	11.8
	40	0.04	12.2	5.7

*Obtained using Eqn. (3.4) and a SA to WV ratio of $\sim 0.275 \mu\text{m}^{-1}$, based on the Krogh model dimensions and the assumed value of V_b .

By incorporating the best fit parameters of water transport in Eqn. (3.4), the theoretically predicted values for optimal rate of freezing mare ovarian tissue sections were obtained and are listed in Table 3.2. To independently verify the predicted rates of optimal freezing mare ovarian tissue, additional numerical simulations were also performed at various cooling rates (5 to 100°C/min) using a Krogh cylinder model and the best fit parameters in Eqn. (3.1). The results from the numerical simulations for cells that were cooled at 0.5°C/min and at 40°C/min from 25° to 4°C in the absence of CPAs are shown in Figs. 3.3 and 3.4, respectively. Similar figures were also obtained in the presence of CPAs but in the interest of brevity are not presented here. In both figures (Figs. 3.3 and 3.4), two different variables are graphed as a

function of temperature: 1) lower part: the nondimensional cellular volume (V/V_0), which decreases due to dehydration during freezing, and 2) upper part: the nondimensional radius of the extracellular space (r_V/r_{V0}), which expands during freezing. The Krogh model simulations in Fig. 3.3 show that ovarian tissue sections that are cooled at $0.5^\circ\text{C}/\text{min}$ from 25° to 4°C in the absence of CPAs are essentially dehydrated for freezing rates $< 60^\circ\text{C}/\text{min}$. At freezing rates $> 60^\circ\text{C}/\text{min}$, the amount of water trapped inside the tissue cells increases rapidly with increasing cooling rate. Similarly, the Krogh model simulations in Fig. 3.4 show that the ovarian tissue sections that are cooled at $40^\circ\text{C}/\text{min}$ from 25° to 4°C in the absence of CPAs are essentially dehydrated for freezing rates $< 10^\circ\text{C}/\text{min}$. At freezing rates $> 10^\circ\text{C}/\text{min}$, the amount of water trapped inside the tissue cells increases rapidly with increasing cooling rate. These observations lend further support to the predicted rates of optimal cryopreservation obtained earlier using Eqn. (3.2) and shown in Table 3.2.

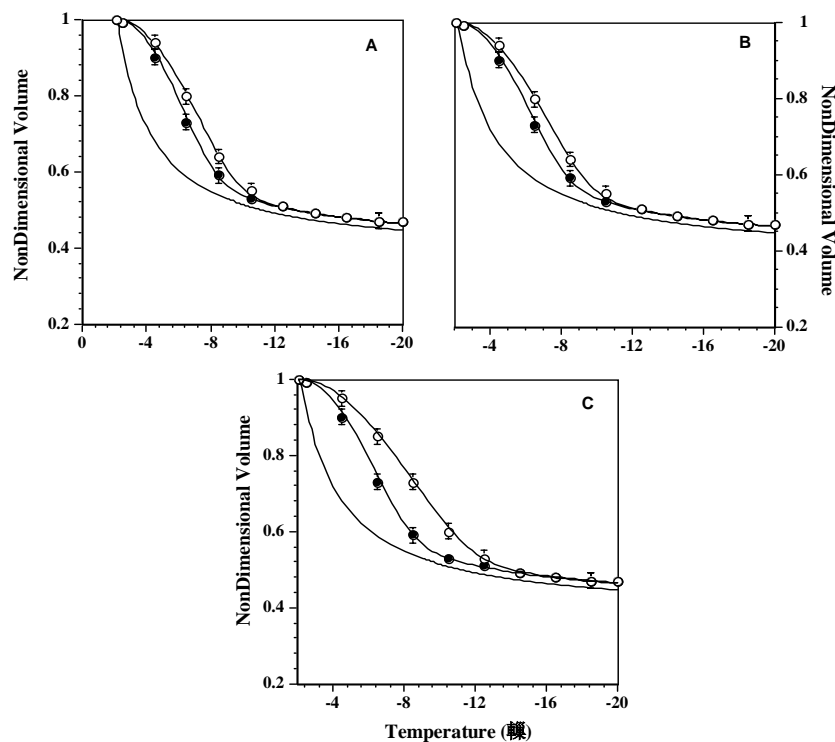


Figure 3.2 Volumetric response of the ovarian tissue as a function of subzero temperatures using the DSC technique, at a freezing rate of $5^\circ\text{C}/\text{min}$.

The water transport data from the ovarian tissue cooled at $0.5^\circ\text{C}/\text{min}$ between 25° to 4°C and at $40^\circ\text{C}/\text{min}$ between 25° to 4°C are shown as filled (\bullet) and open (\circ) circles, respectively.

Figs. 3.2A, 3.2B and 3.2C show the water transport response obtained in the absence of CPAs, in the presence of 0.85 M glycerol and in the presence of 0.85 M DMSO, respectively. The Krogh model simulated response using the predicted best fit membrane permeability parameters in Eqns. (3.1) and (3.2) are also shown (—). The Krogh model simulated equilibrium cooling response obtained assuming $V_b = 0.5V_0$ and $dV/dT = 0$ in Eqn. (3.1), is shown as a dashed line (- - - -). The nondimensional volume is plotted along the y-axis and the subzero temperatures are shown along the x-axis. The error bars represent the standard deviations in the data ($n = 6$).

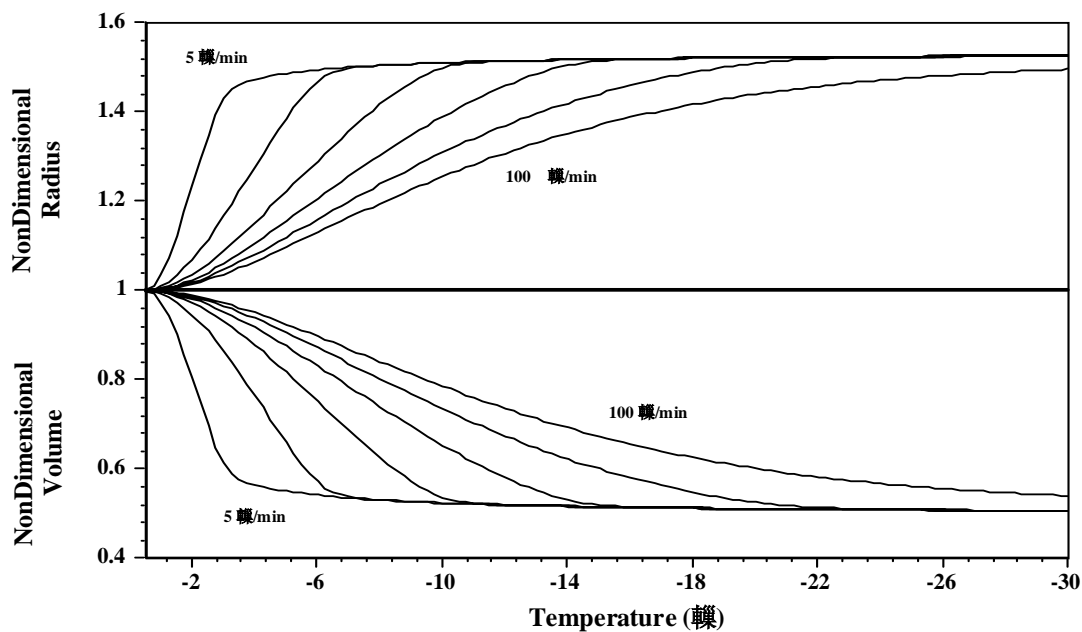


Figure 3.3 Krogh model: Volumetric response of the ovarian tissue at various freezing rates as a function of subzero temperatures using the best fit membrane permeability parameters (see Table 3.2 – cooled at 0.5°C/min between 25° to 4°C and in the absence of CPAs). The subzero temperatures are shown along the x-axis.

Lower Graph: Changes in the normalized (nondimensional) volume of the Krogh model as a function of temperature for different cooling rates (5, 20, 40, 60, 80 and 100 °C/min). Krogh cell volume (—).

Upper Graph: Changes in the normalized (nondimensional) radius of the extracellular space (r_v/r_{v0}) of the vasculature in the Krogh unit as a function of temperature for different cooling rates (5, 20, 40, 60, 80 and 100 °C/min). The normalized radius of the extracellular space is also given as (—).

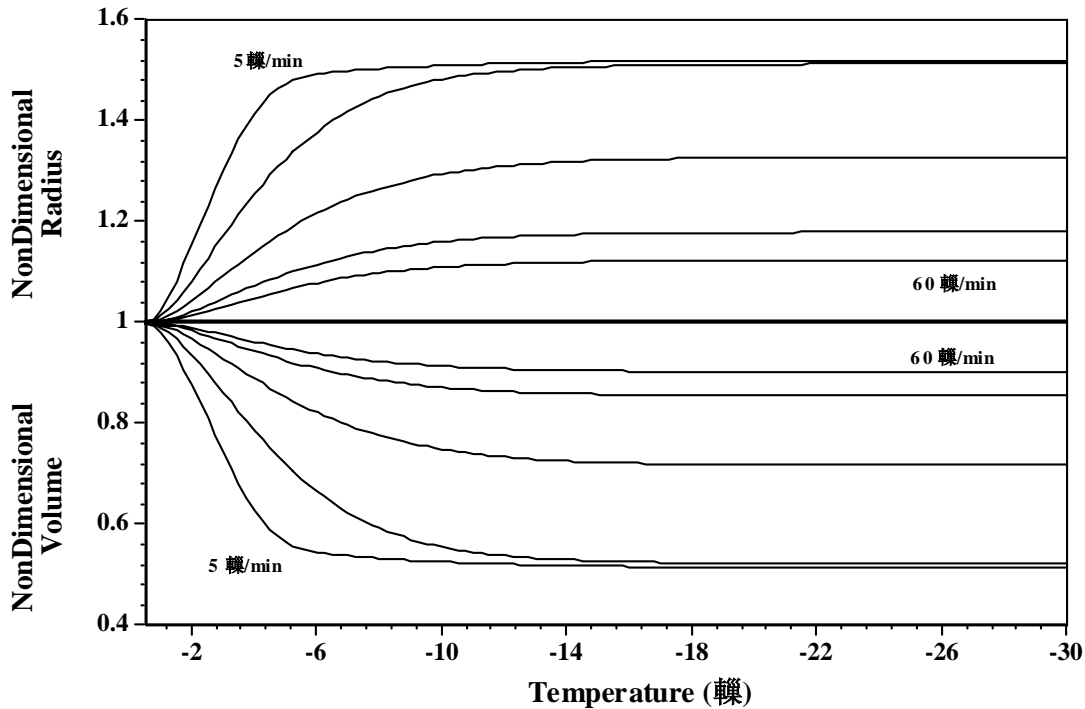


Figure 3.4 Krogh model: Volumetric response of the ovarian tissue at various freezing rates using the best fit membrane permeability parameters (see Table 3.2 – cooled at 40°C/min between 25° to 4°C and in the absence of CPAs). The subzero temperatures are shown along the x-axis.

Lower Graph: Changes in the normalized (nondimensional) volume of the Krogh model as a function of temperature for different cooling rates (5, 10, 20, 40, and 60 °C/min). Krogh cell volume (———).

Upper Graph: Changes in the normalized (nondimensional) radius of the extracellular space (r_v/r_{v0}) of the vasculature in the Krogh unit as a function of temperature for different cooling rates (5, 10, 20, 40, and 60 °C/min). The normalized radius of the extracellular space is also given as (———).

To study the effect of varying the osmotically inactive cell volume on the predicted membrane permeability parameters (L_{pg} and E_{Lp}), the value of V_b was varied from $0.75V_0$ to $0.25V_0$ (i.e. a 50% variation in the assumed value of $0.5V_0$). The DSC data were correspondingly modified (using Eqn. 3.3) and the modified DSC water transport data were fitted to the water transport model (Eqns. 3.1 and 3.2) by use of a nonlinear least squares

curve fitting technique as previously described. The parameters obtained with the new values of V_b are shown in Table 3.3 (for water transport data obtained in the absence of CPAs). Note that the predicted values of the reference membrane permeability parameters (L_{pg}) with assumed values of $0.75V_0$ or $0.25V_0$ (parameters in Table 3.3) as the osmotically inactive cell volume were significantly different from the values obtained with an assumed osmotically inactive cell volume of $0.5V_0$ (parameters in Table 3.2). This variation in the value of L_{pg} is in direct contrast to the behavior of E_{Lp} , which remains essentially unchanged ($\pm 10\%$) when V_b is varied from $0.5V_0$ to either $0.75V_0$ or $0.25V_0$. However, the predicted rates of optimal freezing are essentially unchanged ($\pm 10\%$) when the assumed value of V_b is varied by a factor of 2 (see Tables 3.2 and 3.3). A similar lack of sensitivity of the predicted optimal rates of freezing mare ovarian tissue cells to the assumed value of the osmotically inactive cell volume has been found in the presence of glycerol and DMSO (data not shown). As an independent assessment of the predicted rates of optimal freezing (shown in Table 3.3), a separate set of numerical simulations was also performed with the predicted best fit permeability parameters obtained with the assumed values of $0.75V_0$ and $0.25V_0$ as V_b (data not shown). An analysis of these simulations showed that the ovarian tissue cells are essentially dehydrated (or trap intracellular water) in a similar fashion as observed earlier with an osmotically inactive cell volume of $0.5V_0$ (Figs. 3.3 and 3.4). Thus, errors in the assumed value of V_b do alter the model predicted membrane permeability parameters (shown in Table 3.1) but the trends (and the predicted optimal rates of freezing) remain essentially unaltered. This insensitivity of the predicted optimal rate of freezing to the assumed value of V_b has also been previously noted in rat liver tissue (Devireddy and Bischof, 1998) and for sperm cells of various species (Devireddy et al., 2002c; Devireddy et al., 2004; He et al., 2004; Pinisetty et al., 2005).

And finally to complete our analysis on the effect of suprazero cooling conditions on the measured membrane permeability parameters of mare ovarian tissue, we show in Fig. 3.5 a

contour plot of the goodness of fit parameter, R^2 in the L_{pg} and E_{Lp} space that “fit” the DSC water transport data at both the suprazero cooling conditions studied (in the absence of any CPAs). Any combination of L_{pg} and E_{Lp} shown to be within the contour will “fit” the water transport data at the corresponding suprazero cooling condition with an R^2 value ≥ 0.98 . The predicted best fit parameters are denoted either by an asterisk (*) or a pound (#) sign and fall within both the contours (Table 3.2). Note that there is no overlapping portion in the contour (parametric space) suggesting that there is no “common” range of parameters between cells that were cooled at $0.5^\circ\text{C}/\text{min}$ or at $40^\circ\text{C}/\text{min}$ from 25° to 4°C when frozen in the absence of CPAs. Similarly, in the presence of either glycerol or DMSO, we did not find a “common” range of parameters that can predict the measured water transport response at both the suprazero cooling conditions studied (data not shown, in the interest of brevity).

Table 3.3 Membrane Permeability Parameters for Mare Ovarian Tissue (in the absence of CPAs): A tabulated comparison of the membrane permeability parameters obtained using the DSC water transport data at $5^\circ\text{C}/\text{min}$ with different assumed values of V_b .

<i>Osmotically Inactive Cell Volume</i>	<i>Cooling Rate Between 25°C and 4°C ($^\circ\text{C}/\text{min}$)</i>	<i>$L_{pg}[\text{cpa}]$ ($\mu\text{m}/\text{min-atm}$)</i>	<i>$E_{Lp}[\text{cpa}]$ (Kcal/mole)</i>	<i>B_{opt} ($^\circ\text{C}/\text{min}$)</i>
0.75 V_o	0.5	0.36	19.3	68.3*
	40	0.31	53.1	8.6*
0.5 V_o	0.5	0.73	20.5	65.0**
	40	0.61	53.2	8.2**
0.25 V_o	0.5	1.1	19.1	68.5****
	40	0.94	55.3	7.8****

*Obtained using Eqn. (3.4). The ratio of SA to WV is $\sim 0.55 \mu\text{m}^{-1}$.

**Obtained using Eqn. (3.4). The ratio of SA to WV is $\sim 0.275 \mu\text{m}^{-1}$.

***Obtained using Eqn. (3.4). The ratio of SA to WV is $\sim 0.18 \mu\text{m}^{-1}$.

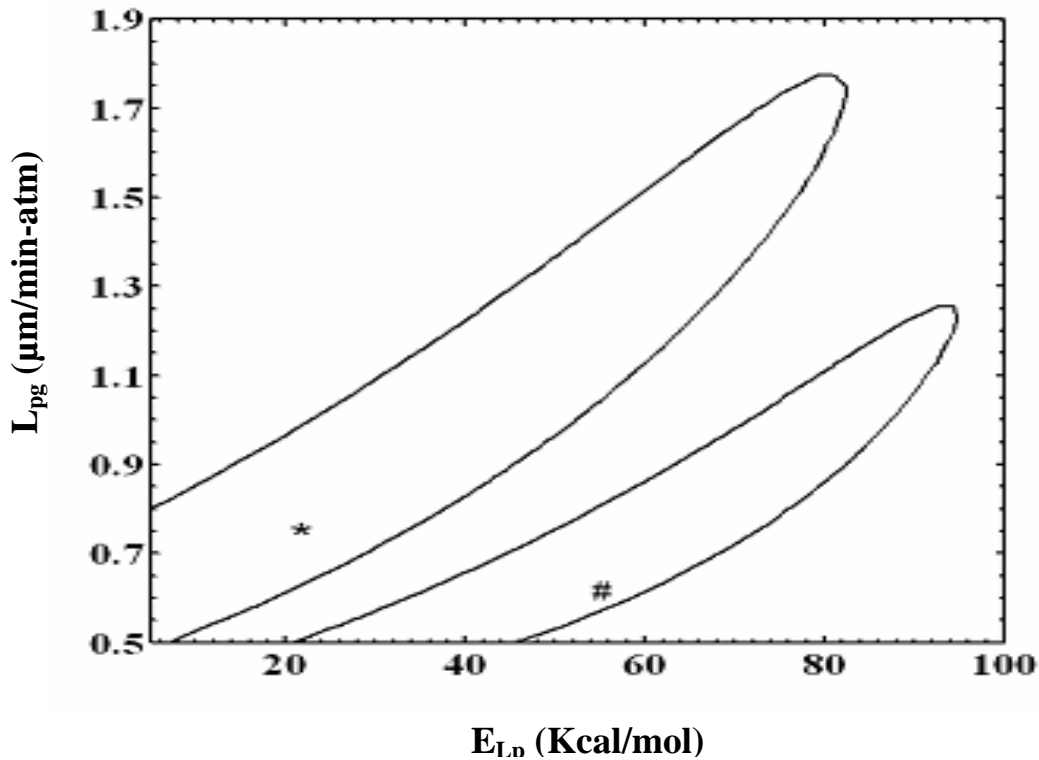


Figure 3.5 Contour plots of the goodness of fit parameter R^2 ($= 0.98$) for the parametric space in ovarian tissue that is cooled at either $0.5^\circ\text{C}/\text{min}$ or at $40^\circ\text{C}/\text{min}$ from 25° to 4°C in the absence of CPAs (assuming $V_b = 0.5V_0$).

The predicted best fit parameters for both the suprazero cooling conditions are shown as (*) and (#) within the respective contours (see Table 3.1 for the numerical values). There is no “common” region between the contours suggesting that there is not any combination of water transport parameters that ‘fit’ the water transport data at both the suprazero cooling conditions studied ($0.5^\circ\text{C}/\text{min}$ and $40^\circ\text{C}/\text{min}$ between 25° to 4°C). The membrane permeability at 0°C , L_{pg} ($\mu\text{m}/\text{min-atm}$) is plotted on the y-axis while the apparent activation energy of the membrane, E_{Lp} (kcal/mole) is plotted on the x-axis.

3.5 Discussion

The primary conclusions from the present study are: (a) the rate of cooling from 25° to 4°C has a significant impact on the subzero water transport response (and consequently, the subzero water permeability parameters L_{pg} and E_{Lp}) of mare ovarian tissues; (b) ovarian tissues cooled at $40^\circ\text{C}/\text{min}$ from 25° to 4°C have a lower value of reference membrane

permeability L_{pg} than those cooled at $0.5^{\circ}\text{C}/\text{min}$; (c) ovarian tissues cooled at $40^{\circ}\text{C}/\text{min}$ from 25° to 4°C have a higher value of reference activation energy E_{Lp} than those cooled at $0.5^{\circ}\text{C}/\text{min}$; (d) the predicted optimal rates of freezing are higher for ovarian tissues cooled at $0.5^{\circ}\text{C}/\text{min}$ from 25° to 4°C than those cooled at $40^{\circ}\text{C}/\text{min}$; (e) the addition of 0.85 M glycerol or DMSO lowers the predicted values of L_{pg} and E_{Lp} considerably for ovarian tissues cooled at either $40^{\circ}\text{C}/\text{min}$ or $0.5^{\circ}\text{C}/\text{min}$ between 25° and 4°C ; (f) the optimal rate of freezing ovarian tissues in the presence of 0.85 M glycerol or 0.85 M DMSO are considerably lower ($>80\%$) than in their absence for tissues cooled at $0.5^{\circ}\text{C}/\text{min}$ between 25° and 4°C ; (g) the optimal rate of freezing ovarian tissues in the presence of 0.85 M glycerol are essentially unchanged ($\pm 10\%$) than in its absence for tissues cooled at $0.5^{\circ}\text{C}/\text{min}$ between 25° and 4°C ; and (h) the predicted rates of optimal freezing obtained using Eqn. (3.4) are comparable to those predicted by a detailed analysis of water transport simulations at a range of freezing rates. Further discussion of these observations and others is provided below.

The measured water transport response for ovarian tissue in the presence and absence of CPAs are significantly different between tissues that were cooled at $0.5^{\circ}\text{C}/\text{min}$ from 25° to 4°C and those that were cooled at $40^{\circ}\text{C}/\text{min}$ between 25° and 4°C , as shown in Fig. 3.2. Also as shown in Table 3.2, the L_{pg} value obtained for ovarian tissue cells cooled at $0.5^{\circ}\text{C}/\text{min}$ from 25° to 4°C are uniformly higher than those obtained for ovarian tissue cells cooled at $40^{\circ}\text{C}/\text{min}$ from 25° to 4°C (both in the presence and absence of CPAs) while the converse is true for the values of E_{Lp} . Taken together these facts suggest an alteration to the ovarian tissue membrane that produces a reduction in the permeability of cell membrane to water, when the ovarian tissues are cooled at $40^{\circ}\text{C}/\text{min}$ from 25° to 4°C . A similar “reduction in the ability of the water to permeate the cell membrane” for an imposed chemical potential difference was also found for equine sperm cells as a function of suprazero cooling conditions (Devireddy et al., 2002c).

As shown in Fig. 3.2 and Table 3.2, our experiments demonstrate that the suprazero cooling conditions effect the predicted membrane permeability parameters of mare ovarian tissue at subzero temperatures. Our observations are consistent with previous experiments by

other investigators who have also shown that suprazero cooling conditions can be related to phase transitions, such as an inverted hexagonal II phase, in the plasma membrane which further correlate to changes in the membrane permeability to ions such as K^+ and Ca^{++} (Blok et al., 1976; Watson, 1981; Quinn, 1985; Caffrey, 1987; Vincent and Johnson, 1992; Drobnis et al., 1993). Changes in the membrane permeability to water caused by suprazero cooling conditions, as shown in our experiments, are also consistent with perturbation of the membrane structure (Wilmot et al., 1975; Steponkus, 1984; Morris, 1987; Pickering et al., 1990; Parks and Lynch, 1992; Parks and Ruffing, 1992; Almeida and Bolton, 1995; Bernard and Fuller, 1996; Eroglu et al., 1998; Zenzes et al., 2001). Thus, the effect of suprazero cooling conditions on the measured water transport response and the predicted permeability parameters appears to be an important variable in ovarian tissue preservation. Future experiments will focus on investigating this phenomenon in other ovarian tissue types (primate and non-primates) and in mare ovarian tissue collected when the animals are in the breeding season. Preliminary experiments with ovarian tissues from *Macaca mulatta* (a non-human primate) suggest a similar response to suprazero cooling conditions to that observed in mare ovarian tissue. Additionally experiments using either Fourier transform infrared (FTIR) spectroscopy or electron microscopy (EM) techniques should also be conducted to study the temperature at which this transition in ovarian tissue cells occurs. Based on previous experience with sperm cells, it is expected that this temperature is in the range of $+8^\circ$ to $+20^\circ C$.

As shown in Table 3.2, for a given suprazero cooling condition, the addition of CPAs (glycerol or DMSO) lowers the value of both L_{pg} (by a factor of ~ 10) and E_{Lp} (by a factor of 2 to 8). The lowering in the value of L_{pg} indicates a “alteration” of the membrane, i.e. the ability of water to permeate through the membrane is lowered, while the lowering of E_{Lp} suggests that the loss of intracellular water continues at lower subzero temperatures, i.e. the temperature range within which the phenomenon of water transport can occur is increased in the presence of CPAs. Thus, a lowering in the value of L_{pg} can be compensated by a lowering in the value of E_{Lp} . However, as noted earlier, the lowering in the value of L_{pg} due

to the addition of CPAs is much larger than the lowering in the value of E_{Lp} . Thus, the net effect is to reduce the predicted rate of optimal freezing in the presence of CPAs when compared with the values obtained in their absence. This result is counter-intuitive as the addition of CPAs is usually found to increase the optimal rate of freezing rather than decreasing it. However, equine sperm cells (Devireddy et al. 2002c) and more recently sperm cells from aquatic organisms (Thirumala et al. 2005; Pinisetty et al., 2005) were found to exhibit a similar behavior in the presence of CPAs, i.e. an increase in the predicted rate of optimal freezing in the absence of CPAs than in their presence. It is also clear from the data shown in Figs. 3.2B and 3.2C that the differences in the measured water transport data between the two suprazero cooling conditions studied are smaller in the presence of glycerol (Fig. 3.2B) than in the presence of DMSO (Fig. 3.2C). It is as yet unclear if, a) this is a unique effect of glycerol on mare ovarian tissue or a general characteristic for all mammalian ovarian tissue and b) if varying the concentrations of glycerol and DMSO from the 0.85 M used in the present study will “enhance” or “reduce” the differences in the measured water transport data for different suprazero cooling conditions. Clearly, further studies are necessary to delineate the effect of CPAs on cell membrane transport and structural properties (Pinisetty, 2005).

Permeability to water and its activation energy are among the principal determinants of the response of all types of cells to freezing and thawing (Mazur 1963; Mazur et al., 1972; Leibo, 1980). Although coefficients of water permeability at subzero temperatures have not yet been reported for ovarian tissue (this being the first such study), these parameters have been reported in the literature for human ovarian tissues at suprazero temperatures (Newton et al., 1998; Devireddy, 2005) and oocytes from various species at suprazero and subzero temperatures (Leibo 1980; Myers et al., 1987; Hunter et al., 1992; Ruffing et al., 1993; Le Gal et al., 1995; McGrath et al., 1995; Younis et al., 1996; Paynter et al., 2001; Songsasen et al., 2002a). In general, the permeability parameters obtained in the present study for mare ovarian tissues are comparable to those obtained during freezing (i.e. in the presence of extracellular ice) of mammalian oocytes (see review by Critser et al., 1997). However, a comparison of suprazero mammalian oocyte membrane permeability parameters, i.e. those

obtained in the absence of extracellular ice and at suprazero temperature with the permeability parameters obtained in the present study show significant differences, especially in the presence of CPAs. The reference membrane permeability values obtained in the presence of extracellular ice (Table 3.2) are significantly lower (by a factor of 10 to 100) than those obtained in the absence of extracellular ice. The opposite effect is seen for the predicted values of activation energies, i.e. the activation energy obtained in the presence of extracellular ice is significantly higher (by a factor of 2 to 3) than those obtained in its absence. These observations are comparable to those obtained for sperm cells of various species (Devireddy et al., 2002c; Devireddy et al., 2004; He et al., 2004; Thirumala et al., 2005) and such observations suggest that the ovarian tissue membrane permeability parameters are also significantly effected by the presence of extracellular ice. Clearly, further studies are needed to understand the effect of suprazero cooling conditions on the subzero water transport properties of mammalian and non-mammalian ovarian tissues.

3.6 Conclusion

This study presents the first measured changes in the water transport response of mare ovarian tissues due to variations in suprazero cooling conditions. Significant changes were found to occur in the mare ovarian tissue plasma membrane due to the imposed suprazero cooling conditions. It is well known that adverse suprazero cooling is detrimental to the function of ovarian tissue, although an effect on membrane permeability to water during freezing had not been previously demonstrated. The results of this study suggest that suprazero cooling conditions do affect the water transport response of mare ovarian tissues and thereby potentially alter their response to an established cryopreservation protocol.

Chapter 4

Subzero Water Transport Characteristics and Optimal Rates of Freezing *Macaca Mulatta*(Rhesus Monkey) Ovarian Tissue

4.1 Introduction

Aggressive treatments of women of child-bearing age suffering from various malignant diseases have resulted in significant increases in long-term survival of such patients. However, the consequences of treatment are often premature ovarian failure and irreversible loss of fertility (Nicosia et al., 1985; Gradishar and Schilsky 1989; Howell, Shalet 1998; Meirou, 2000; Donnez et al., 2005). This has prompted innovative research to develop methods to cryopreserve mammalian ovarian cells and tissues, including those of mice (Parrott, 1960; Harp et al., 1994), marmosets (Candy et al., 1995), sheep (Baird et al., 1999; Aubard et al., 1994), bovines (Martino et al., 1996; Semple et al., 2000), primates (Schnorr et al., 2002; Lee et al., 2004), and humans (Gosden, 2000; Oktay and Karlikaya, 2000; Picton et al., 2000; Oktay et al., 2004; Sonzemer 2005; Lobo, 2005). The ultimate goal is to restore fertility of cancer survivors. Although it is well known that suprazero cooling conditions have a deleterious effect on the functionality and viability of mammalian reproductive cells (Parks and Ruffing, 1992; Vincent and Johnson, 1992; Zenzes et al., 2001; Songsasen et al., 2002a), there have been very few studies of the effect of suprazero cooling conditions on subzero water transport properties in mammalian reproductive cells or tissues. Non-human primates seem an especially relevant surrogate model for humans, since much is known about their folliculogenesis (Goodman, 1977) and radiation- and chemo-therapeutic-induced ovarian failure (Ataya et al., 1995; Ataya et al., 1995). In the current study, we determined the effect of two suprazero cooling conditions on the subzero water transport characteristics of rhesus monkey (*Macaca mulatta*) ovarian tissue in the presence of extracellular ice and cryoprotective agents (CPAs). Our goal is to develop a mechanistic understanding of the freezing response in ovarian tissue, and to aid in the development of efficacious methods to cryopreserve ovarian tissue of humans.

Qualitative effects of freezing have been recorded in tissue systems using uncontrolled slow freezing and freeze-substitution techniques as early as the 1960s by Trump et al. and Love (1966) and more recently by Rubinsky et al. (1987). These studies showed that ice

forms initially in the extracellular or the vascular space. More recently, Pazhayannur and Bischof (1997) and Devireddy and Bischof (1998) developed two complementary and independent techniques to measure the dynamic water transport response of tissues during freezing. The first technique utilizes a combination of directional cooling and freeze-substitution (Devireddy et al., 1999) while the second technique is based on a differential scanning calorimeter (DSC) (Devireddy 1998). These techniques have been used to study water transport during freezing of normal rat liver (Pazhayannur and Bischof, 1997; Devireddy and Bischof, 1998), wood frog liver (Devireddy et al., 1999) on rat prostate tumor (Devireddy et al., 1999), on uterine fibroid tumor (Devireddy et al., 2001) and more recently in equine ovarian tissue (Devireddy et al., 2005).

In the present study, these techniques were used to measure the water transport processes in rhesus monkey ovarian tissue that was cooled from 25° to 4°C at 0.5°C/min or at 40°C/min. Water transport response during freezing of macaque ovarian tissue was measured at a freezing rate of 5°C/min by means of the calorimetric method. To distinguish between the rate of temperature change at suprazero and subzero temperatures, we will denote the former as “cooling rate” and the latter as “freezing rate”. The fitting of a model of water transport to the measured water transport response during freezing of ovarian tissue yielded the membrane permeability parameters (reference membrane permeability to water, L_{pg} and the activation energy, E_{Lp}). The experimentally determined membrane permeability parameters were then used to calculate theoretical optimal rates of freezing of macaque ovarian tissue.

The *Macaca mulatta* (rhesus monkey) ovarian tissue are chosen because their biologically close relationship to human. The theoretical background for this study is the same as that introduced in chapter 3.2.

4.2 Materials and Methods

4.2.1 Tissue Collection and Isolation

Water transport experiments were performed on excised macaque ovarian tissue from 12 adult female monkeys aged between 6 and 8 years that were euthanized at the Louisiana State University (LSU) Veterinary School (during the months of May and August in 2005). All ovarian tissue samples were excised from euthanized animals by trained veterinary surgeons.

The animals were euthanized for unrelated experiments and all protocols and handling procedures were approved by the Institutional Animal Care and Usage Committee (IACUC) at LSU. Upon excision, the tissue was placed in a petri dish with D-PBS solution (GIBCO BRL, Rockville, MD) and transported from the Veterinary School to the LSU Bioengineering Laboratory (a distance of less than a mile). As stated earlier, water transport experiments were carried out both in the absence and presence of CPAs. Experiments were conducted in the presence of three permeating CPAs (glycerol, dimethylsulfoxide or DMSO and ethylene glycol or EG) at 0.85 M. Stepwise addition of CPAs was performed at room temperature to minimize the osmotic injury or the volumetric excursions of the ovarian tissue during the CPA loading process (Hovatta et al., 1996; Newton et al., 1998). At room temperature of 25 °C a stock of 1.7 M CPA was added to ovarian tissue in 5 equal volume steps at 5 min intervals such that the final concentration of the CPA was 0.85 M. The equilibration time and the number of steps were chosen based on an analysis of the Kedem and Katchalsky equations (Kedem and Katchalsky, 1958) as described elsewhere (Devireddy, 2005). All water transport experiments were completed within 6 hours after excision of the ovaries.

4.2.2 Water Transport Experiments

Water transport experiments were performed on ovarian tissue using a Differential Scanning Calorimeter, DSC (DSC-7, Perkin Elmer corporation, Norwalk, CT). The tissue was cut into small pieces (1-1.5 mm³) using a razor blade. The tissue slices were then patted externally using a blotting paper and their weight was measured (1-1.5 mg). The samples were then placed in standard aluminum sample pans (Perkin Elmer Corporation, Norwalk, CT) and a small drop (< 8 µl) of freezing medium was added to keep the tissue slice hydrated. A natural ice nucleator *Pseudomonas syringae* (ATCC, Rockville, MD) was sprinkled (~0.1 mg) before the pans were sealed and reweighed. The ice nucleating agent *P. syringae* always nucleated the vascular/extracellular space at temperatures $\geq -4^{\circ}\text{C}$ in order to avoid damaging intracellular ice formation, which occurs predominantly at temperatures below -5°C in most cell systems (Toner, 1993). The total sample weight was always kept ≤ 10 mg.

The calorimetric protocol developed to measure water transport out of ovarian tissue is the same as the one detailed recently for equine ovarian tissue (Devireddy et al., 2005) and

earlier for a variety of tissue systems (Devireddy and Bischof, 1998; Devireddy et al., 1999a; Devireddy et al., 1999b; Devireddy et al. 2001; Devireddy et al., 2005). In the calorimetric method, the heat release measurements of interest are Δq_{dsc} and $\Delta q(T)_{dsc}$ that are the total and fractional difference between the heat releases measured by integration of the heat flows during freezing of osmotically active (live) cells in medium and during freezing of osmotically inactive (dead) cells in medium. This difference in heat release has been shown to be related to cell volume changes in several tissue systems (Devireddy and Bischof, 1998; Devireddy et al., 1999a; Devireddy et al., 1999b; Devireddy et al. 2001; Devireddy et al., 2005; Devireddy et al., 1998) as:

$$V(T) = V_o - \frac{\Delta q(T)_{dsc}}{\Delta q_{dsc}} \cdot (V_o - V_b). \quad (4.1)$$

Recently, this method to measure volume changes has been independently verified by Yuan and Diller (2005). Note that the heat release readings $\Delta q(T)_{dsc}$ and Δq_{dsc} are obtained separately at a freezing rate of 5°C/min in the four different freezing media (without CPAs, or with DMSO, or with glycerol or with EG) for ovarian tissue that was either cooled at 0.5°C/min or 40°C/min between 25° and 4°C. The unknowns needed in Equation (4.1) apart from the DSC heat release readings are V_o (the initial or the isotonic cell volume) and V_b (the osmotically inactive cell volume). The Krogh model dimensions (or V_o) were taken from previously published results for mammalian ovarian tissues (Hartman and Straus, 1961; Szebenyi, 1969; Berringer et al., 1968; Van and Simpson, 1973), as described earlier. The value of V_b was assumed to be 0.2 V_o , a value reported earlier for macaque oocytes (Songsasen et al., 2002b)

As stated above, the differential scanning calorimeter (DSC) experiments were conducted at a freezing rate of 5°C/min. Since the DSC cannot distinguish between the heat released due to dehydration (water transport) and intracellular ice formation (IIF), additional experiments were not performed at higher cooling rates (> 5 °C/min), where there is a strong possibility of IIF. To ensure the accuracy and repeatability of the experimental data, a set of calibration

and control experiments were also performed (Devireddy et al., 1998). These included a) calibration and minimization of the thermal lag; b) baseline determination of the thermogram (a sigmoidal baseline was used as described in the DSC-7 manual). In addition, the DSC technique is relatively insensitive to the baseline used since the heat releases are differences and not absolute values; c) energy conservation during freezing and thawing; d) error due to condensation effects; e) effect of *P. syringae* on DSC heat release readings; f) experiments with osmotically inactive (lysed) tissues ($\Delta q_{dsc} = 0$) and g) error due to noise in the DSC readings ($< 1\%$ of Δq_{dsc}). In summary the total error in the measured cellular heat release reading is estimated at $< 5\%$ of Δq_{dsc} or the measured heat release (proportional to tissue water transport).

4.2.3 Numerical Simulations and Optimal Cooling Rates

The numerical methods and simulations used to calculate the best-fit membrane permeability parameters (L_{pg} and E_{Lp}) and to simulate biophysical response of tissue under a variety of cooling rates is the same as introduced in 2.2.7. Once the cell level parameters L_{pg} and E_{Lp} are determined, the optimal cooling rates could be obtained by equation (2.4).

4.3 Results

The water transport data and simulation for macaque ovarian tissue frozen at $5^\circ\text{C}/\text{min}$ are shown in Fig. 4.1 and Fig. 4.2. Fig. 4.1 shows the measured water transport data obtained in the absence of CPAs while Figs. 4.2A, 4.2B and 4.2C show the water transport response in the presence of 0.85 M DMSO, glycerol or EG, respectively. In all the figures, the open (o) and filled (•) circles represent the dynamic DSC water transport data for cells that were cooled at $0.5^\circ\text{C}/\text{min}$ or at $40^\circ\text{C}/\text{min}$ from 25° to 4°C , respectively. The dynamic portion of the cooling curve is between -0.53° to $\sim -8^\circ\text{C}$ in the absence of CPAs (Fig. 4.1) and is between -2.1° and $\sim -18^\circ\text{C}$ in the presence of CPAs (Figs. 4.2A-4.2C). The best fit parameters of water transport obtained by fitting Eqn. (2.2) to the experimentally determined water transport data for rhesus monkey ovarian tissue sections are shown in Table 4.1. The volumetric response generated by these parameters in Eqn.(2.2) are shown in Figs. 4.1 and

4.2, as solid lines (————). The response of cells cooled infinitely slowly (equilibrium cooling) as predicted by the model is also shown in both figures as a dashed line (- - - -).

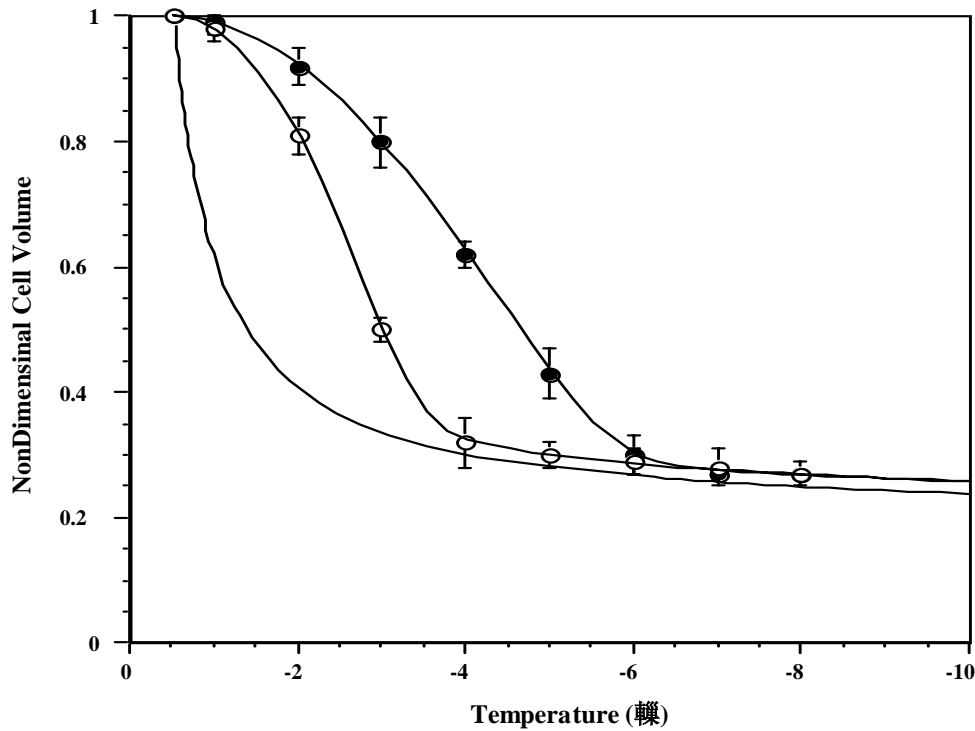


Figure 4.1 Volumetric response of ovarian tissue as a function of subzero temperatures using the DSC technique, at a freezing rate of 5°C/min and in the absence of CPAs.

The water transport data from the ovarian tissue cooled at 0.5°C/min or at 40°C/min between 25° and 4°C are shown as open (○) and filled (●) circles, respectively. The Krogh model simulated response, using the predicted best fit membrane permeability parameters in Eqns. (2.2) and (2.3) are also shown (————). The Krogh model simulated equilibrium cooling response, obtained assuming $V_b = 0.2V_0$ and $dV/dT = 0$ in Eqn. (2.2), is shown as a dashed line (- - - -). The nondimensional volume is plotted along the y-axis and the subzero temperatures are shown along the x-axis. The error bars represent the standard deviations in the data ($n = 10$).

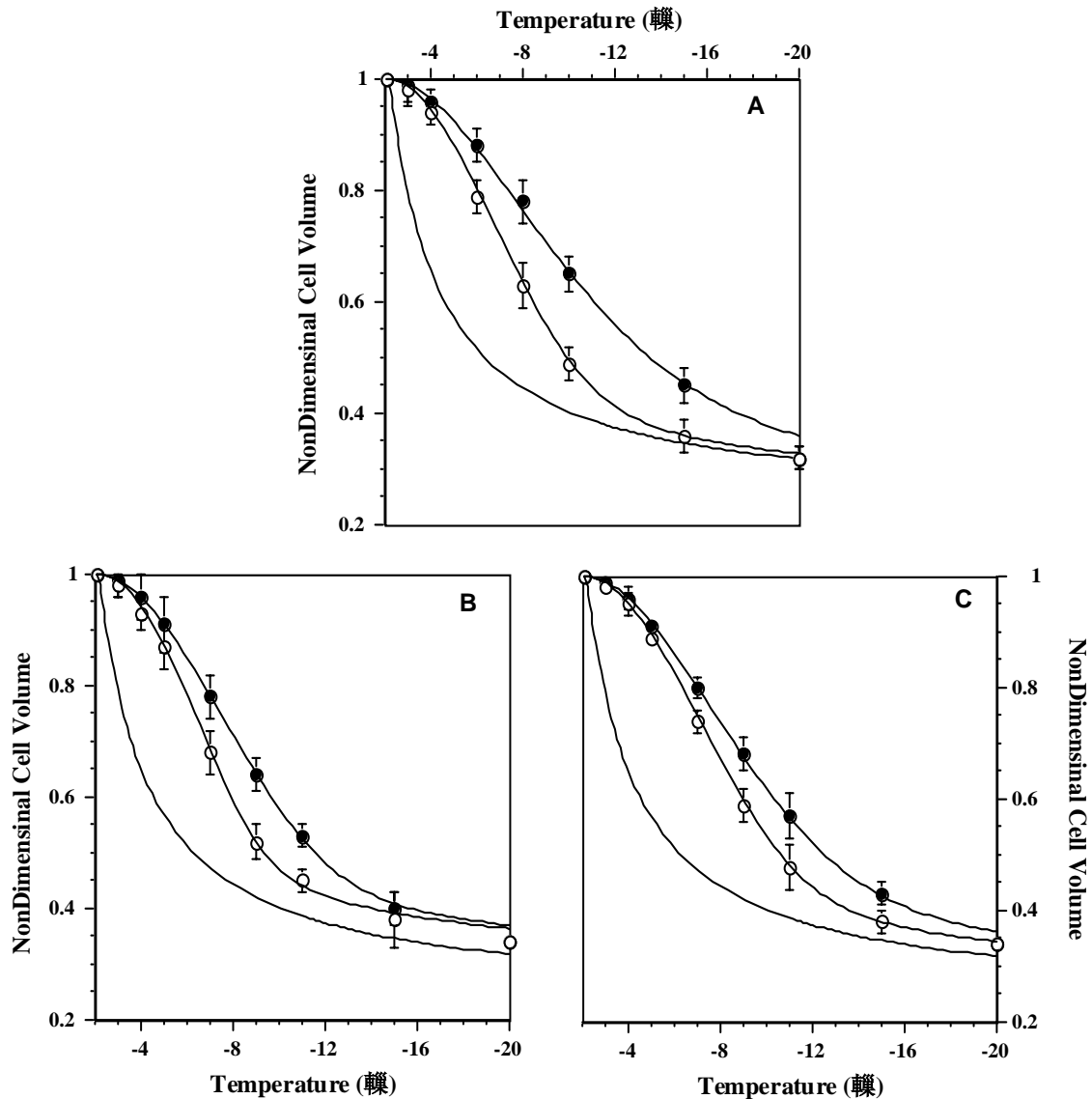


Figure 4.2 Volumetric response of the ovarian tissue as a function of subzero temperatures using the DSC technique at 5 °C/min in the presence of 0.85 M DMSO (2A), 0.85 glycerol (2B) or 0.85 M EG (2C).

In all the figures, the water transport data from the ovarian tissue cooled at 0.5°C/min or at 40°C/min between 25° and 4°C are shown as open (○) and filled (●) circles, respectively. The Krogh model simulated response using the predicted best fit membrane permeability parameters in Eqns. (2.2) and (2.3) are also shown (—). The Krogh model simulated equilibrium cooling response, obtained assuming $V_b = 0.2V_0$ and $dV/dT = 0$ in Eqn. (2.2), is shown as a dashed line (- - - -). The nondimensional volume is plotted along the y-axis and the subzero temperatures are shown in the x-axis. The error bars represent the standard deviations in the data (n = 10).

The theoretically predicted optimal rates of cryopreservation values for freezing macaque ovarian tissue were obtained using Eqn. (2.4) and are also shown in Table 4.1. To further corroborate the predicted rates of optimal freezing for ovarian tissue, additional numerical simulations were also performed at various cooling rates (5–100 °C/min) using a Krogh cylinder model and the best fit parameters in Eqn. (2.2). The results from the numerical simulations for the macaque ovarian tissue cooled at either 0.5°C/min or 40°C/min from 25° to 4°C in the presence of 0.85 M glycerol are shown in Figs. 4.3 and 4.4, respectively. Similar figures were also obtained in the absence of CPAs, in the presence of DMSO and EG but are not presented here in the interest of brevity. In Figs. 4.3 and 4.4, two variables are graphed as a function of temperature: 1) lower part: the nondimensional cellular volume (V/V_0), which decreases due to dehydration during freezing, and 2) upper part: the nondimensional radius of the extracellular space (r_V/r_{V0}), which expands during freezing. The Krogh model simulations in Fig. 4.3 show that ovarian tissue sections equilibrated with 0.85 M glycerol and cooled at 0.5°C/min from 25° to 4°C are essentially completely dehydrated at freezing rates $< 9^\circ\text{C}/\text{min}$. At freezing rates $> 9^\circ\text{C}/\text{min}$, the amount of water trapped inside the tissue increases rapidly with increasing cooling rate. Similarly, the Krogh model simulations in Fig. 4.4 show that the ovarian tissue sections equilibrated with 0.85 M glycerol and cooled at 40°C/min from 25° to 4°C, are completely dehydrated for freezing rates $< 6^\circ\text{C}/\text{min}$. At freezing rates $> 6^\circ\text{C}/\text{min}$, the amount of water trapped inside the tissue increases rapidly with increasing cooling rate. These observations lend further support to the predicted rates for optimal cryopreservation obtained earlier using Eqn. (2.4) and shown in Table 4.1.

To study the effect of varying the osmotically inactive cell volume on the predicted membrane permeability parameters (L_{pg} and E_{Lp}), the value of V_b was varied from $0.1V_0$ to $0.4V_0$ (i.e. the assumed value of $0.2V_0$ was doubled and halved). The DSC data were correspondingly modified (using Eqn. 2.1) and the modified DSC water transport data were fitted to the water transport model (Eqns. 2.2 and 2.3) by use of the nonlinear least squares fitting technique as previously described. The parameters obtained with the new values of V_b are shown in Tables 4.2 and 4.3. Note that the predicted values of the reference membrane

permeability parameters (L_{pg}) using $0.1V_O$ and $0.4V_O$ (parameters in Tables 4.2 and 4.3) as the osmotically inactive cell volume are significantly different from the values obtained when the osmotically inactive cell volume is assumed to be $0.2V_O$ (parameters in Table 4.1). This variation in the value of L_{pg} is in direct contrast to the behavior of E_{Lp} , which remains essentially unchanged ($\pm 10\%$) when V_b is varied from $0.2V_O$ to either $0.1V_O$ or $0.4V_O$. However, and more importantly, the predicted rates of optimal freezing are essentially unchanged ($\pm 10\%$) when the assumed value of V_b is varied by a factor of 2 (see Tables 4.1, 4.2 and 4.3). A similar lack of sensitivity of the optimal rates of freezing to the value of the osmotically inactive cell volume has been previously noted in rat liver tissue (Montgomery and Runger, 1994), Dunning AT-1 rat prostate tumor tissue (Thirumala and Devireddy, 2005), equine ovarian tissue (Devireddy et al., 2005) and also in spermatozoa from various species (Paynter et al., 2005; Younis et al., 1996; Leibo, 1986; Critser et al., 1997). A separate set of numerical simulations were also performed with the predicted best fit permeability parameters obtained with $0.1V_O$ and $0.4V_O$ as the assumed value of V_b (data not shown) for the eight conditions studied. Analysis of these simulations showed that the ovarian tissue is essentially dehydrated (or trap intracellular water) in a similar fashion as observed earlier with an osmotically inactive cell volume of $0.2V_O$ (Figs. 4.3 and 4.4). Thus, errors in the assumed value of V_b do alter the model predicted membrane permeability parameters (shown in Table 4.1) but the predicted optimal rates of freezing remain essentially unaltered.

The data in Figs. 4.5 and 4.6 show a contour plot of the goodness of fit parameter, R^2 , in the L_{pg} and E_{Lp} space that “fit” the DSC water transport data at both the suprazero cooling conditions studied, in the absence of CPAs (Fig. 4.5) and in the presence of CPAs (Figs. 4.6B–4.6C). Any combination of L_{pg} and E_{Lp} shown to be within the contour will “fit” the water transport data at that cooling rate with an R^2 value ≥ 0.96 .

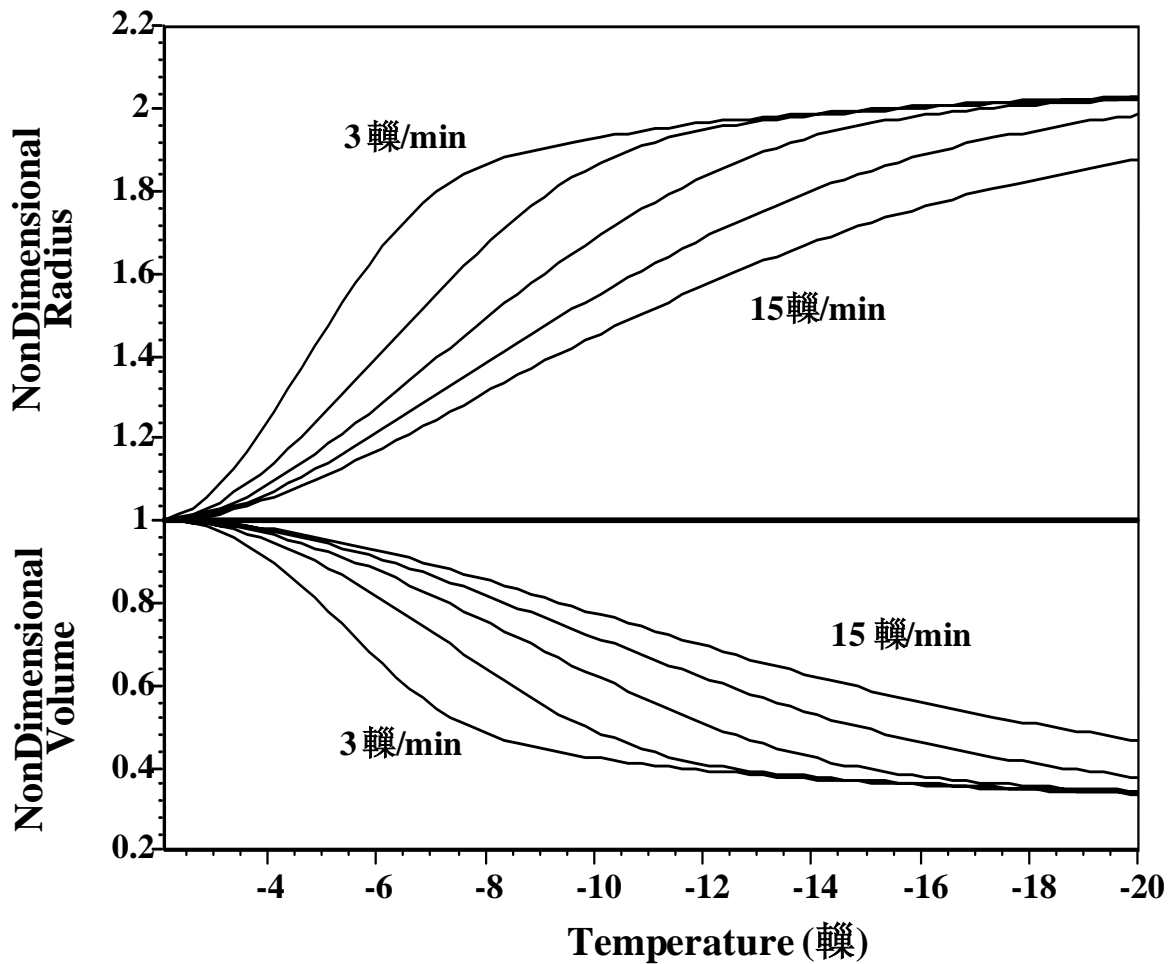


Figure 4.3 Krogh model: Volumetric response of the ovarian tissue at various freezing rates as a function of subzero temperatures using the best fit membrane permeability parameters (see Table 4.1– cooled at 0.5°C/min from 25 to 4°C in the presence of 0.85 M glycerol). The subzero temperatures are shown along the x-axis.

Lower Graph: Changes in the normalized (nondimensional) volume of the Krogh model as a function of temperature for different cooling rates (3, 6, 9, 12 and 15 °C/min). Krogh cell volume (——).

Upper Graph: Changes in the normalized (nondimensional) radius of the extracellular space (r_V/r_{V0}) of the vasculature in the Krogh unit as a function of temperature for different cooling rates (3, 6, 9, 12 and 15 °C/min). The normalized radius of the extracellular space is also given as (——).

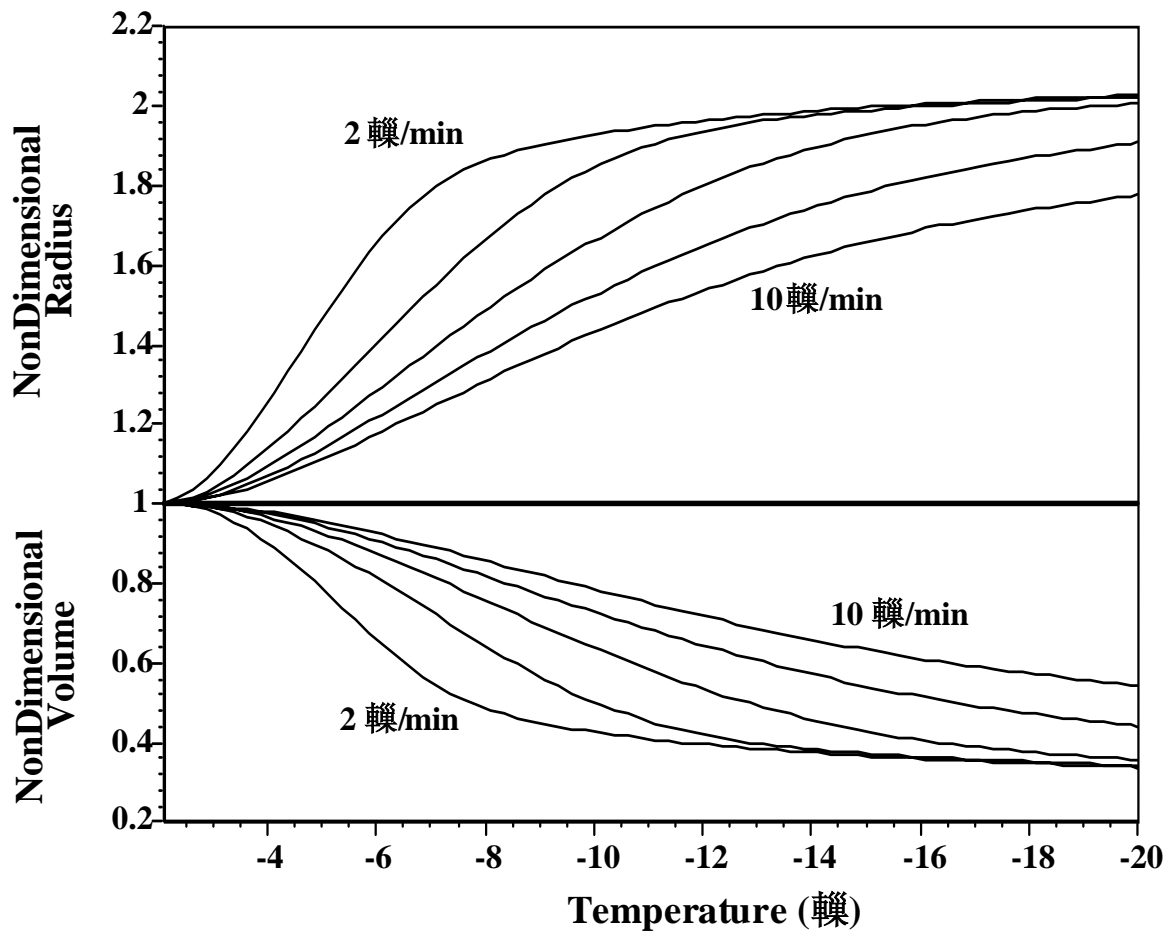


Figure 4.4 Krogh model: Volumetric response of the ovarian tissue at various freezing rates using the best fit membrane permeability parameters (see Table 4.1—cooled at 40°C/min from 25 to 4°C in the presence of 0.85 M glycerol). The subzero temperatures are shown along the x-axis.

Lower Graph: Changes in the normalized (nondimensional) volume of the Krogh model as a function of temperature for different cooling rates (2, 4, 6, 8 and 10 °C/min). Krogh cell volume (——).

Upper Graph: Changes in the normalized (nondimensional) radius of the extracellular space (r_v/r_{v0}) of the vasculature in the Krogh unit as a function of temperature for different cooling rates (2, 4, 6, 8 and 10 °C/min). The normalized radius of the extracellular space is also given as (——).

Table 4.1 Membrane Permeability Parameters for Rhesus Monkey Ovarian Tissue ($V_b=0.2V_o$): A tabulated comparison of the membrane permeability parameters obtained using the DSC water transport data at 5°C/min assuming a Krogh cylinder geometry.

<i>Freezing Media</i>	<i>Cooling Rate Between 25° and 4°C (°C/min)</i>	<i>L_{pg}[cpa] (μm/min-atm)</i>	<i>E_{Lp}[cpa] (Kcal/mole)</i>	<i>B_{opt}** (°C/min)</i>
No CPA	0.5	0.70	31.2	20.1
	40	0.30	32.1	8.2
0.85M DMSO	0.5	0.21	28.9	6.8
	40	0.14	30.5	3.2
0.85M Glycerol	0.5	0.19	22.1	9.0
	40	0.15	26.4	5.6
0.85M EG	0.5	0.18	27.8	6.2
	40	0.15	29.1	3.8

**Obtained using Eqn. (2.4) with $\left(\frac{A_c}{V_o - V_b}\right) = 0.156 \mu\text{m}^{-1}$.

The predicted “best fit” parameters shown in Table 4.1 are denoted by a star (*) and fall within the contours. The lack of a “common” region between the contours suggests that there

does not exist a combination of L_{pg} and E_{LP} that will “fit” the data at both the suprazero cooling conditions concurrently in a given media

Table 4.2 Membrane Permeability Parameters for Rhesus Monkey Ovarian Tissue($V_b=0.4V_o$): A tabulated comparison of the membrane permeability parameters obtained using the DSC water transport data at 5°C/min assuming a Krogh cylinder geometry.

<i>Freezing Media</i>	<i>Cooling Rate Between 25° and 4°C (°C/min)</i>	$L_{pg}[cpa]$ <i>($\mu\text{m}/\text{min-atm}$)</i>	$E_{LP}[cpa]$ <i>(Kcal/mole)</i>	B_{opt}^{**} <i>(°C/min)</i>
No CPA	0.5	0.51	32.2	18.9
	40	0.22	33.1	7.3
0.85M DMSO	0.5	0.15	29.2	6.7
	40	0.10	31.2	3.0
0.85M Glycerol	0.5	0.14	23.1	8.5
	40	0.11	27.4	5.3
0.85M EG	0.5	0.13	28.1	6.1
	40	0.11	29.3	3.8

** Obtained using Eqn. (2.4) with $\left(\frac{A_c}{V_o - V_b}\right) = 0.21 \mu\text{m}^{-1}$.

Table 4.3 Membrane Permeability Parameters for Rhesus Monkey Ovarian Tissue($V_b=0.1V_o$): A tabulated comparison of the membrane permeability parameters obtained using the DSC water transport data at $5^\circ\text{C}/\text{min}$ assuming a Krogh cylinder geometry.

<i>Freezing Media</i>	<i>Cooling Rate Between 25° and 4°C (°C/min)</i>	<i>L_{pg}[cpa] (μm/min-atm)</i>	<i>E_{Lp}[cpa] (Kcal/mole)</i>	<i>B_{opt}** (°C/min)</i>
No CPA	0.5	0.95	33.4	21.6
	40	0.4	36.1	8.0
0.85M DMSO	0.5	0.28	31.2	7.3
	40	0.19	33.2	3.4
0.85M Glycerol	0.5	0.26	25.7	8.9
	40	0.2	29.2	5.8
0.85M EG	0.5	0.24	30.1	6.6
	40	0.2	31.2	5.2

** Obtained using Eqn. (2.4) with $\left(\frac{A_c}{V_o - V_b}\right) = 0.14 \mu\text{m}^{-1}$.

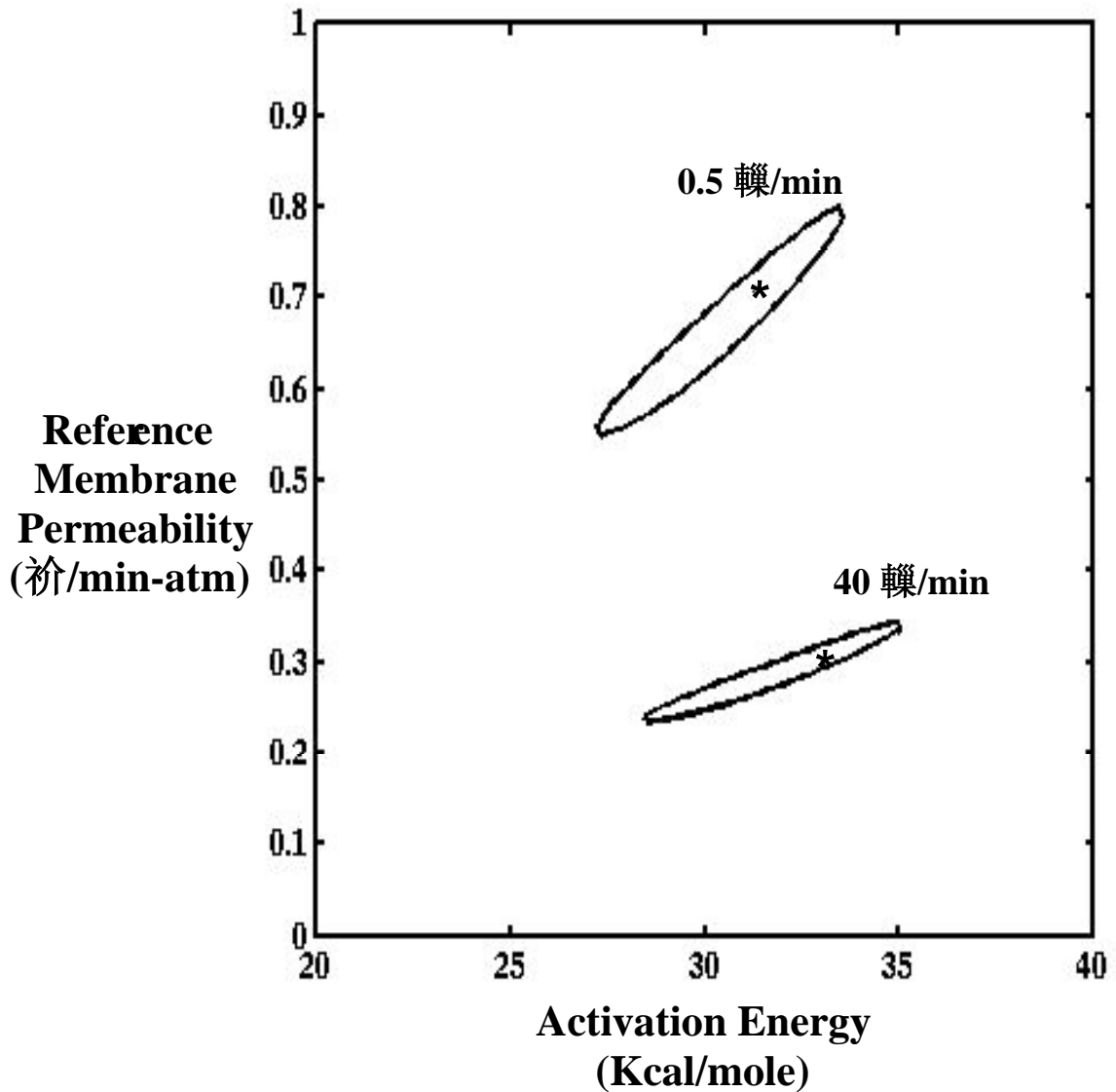


Figure 4.5 A contour plot of the goodness of fit parameter R^2 ($= 0.96$) for the parametric space in ovarian tissue that is cooled at $0.5^\circ\text{C}/\text{min}$ between 25° and 4°C or at $40^\circ\text{C}/\text{min}$ between 25° and 4°C in the absence of CPAs ($V_b = 0.2V_0$).

The predicted best fit parameters for both suprazero cooling conditions are shown as (*) and are within the respective contours (see Table 4.1 for the numerical values and text for further details). The membrane permeability at 0°C , L_{pg} ($\mu\text{m}/\text{min-atm}$) is plotted on the y-axis while the apparent activation energy of the membrane, E_{LP} (kcal/mole) is plotted on the x-axis.

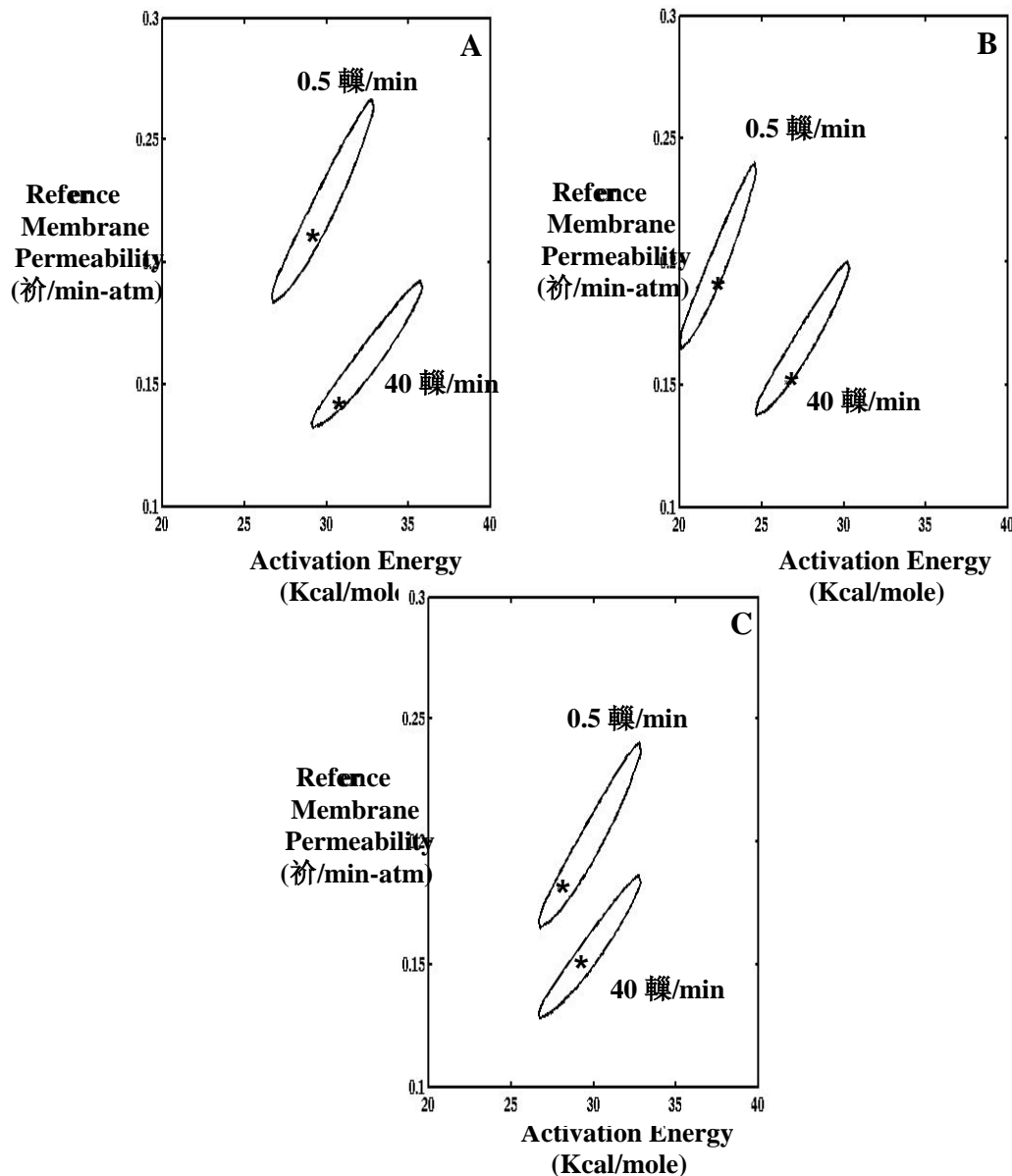


Figure 4.6 A contour plot of the goodness of fit parameter R^2 ($= 0.96$) for the parametric space in ovarian tissue that is cooled at $0.5^\circ\text{C}/\text{min}$ between 25° and 4°C or at $40^\circ\text{C}/\text{min}$ between 25° and 4°C in the presence of 0.85 M DMSO (Fig. 6A), Glycerol (Fig. 6B) and EG (Fig. 6C).

The predicted best fit parameters for both the suprazero cooling conditions are shown as (*) and are within the respective contours (see Table 4.1 for the numerical values and text for further details). The membrane permeability at 0°C , $L_{pg}[\text{cpa}]$ ($\mu\text{m}/\text{min}\text{-atm}$) is plotted on the y-axis while the apparent activation energy of the membrane, $E_{Lp}[\text{cpa}]$ (kcal/mole) is plotted on the x-axis.

4.4 Discussion

The best fit membrane permeability parameters of water transport for macaque ovarian tissue are significantly different between the samples that were cooled at $\sim 0.5^\circ\text{C}/\text{min}$ from 25° to 4°C and those that were cooled at $40^\circ\text{C}/\text{min}$ (Figs. 4.1 and 4.2; Tables 4.1 to 4.3). As also shown in Table 4.1, the L_{pg} value obtained for cooled ovarian tissue cooled at $0.5^\circ\text{C}/\text{min}$ from 25° to 4°C are uniformly higher than those obtained for ovarian tissue cooled at $40^\circ\text{C}/\text{min}$ (both in the presence and absence of CPAs) while the opposite affect is seen in the predicted values of E_{Lp} . Taken together, these observations suggest a loss of fluidity or hardening or a loss in the ability of the water to permeate the cell membrane in ovarian tissues cooled at $40^\circ\text{C}/\text{min}$ from 25° to 4°C when compared to those tissues cooled at $0.5^\circ\text{C}/\text{min}$. A similar difference was observed in equine ovarian tissue sections (Devireddy et al., 2005a) and to a lesser degree in equine sperm cells that were cooled (from 25° to 4°C) and collected under different conditions (Devireddy et al., 2002). Our observations are also consistent with previous experiments by other investigators showing that the suprazero cooling conditions can be related to phase transitions, such as an inverted hexagonal II phase, in the plasma membrane which further correlate to changes in the membrane permeability to ions such as K^+ and Ca^{++} (Morris and Watson, 1984; Caffrey, 1987; Drobnis et al., 1993; Zeron et al., 2002). Changes in the membrane permeability to water caused by abrupt changes in suprazero temperature, as shown in our experiments, are also consistent with perturbation of the membrane structure (Parks and Ruffing, 1992; Vincent and Johnson, 1992; Zenzes et al., 2001; Songsasen et al., 2002a; Steponkus and Weist, 1979). Thus, suprazero cooling conditions appear to have an influence on determination of optimal freezing rates for mammalian ovarian tissue. Future experiments will focus on investigating this phenomena in other mammalian (bovine, sheep and human) ovarian tissues. Additionally, experiments with either Fourier transform infrared (FTIR) spectroscopy or electron microscopy (EM) techniques may also help to determine the temperature at which this transition in ovarian tissue occurs. Based on previous experience in sperm cells, it is expected that this temperature is in the range of $+8^\circ$ to $+20^\circ\text{C}$ (Drobnis et al., 1993).

For a given suprazero cooling condition, the addition of CPAs (glycerol, DMSO or EG)

lowers the value of both L_{pg} by 30 to 70% and E_{Lp} by 10 to 20%. A similar, but more dramatic, lowering of membrane permeability parameters was also observed in equine ovarian tissue (Devireddy et al., 2005a). As described earlier, this lowering in the value of L_{pg} indicates an “alteration” of the membrane, i.e. the ability of intracellular water to permeate through the membrane is lowered, while the lowering of E_{Lp} suggests that the loss of intracellular water continues at lower subzero temperatures, i.e. the temperature range within which the phenomenon of water transport can occur is increased in the presence of CPAs. Thus, a lowering in the value of L_{pg} can be compensated by a lowering in the value of E_{Lp} . However, an examination of the data in Tables 4.1 to 4.3 shows that the lowering in the value of L_{pg} due to the addition of CPAs is much larger than the lowering in the value of E_{Lp} . As also shown in Eqn. (2.4), the optimal rate of freezing is directly proportional to the value of L_{pg} . Thus, the overall effect of adding CPAs is to reduce the predicted rate of optimal freezing. This result is somewhat surprising as the addition of CPA is typically expected to increase the optimal rate of freezing rather than decreasing it. However, canine (Thirumala et al., 2003) and porcine (Devireddy et al., 2004) sperm cells were also found to exhibit a similar behavior in the presence of a CPA, i.e. a decrease in the predicted rate of optimal freezing in the presence of CPAs compared to their absence. It is also quite clear from the data shown in Fig. 2 that the differences in the measured water transport data between the two suprazero cooling conditions studied are smaller in the presence of glycerol (Fig. 2A) or EG (Fig. 2C) than in the presence of DMSO (Fig. 4.2B). A similar “reduction” in the differences in the measured water transport was also obtained in the presence of glycerol (when compared with DMSO) for equine ovarian tissue (Devireddy et al., 2005a). It is as yet unclear if varying the concentrations of CPAs (glycerol, DMSO and EG) from 0.85 M or using a combination of these CPAs will “enhance” or “reduce” the differences in the measured water transport data for different suprazero cooling conditions. Clearly, further studies are necessary to delineate the effect of CPAs on cell membrane transport and structural properties.

Membrane permeability to water and its activation energy are among the most important variables that determine the response of any biological system to an imposed freezing or thawing procedure. Thus, coefficients of water permeability have been determined for oocytes of mice (Leibo, 1980; Paynter et al., 1999; Jackowski et al., 1980; Hunter et al., 1992; McWilliams et al., 1995), rats (Agca et al., 2000), goats (Le et al., 1995), cattle (Myers et al., 1987; Ruffing et al., 1993), humans (McGrath et al., 1995; Paynter et al., 2001; Paynter et al., 2005), cynomolgus monkey (Younis et al., 1996) and rhesus monkey (Songsasen et al., 2002b). In general, the permeability parameters obtained in the present study for macaque ovarian tissue are comparable to those obtained during freezing or in the presence of extracellular ice of mammalian oocytes (Leibo, 1996; Critser et al., 1997). However, a comparison of suprazero mammalian oocyte membrane permeability parameters or parameters obtained in the absence of extracellular ice with the permeability parameters obtained in the present study show significant differences, especially in the presence of CPAs. The reference membrane permeability values obtained in the presence of extracellular ice (Tables 4.1 to 4.3) are significantly lower (sometimes by a factor of 10) than those obtained in the absence of extracellular ice. In direct contrast, the activation energy obtained in the presence of extracellular ice is somewhat higher (by a factor of 2) than those obtained in its absence. These observations are quite comparable to those obtained for a variety of mammalian cells (Devireddy et al., 2002c; Thirumala et al., 2003; Devireddy et al., 2004) and suggest that ovarian tissue membrane permeability parameters are significantly affected by the presence of extracellular ice.

In conclusion, this study presents dynamic water transport data during freezing of macaque ovarian tissue cooled at two rates between +25° and +4°C in the presence or absence of three cryoprotective agents. A Krogh model of water transport was then fitted to the experimentally measured water transport data at 5°C to obtain the reference membrane permeability coefficient, L_{pg} , and the apparent activation energy, E_{Lp} , of ovarian tissue as a function of the suprazero cooling condition and the composition of the freezing medium. By incorporating these parameters into a recently developed optimal cooling rate equation, we determined the optimal rates of freezing ovarian tissue for the various conditions investigated.

This study shows that the membrane permeability parameters and consequently the optimal rates of cryopreservation for a rhesus monkey ovarian tissue are significantly impacted by the cooling conditions between 25° and 4°C. This fact should be considered when mammalian ovarian tissue is collected for use in assisted reproductive techniques or as an alternative to hormone replacement therapy in human cancer survivors.

Chapter 5

Conclusion and Future Work

Cryopreservation is an effective and useful way to store reproductive cells and tissues. In this study, the DSC measured volume response of cells was coupled with water transport model to get the fitted permeability parameters of membrane for bovine sperm, equine and macaca mulatta ovary. For rhesus and equine ovarian tissue, these parameters suggest that the optimal rates of cryopreservation are significantly dependent upon suprazero cooling conditions and the choice of cryoprotective agents (CPAs). For bovine sperm, these subzero water transport parameters are significantly different than the suprazero membrane permeability values (obtained in the absence of extracellular ice) reported in literature. With these obtained parameters, the theoretical response of bull sperm at subzero temperatures was calculated and the result suggest that the optimal cooling rates to cryopreserve bovine spermatozoa range from 45 to 60 °C/min and agrees quite closely with experimentally determined rates of freezing bovine sperm. For equine ovarian tissues, the theoretical calculation of cellular response at subzero temperatures show that the optimal cooling rates to cryopreserve ovarian tissue are significantly dependent upon suprazero cooling conditions. In conclusion, to optimize the cryopreservation protocol of mammalian reproductive cell and tissues, the physical conditions and the biochemical environment during freezing and thawing should be properly controlled.

In future, the effect of biochemical environment and cooling conditions on the viability of reproductive tissues during cryopreservation process should be further studied and the biophysical response of cells and tissues during freezing and thawing need be more clearly understood. More sensitive criteria of the objective assessment of viability, motility, energy status of biological systems during cryopreservation should be found out. Cellular damage study should be extended to the subcellular elements, such as plasma membrane destabilization, chromatin stability and chromosomal damage and effective ways need to be found to assess the ultra-structure cellular damage. The relationship between cellular structure and functions should be specified so that the mechanism of cell injury could be more clearly understood. The final goal is to find optimal protocols for different mammalian

reproductive cell and tissues and to achieve the best preservation effect in all applications.

My current work is focused on the cryopreservation of animal reproductive tissues. Based on the cellular model of animal cells during freezing, the cryopreservation technique needs to be extended and further applied to human reproductive tissues. The difference between human and animal reproductive tissues need be clarified used to guide the optimization of the cryopresearvation procedure for human tissues.

References

- Almeida PA, Bolton VN. 1995. The effect of temperature fluctuations on the cytoskeletal organization and chromosomal constitution of the human oocyte. *Zygote* 3: 357-365.
- Amirat L, Anton M, Tainturier D, Chatagnon, Battut GI and Courtens JL. 2005. Modifications of bull spermatozoa induced by three extenders: Biociphos, low density lipoprotein and Triladyl, before, during and after freezing and thawing. *Reproduction* 129: 535 - 543.
- Awad MM, Graham JK. 2002. Effect of adding cholesterol to bovine spermatozoa on motility parameters and cell viability after cryopreservation. *Cryobiology* 45:256-257.
- Bailey JL, Bilodeau JF, Cormier N. Semen cryopreservation in domestic animals: a damaging and capacitating phenomenon. *J Androl* 21:1-7.
- Baird DT, Webb R, Campbell BK, Harkness LM, Gosden RG. 1999. Long-term ovarian function in sheep after ovariectomy and transplantation of autografts stored at -196 C . *Endocrinology* 140:462-471.
- Barthelemy C, Royere D, Hamamah.1990. Ultrastructural changes in the membrane and acrosome of human sperm heads during freezing-thawing process. *Arch Androl* 25:29-40.
- Bernard A, Fuller BJ. 1996. Cryopreservation of human oocytes: a review of current problem and perspectives. *Hum Reprod Update* 2:193-207.
- Berringer OM Jr, Browning FM, and Schroeder CR. *An Atlas and Dissection Manual of Rhesus Monkey Anatomy*, Tallahassee, FL: Anatomy Laboratory Aids, 1968.
- Bevington PR, Robinson DK. 1992. *Data Reduction and Error Analysis for the Physical Sciences* (2nd ed). McGraw-Hill, New York.
- Bischof JC, Smith D, Pazhayannur PV, Mamivel C, Hulbert J, Roberts KP. 1997. Cryosurgery of Dunning AT-1 rat prostate tumor: Thermal, biophysical, and viability response at the cellular and tissue level. *Cryobiology* 34:42-69.
- Bischof JC. 2000. Quantitative measurement and prediction of biophysical response during freezing in tissues. *Ann Rev Biomed Eng* 2:257-288.
- Blok MC, Van Dennen LMM, DeGier J. 1976. Effect of gel to liquid crystalline phase transition on the osmotic behavior of phosphatidylcholine liposomes. *Biochim Biophys Acta* 433:1-12.
- Caffrey M. 1987. The combined and separate effects of low temperature and freezing on membrane lipid mesomorphic phase behavior: Relevance to cryobiology. *Biochim Biophys Acta* 896:123-127.

Carroll J, Gosden R. 1993. Transplantation of frozen-thawed mouse primordial follicles. *Hum Reprod* 8:1163-1167.

Carroll J, Whittingham DG, Wood MJ, Telfer E and Gosden RG. 1990. Extra-ovarian production of mature viable mouse oocytes from frozen primary follicles. *J Reprod Fert* 90:321-327.

Candy CJ, Wood MJ, Whittingham DG. 1995. Follicular development in cryopreserved marmoset ovarian tissue after transplantation. *Hum Reprod* 10:2334-2338.

Chaveiro A, Liu J, Mullen S, Woelders, H and Critser JK. 2004. Determination of bull sperm membrane permeability to water and cryoprotectants using a concentration-dependent self-quenching fluorophore. *Cryobiology* 48: 72-80.

Chen C. 1986. Pregnancy after human oocytes cryopreservation. *Lancet* 1:884-886.

Critser JK, Agca Y, Gunasena KT. 1997. The cryobiology of mammalian oocytes. In Karow, A.M. and Critser, J.K. (eds), *Reproductive Tissue Banking: Scientific Principles*. Academic Press, San Diego, pp. 329–358

Cosman MD, Toner M, Kandel J, Cravalho EG. 1989. An integrated cryomicroscopy system. *CryoLetters* 10:17-38.

Cummins JM, Woodall PE. 1985. On mammalian sperm dimensions. *J Reprod Fert* 75:153-175.

Curry M. 2000. Cryopreservation of semen from domestic livestock. *Rev Reprod* 5: 46-52.

Curry MR, Kleinhans FW, Watson PF. 2000. Measurement of the water permeability of the membranes of boar, ram, and rabbit spermatozoa using concentration-dependent self-quenching of an entrapped fluorophore. *Cryobiology* 41: 167-173.

Day SH, Nicoll-Griffith DA, Silva JM. 1999. Cryopreservation of rat and human liver slices by rapid freezing. *Cryobiology* 38:154-159.

De Leeuw FE, De Leeuw AM, Den Daas JHG, Colenbrander B and Verkleij AJ. 1993. Effects of various cryoprotective agents and membrane-stabilizing compounds on bull sperm membrane integrity after cooling and freezing. *Cryobiology* 30: 32-44.

De Gier J. Osmotic properties of liposomes. In: Benga G, ed. *Water transport in biological membranes*. Vol 1. From model membranes to isolated cells. Boca Raton, FL: CRC Press, 1989:77-98. Drevius L-O, Erickson.

De Jonge C. 2005. Biological basis for human capacitation. *Hum Reprod Update* 11: 205-214.

Devireddy RV, Bischof JC. 1998. Measurement of water transport during freezing in

mammalian liver tissue - Part II: The use of differential scanning Calorimetry. Amer Soc Mech Eng J Biomech Eng 120:559-569.

Devireddy RV, Raha D and Bischof JC. 1998. Measurement of water transport during freezing in cell suspensions using a differential scanning calorimeter. Cryobiology 36:124-155.

Devireddy RV, Barratt PR, Storey KB, Bischof JC. 1999(a). Liver freezing response of the freeze tolerant wood frog, *Rana sylvatica*, in the presence and absence of glucose. I. Experimental Measurements. Cryobiology 38:310-326.

Devireddy RV, Smith DJ, Bischof JC. 1999(b). Mass transfer during freezing in rat prostate tumor tissue. AIChE J 45:639-654.

Devireddy RV, Swanlund DJ, Roberts KP and Bischof JC. 1999(c). Subzero membrane permeability parameters of mouse spermatozoa in the presence of extracellular ice and cryoprotective agents. Biol Reprod 61:764-775.

Devireddy RV, Swanlund DJ, Roberts KP, Pryor JL and Bischof JC. 2000. The effect of extracellular ice and cryoprotective agents on the water permeability parameters of human sperm plasma membrane during freezing. Hum Reprod 15:1125-1135.

Devireddy RV, Coad JE, Bischof JC. 2001. Microscopic and calorimetric assessment of freezing processes in uterine fibroid tissue. Cryobiology 42:225-243.

Devireddy RV, Swanlund DJ, Olin T, Vincente W, Troedsson MHT, Bischof JC, Roberts KP. 2002(a). Cryopreservation of equine spermatozoa: Optimal cooling rates In the presence and absence of cryoprotective agents. Biol Reprod 66:222-231.

Devireddy RV, Swanlund DJ, Olin T, Vincente W, Troedsson MHT, Bischof JC and Roberts KP 2002(b). Measured effect of collection and cooling conditions on the motility and the water transport parameters at subzero temperatures of equine spermatozoa. Reproduction 124 643-648.

Devireddy RV, Swanlund DJ, Alghamdi AS, Duoos LA, Troedsson MHT, Bischof JC, Roberts KP. 2002(c). Measured effect of collection and cooling conditions on the motility and the water transport parameters at subzero temperatures of equine spermatozoa. Reproduction 124:643-648

Devireddy RV, Fahrig B, Godke RA, Leibo SP. 2004. Subzero water transport characteristics of boar spermatozoa confirm observed optimal cooling rates. Mol Reprod Dev 67:446-457.

Devireddy RV, Li G, Leibo SP. 2005. Suprazero Cooling Conditions Significantly Influence Subzero Permeability Parameters of Mammalian Ovarian Tissue. Mol Reprod Dev In Press.

Devireddy RV. 2005. Predicted permeability parameters of human ovarian tissue cells to various cryoprotectants and water. Mol Reprod Dev 70:333-343.

Diller KD. 2005. Bioheat and mass transfer as viewed through a microscope. *Amer Soc Mech Eng J Biomech Eng* 127:67-84.

Drevius L-O. 1971. Permeability coefficients of bull spermatozoa for water and polyhydric alcohols. *Exp Cell Res* 69: 212-216.

Drevius L-O. 1972. Bull spermatozoa as osmometers. *J Reprod Fertil* 28:29-39.

Drobnis EZ, Crowe LM, Berger T, Anchordoguy TJ, Overstreet JW, Crowe JH. 1993. Cold shock damage is due to lipid phase transitions in cell membranes: A demonstration using sperm as a model. *J Exp Zool* 265:432-437.

Donnez J, Dolmans MM, Demylle D, Jadoul P, Pirard C, Squifflet J, Martinez-Madrid B, Van Langendonck A. 2004. Livebirth after orthotopic transplantation of cryopreserved ovarian tissue. *Lancet* 364:1405-1410.

Donnez J, Dolmans MM, Martinez-Madrid B, Demylle D, Van Langendonck A. 2005. The role of cryopreservation for women prior to treatment of malignancy. *Curr Opin Obstet Gynecol*. 17:333-8.

Duncan AE and Watson PF. 1992. Predictive water loss curves for ram spermatozoa during cryopreservation: comparison with experimental results. *Cryobiology* 29: 95-105.

Ehrenwald E, Foote RH, Parks JE. 1998. Cholesterol efflux from bovine sperm. I. Induction of the acrosome reaction with lysophosphatidylcholine after reducing sperm cholesterol. *Gamete Res* 20:1-13.

Eroglu A, Toth TL, Toner M. 1998. Alterations of the cytoskeleton and polyploidy induced by cryopreservation of M-II mouse oocytes. *Fert Steril* 69: 944-957.

Farrant J. 1963. Water transport and cell survival in cryobiological procedure. *J Gen Physiol* 47:347-369.

Farrant J. 1980. General observations on cell preservation. In: M.J. Ashwood-Smith and J. Farrant, Eds. *Low Temperature Preservation in Medicine and Biology*, Pitman Medical Limited, Kent, England, p. 1-18.

Foote RH, Parks JE. 1993. Factors affecting preservation and fertility of bull sperm: a brief review. *Reprod Fertil Dev* 5: 665-673.

Foote RH. 1999. Review: Development of reproductive biotechnologies in domestic animals from artificial insemination to cloning: A perspective. *Cloning* 3: 133-142.

Foote RH. 2002. The history of artificial insemination: Selected notes and notables *Am Soc Anim Sci* 80: 1-10.

Gage AA. 1992. Cryosurgery in the treatment of cancer. *Surg Gynecol Obstet* 37:171-86.

- Gage AA, Baust J. 1998. Mechanisms of tissue injury in cryosurgery. *Cryobiology* 37:171-86.
- Gao DY, Mazur P, Critser JK. Fundamental cryobiology of mammalian spermatozoa. In: Karow AM, Critser JK (eds.), *Reproductive Tissue Banking*. San Diego: Academic Press; 1997: 263–328.
- Gilmore JA, McGann LE, Liu J, Gao DY, Peter AT, Kleinhans FW, Critser JK. 1995. Effect of cryoprotectant solutes on water permeability of human spermatozoa. *Biol Reprod* 53: 985-995.
- Gilmore JA, Liu J Gao DY. Critser JK. 1997. Determination of optimal cryoprotectants and procedures for their addition and removal from human spermatozoa. *Hum Reprod* 12:112-118.
- Gitler C.1972. Plasticity of biological membranes. *Annu Rev Biophys Bioeng.* 1: 51-92.
- Gradishar WJ, Schilsky RL. 1989. Ovarian function following radiation and chemotherapy for cancer. *Semin Oncol* 16:425-436.
- Graham EF. 1978. Fundamentals of the preservation of spermatozoa. In: *The Integrity of Frozen Spermatozoa. Proc Conf Natl Acad Sci Washington, DC.* pp 4–44.
- Graham JK, Foote RH. 1987. Effect of several lipids, fatty acyl chain length, and degree of unsaturation on the motility of bull spermatozoa after cold shock and freezing. *Cryobiology* 24: 42-52.
- Graham JK.1996. Cryopreservation of stallion spermatozoa. *Reprod Technol* 199 12:131–147.
- Gravance CG, Liu IKM, Davis RO, Hughes JP, Casey PJ. 1996. Quantification of normal head morphometry of stallion spermatozoa: *J Reprod Fertil* 108:41–46.
- Goodman AL, Nixon WE, Johnson DK, Hodgen GD. 1977. Regulation of folliculogenesis in the cycling rhesus monkey: Selection of the dominant follicle. *Endocrinology* 100:155-161.
- Gosden R, Baird DT, Wade JC, Webb R. 1994. Restoration of fertility to oophorectomized sheep by ovarian autografts stored at -196°C. *Hum Reprod* 9:597-603.
- Gosden RG. 2000. Low temperature storage and grafting of human ovarian tissue. *Mol Cell Endocrin* 163:125-129.
- Gosden RG. 2000. Low temperature storage and grafting of human ovarian tissue. *Mol Cell Endocrin* 163:125-129.
- Guthrie HD, Liub J, Critser JK. 2002. Osmotic tolerance limits and effects of cryoprotectants on motility of bovine spermatozoa. *Biol Reprod* 67: 1811-1816.
- Hammerstedt RH, Keith AD, Snipes W, Amann RP, Arruda D, Griel LC. 1978. Use of spin labels to evaluate effects of cold shock and osmolality on sperm. *Biol Reprod* 18:686-696.

- Hammerstedt RH, Graham JK, Nolan JP. 1990. Cryopreservation of mammalian sperm: what we ask them to survive. *J Androl.* 11: 73-88.
- Harp R, Leibach J, Black J, Keldahl C, Karow A. 1994. Cryopreservation of murine ovarian tissue. *Cryobiology* 31:336-343.
- Hartman CG, and Straus WL Jr. *The Anatomy of the Rhesus Monkey.*, New York: Hafner, 1961.
- He L, Bailey JL, Buhr MM. 2001. Incorporating lipids into boar sperm decreases chilling sensitivity but not capacitation potential. *Biol Reprod* 64: 69-79.
- He Y, Dong Q, Tiersch TR, Devireddy RV. 2004. Variation in the membrane transport properties and predicted optimal rates of freezing for spermatozoa of diploid and tetraploid pacific oyster *Crassostrea gigas*. *Biol Reprod* 70:1428-1437.
- Holt WV. 2000. Basic aspects of frozen storage of semen. *Anim Reprod Sci.* 62 3-22.
- Holt W.V. 2001. Fundamental Aspects of Sperm Cryobiology: The Importance of Species and Individual Differences. *Theriogenology* 53, Number 1, 1 January 2000, pp. 47-58(12).
- Howell S, Shalet S. 1998. Gonadal damage from chemotherapy and radiotherapy. *Endocrinol Metab Clin North Am* 27:927-943.
- Hovatta O, Silye R, Krausz T, Abir R, Margare R, Trew G, Lass A, Winston RML. 1996. Cryopreservation of human ovarian tissue using dimethylsulphoxide and propanediol-sucrose as cryoprotectants. *Hum Reprod* 11:1268-1272.
- Hubel A. 1997. Parameters of cell freezing: implications for the cryopreservation of stem cells. *Transfusion Medicine Reviews* 11:224-233.
- Hunter JE, Bernard A, Fuller BJ, McGrath JJ, Shaw RW. 1992. Measurement of the membrane water permeability (L_p) and its temperature dependence (activation energy) in human fresh and failed-to-fertilize oocytes and mouse oocytes. *Cryobiology* 29:240-249.
- Karlsson JO, Cravalho EG, Toner M. 1994. A model of diffusion-limited ice growth inside biological cells during freezing. *J Appl Phys* 75:4442-4455.
- Keanini RG, Rubinsky B. 1992. Optimization of Multiprobe Cryosurgery. *Journal of Heat Transfer* 114:796-801.
- Kedem O, Katchalsky A. 1958. Thermodynamic analysis of the permeability of biological membranes to non-electrolytes. *Biochim Biophys Acta* 27:229-246.
- Kim SS, Soules MR, Battaglia DE. 2002. Follicular development, ovulation, and corpus luteum formation in cryopreserved human ovarian tissue after xenotransplantation. *Fert Steril* 78:77- 82.

- Khorasani AM, Cheung AP, Lee CYG. 2000. Cholesterol inhibitory effects on human sperm-induced acrosome reaction. *J Androl.* 21:586-594.
- Klein U, Gimpl G, Fahrenholz F. 1995. Alteration of the myometrial plasma membrane cholesterol content with β -cyclodextrin modulates the binding affinity of the oxytocin receptor. *Biochem.* 34:13784-13793.
- Kumar S, Millar JD, Watson PF. 2003. The effect of cooling rate on the survival of cryopreserved bull, ram, and boar spermatozoa: a comparison of two controlled-rate cooling machines. *Cryobiology.* 46:246-253.
- Langlais J, Roberts KD. 1985. A molecular membrane model of sperm capacitation and the acrosome reaction of mammalian sperm. *Gamete Res* 12:183-224.
- Lee DM, Yeoman RR, Battaglia DE, Stouffer RL, Zelinski-Wooten MB, Fanton JW, Wolf DP. 2004. Live birth after ovarian tissue transplant. *Nature* 428:137-138.
- Le Gal F, Gasqui P, Renard JP. 1995. Evaluation of intracellular cryoprotectant concentration before freezing goat oocytes. *CryoLetters* 16:3-12.
- Leibo SP, McGrath JJ, Cravalho EG. 1978. Microscopic observation of intracellular ice formation in unfertilized mouse ova as a function of cooling rate. *Cryobiology.* 15:257-271.
- Leibo SP. 1980. Water permeability and its activation energy of fertilized and unfertilized mouse ova. *J Membr Biol* 53:179-188.
- Levin RL, Cravalho EG, Huggins CG. 1976. A membrane model describing the effect of temperature on the water conductivity of erythrocyte membranes at subzero temperatures. *Cryobiology* 13:415-429.
- Liu Z and Foote RH. 1998. Osmotic effects on volume and motility of bull sperm exposed to membrane permeable and nonpermeable agents. *Cryobiology* 37:207-218.
- Lobo RA. 2005. Potential options for preservation of fertility in women. *N Engl J Med* 353:64-73.
- Love RM. 1966. The freezing of animal tissue. In: Meryman HT (ed.), *Cryobiology*, Chap.7, New York: Academic Press; 317-405.
- Martino A, Songsasen N, Leibo SP. 1996. Development into blastocysts of bovine oocytes cryopreserved by ultra-rapid cooling. *Biol Reprod* 54:1059-69.
- Mazur P. 1963. Kinetics of water loss from cells at subzero temperatures and the likelihood of intracellular freezing. *J Gen Physiol* 47:347-369.
- Mazur P, Leibo SP, Chu EHY. 1972. A two-factor hypothesis of freezing injury. *Exp Cell Res* 71:345-355.

- Mazur P. 1977. The Kinetics of Water Loss from Cells at Subzero Temperatures and the Likelihood of Intracellular Ice Formation. *Philosophical Transactions of the Royal Society of London B: Biological Sciences*. Mar 29;278(959):191-205.
- Mazur P. 1984. Freezing of living cells: mechanics and implications. *Am. J. Physiology* 247:c125-c142.
- Mazur P, Cole KW. 1989. Roles of unfrozen fraction, salt concentration and change in cell volumes in the survival of frozen human erythrocytes. *Cryobiology* 26:1-29.
- Mazur P, Leibo SP, Chu EHY. 1972. A two factor hypothesis of freezing injury. *Experimental Cell Research* 71:345-355.
- McCaa C, Diller KD, Aggarawal SJ, Takahashi T. 1991. Cryomicroscopic determination of the membrane osmotic properties of human monocytes at subfreezing temperatures. *Cryobiology* 28:391-399.
- McGrath JJ. 1988. Membrane transport properties: In: McGrath JJ, Diller KR (eds.), *Low Temperature Biotechnology: Emerging Applications and Engineering Contributions*, BED-vol. 10, HTD-vol. 98. New York: American Society of Mechanical Engineers Press; 1988: 273-330.
- Meirow D. 2000. Reproduction post-chemotherapy in young cancer patients. *Mol Cell Endocrinol* 169:123-131.
- Molisch, H. 1897. *Untersuchen über das Erfrieren der Pflanzen*. Fisher, Jena. Reprinted in English 1982 in *CryoLetters* 3:332-390.
- Montgomery DC, Runger GC. *Applied statistics and probability for engineers*. New York: John Wiley & Sons; 1994: 471-529.
- Moore Ai, Squire EL and Graham JK (2005) Adding cholesterol to the stallion sperm plasma membrane improves cryosurvival. *Cryobiology* Epublished: 24 August 2005.
- Morris GJ, Watson PF. 1984. Cold shock injury – a comprehensive bibliography. *Cryoletters* 5:352-357.
- Morris GJ. 1987. Direct chilling injury. In: Grout BWW, Morris GJ (eds), *The Effects of Low Temperatures on Biological Systems*, Edward Arnold, London: 120-146.
- McGrath J. 1987. Temperature-controlled cryogenic light microscopy: An introduction to cryomicroscopy, In Grout BWW, Morris GJ, editors. *The Effects of Low Temperature on Biological Systems*. Edward Arnold Press, London, UK. pp. 234-267.
- McGrath JJ, Fuller BJ, Hunter JE, Paynter S, Bernard AG. 1995. The permeability of fresh pre-ovulatory human oocytes to dimethylsulfoxide at 3°C. *CryoLetters* 16:79-84.
- Myers SP, Lin TT, Pitt RA, Steponkus PL. 1987. Cryobehavior of immature bovine oocytes. *CryoLetters* 8:260-275.

- Nicosia SV, Matus-Ridley M, Meadows AT. 1985. Gonadal effects of cancer therapy in girls. *Cancer* 55:2364-2372.
- Newton H, Aubard Y, Rutherford A, Sharma V, Gosden RG. 1996. Low temperature storage and grafting of human ovarian tissue. *Hum Reprod* 11:1487-1491.
- Newton H, Fisher J, Arnold JRP, Pegg DE, Faddy MJ, Gosden RG. 1998. Permeation of human ovarian tissue with cryoprotective agents in preparation for cryopreservation. *Hum Reprod* 13:376-380.
- Nolan JP, Graham JK, Hammerstedt RH. 1992. Artificial induction of exocytosis in bull sperm *Arch Biochem Biophys* 292:311-322.
- Noiles EE, Bailey JL, Storey BT. 1995. The temperature dependence in the hydraulic conductivity, L_p , of the mouse sperm plasma membrane shows a discontinuity between 4 and 0 degrees °C. *Cryobiology* 32:220-238.
- Oegema TR, Deloria LB, Fedewa M, Bischof JC, Lewis JL. 1999. A simple cryopreservation method for the maintenance of cell viability and mechanical integrity of cultured cartilage analog. *Cryobiology* 40(6):370-375.
- Oktay K, Karlikaya G. 2000. Ovarian function after transplantation of frozen, banked autologous tissue. *Engl J Med* 342:1919.
- Oktay K, Buyuk E, Veeck L, Zaninovic N, Xu K, Takeuchi T, Opsahl M, Rosenwaks Z. 2004. Embryo development after heterotopic transplantation of cryopreserved ovarian tissue. *Lancet* 363:837-840.
- Parkinson TJ, Whitfield CH. 1987. Optimization of freezing conditions for bovine spermatozoa *Theriogenology* 27:781-797.
- Parks JE, Lynch DV. 1992. Lipid composition and thermotropic phase behavior of boar, bull, stallion, and rooster sperm membranes. *Cryobiology* 29:255-266.
- Parks JE, Ruffing NA. 1992. Factors affecting low temperature survival of mammalian oocytes. *Theriogenology* 37:59-73.
- Parrott DMV. 1960. The fertility of mice with orthotropic ovarian grafts derived from frozen tissue. *J Reprod Fertil* 1:230-241.
- Paynter SJ, Cooper A, Fuller BJ, Shaw RW. 1999. Cryopreservation of bovine ovarian tissue: Structural normality of follicles after thawing and culture *in vitro*. *Cryobiology* 38:301-309.
- Paynter SJ, O'Neil L, Fuller BJ, Shaw RW. 2001. Membrane permeability of human oocytes in the presence of the cryoprotectant propane-1,2-diol. *Fert Steril.* 75:532-538.
- Paynter SJ, Borini A, Bianchi V, De Santis L, Flamigni C, Coticchio G. 2005. Volume changes of mature human oocytes on exposure to cryoprotectant solutions used in slow cooling

procedures. Hum Reprod 20:1194–1199.

Pazhayannur P, Bischof JC. 1997. Measurement and simulation of water transport during freezing in mammalian liver tissue. Amer Soc Mech Eng J Biomech Eng 119:269-277.

Pickering SJ, Cant A, Braude PR, Currie J. 1990. Transient cooling to room temperature can cause irreversible disruption of the meiotic spindle in the human oocytes. Fert Steril 54:102-108.

Picton HM, Kim SS, Gosden RG. 2000. Cryopreservation of gonadal tissue and cells. Br Med Bull 56:603-615.

Picton HM, Gosden RG, Leibo SP, 2002. Cryopreservation of oocytes and ovarian tissue. In Vayena E, Rowe P, Griffin PD, editors. Current Practice and Controversies in Assisted Reproduction. World Health Organization, Geneva, pp. 142-151.

Pinisetty D, Huang C, Dong Q, Tiersch TR, Devireddy RV. 2005. Subzero water permeability parameters and optimal freezing rates for sperm cells of the southern platyfish, *Xiphophorus maculatus*. Cryobiology 50:250-263.

Pinisetty D. 2005. Molecular dynamic simulations of biological membranes in the presence of cryoprotectants. Master's Thesis, Louisiana State University, LA.

Polge C, Smith AU, Parkes AS. 1949. Revival of spermatozoa after vitrification and dehydration at low temperatures. Nature 164: 666.

Practice Committee of the American Society for Reproductive Medicine. 2004. Ovarian tissue and oocyte cryopreservation. Fert Steril 82:993-998.

Purdy PH, Graham JK. 2003. Effect of cholesterol-loaded cyclodextrin on the cryosurvival of bull sperm. Cryobiology 48:36-45.

Purdy PH, Graham JK. 2004(a). Effect of cholesterol-loaded cyclodextrin on the cryosurvival of bull sperm. Cryobiology 48: 36-45.

Purdy PH, Graham JK. 2004(b). Effect of adding cholesterol to bull sperm membranes on sperm capacitation, the acrosome reaction and fertility. Biol Reprod 71: 522-527.

Purdy PH, Fox MH, Graham JK. 2005. The fluidity of Chinese hamster ovary cell and bull sperm membranes after cholesterol addition. Cryobiology 51: 102-112.

Quinn PJ. 1985. A lipid-phase separation model of low-temperature damage to biological membranes. Cryobiology 22:128-146.

Ravie O, Lake PE. 1982. Prediction of ice formation in fowl spermatozoa at particular cooling rates. Cryolett 3:91-100.

Révay, T, Nagy S, Kovács B, Edvi ME, Hidas H, Rens W, Gustavsson IG. 2004. Head area measurements of dead, live, X- and Y-bearing bovine spermatozoa. Reprod Fert Dev 16:

681-687.

Robbins RK, Saacke RG, Chandler PT. 1976. Influence of freeze rate, thaw rate and glycerol level on acrosomal retention and survival of bovine spermatozoa frozen in French straws. *J Anim Sci* 42:145-54.

Rodriguez OL, Berndtson WE, Ennen BD, Pickett BW. 1975. Effect of rates of freezing, thawing and level of glycerol on the survival of bovine spermatozoa in straws. *J Anim Sci* 41:129-136.

Roy H, Hammerstedt, James K, Graham, John P, Nolan. 1998. Cryopreservation of mammalian sperm: what we ask them to survive. Annual Meeting of the American Society of Andrology.

Royere D, Barthelemy C, Hamamah S, Lansac J. 1996. Cryopreservation of spermatozoa: a 1996 review. *Human Reproduction Update* 2(6): 553-559.

Rubin SC, Sutton GP. 1993. *Ovarian Cancer*. London: McGraw-Hill Education.

Rubinsky B, Lee CY, Bastacky J, Hayes TL. 1987. The mechanism of freezing process in biological tissue. *Cryo-Letters* 8:370-381.

Rubinsky B, Pegg DE. 1988. A mathematical model for the freezing process in biological tissue. *Proc R Soc Lond: Series B* 234:343-358.

Ruffing NA, Steponkus PL, Pitt RE, Parks JE. 1993. Osmotic behavior, hydraulic conductivity, and incidence of intracellular ice formation in bovine oocytes at different developmental stages. *Cryobiology* 30: 562-580.

Schneider U, Mazur P. 1984. Osmotic consequences of cryoprotectant permeability and its relation to the survival of frozen-thawed embryos. *Theriogenology* 21:68-79.

Schneider U. 1986. Cryobiological principles of embryo freezing. *J In Vitro Fert Embryo Trans* 3: 3-9.

Schnorr J, Oehninger S, Toner J, Hsiu J, Lazendorf S, Williams R, Hodgen G. 2002. Functional studies of subcutaneous ovarian transplants in non-human primates: steroidogenesis, endometrial development, ovulation, menstrual patterns and gamete morphology. *Hum Reprod* 17:612-619.

Semple E, Weissman A, Gotlieb L, Casper RF, Leibo SP. 2000. Transplantation of fresh or cryopreserved bovine ovarian cortex to NOD-SCID mice. *Theriogenology* 53:264.

Silber SJ, Lenahan KM, Levine DJ, Pineda JA, Gorman KS, Friez MJ, Crawford EC, Gosden RG. 2005. Ovarian transplantation between monozygotic twins discordant for premature ovarian failure. *N Engl J Med* 353:58-63.

Smith DJ, Schulte M, Bischof JC. 1998. The effect of dimethylsulfoxide on the water

transport response of rat hepatocytes during freezing. Amer Soc Mech Eng J Biomech Eng 120:549-558.

Songsasen N, Yu I-J, Ratterree MS, VandeVoort CA, Leibo SP. 2002(a). Effect of chilling on organization of tubulin and chromosomes in rhesus monkey oocytes. Fert Steril 2002; 77:818-825.

Songsasen N, Ratterree MS, VandeVoort CA, Pegg DE, Leibo SP. 2002(b). Permeability characteristics and osmotic sensitivity of rhesus monkey (*Macaca mulatta*) oocytes. Hum Reprod 17:1875-1884

Sonzemer M, Oktay K. Fertility preservation in female patients. 2005. Hum Reprod Update 10:251-266.

Steponkus PL. 1984. Role of the plasma membrane in freezing injury and cold acclimation. Ann Rev Plant Physiol 35:543-584.

Stevens A, Lowe J. 1996. Human Histology (2nd Ed). The Netherlands: Elsevier Health Science.

Stewart DL. 1951. Storage of bull spermatozoa at low temperatures. Vet Rec 63:65-66.

Szebenyi ES. *Atlas of Macaca mulatta.*, Cranbury, NJ: Associated University Press, 1969.

Thirumala S, Ferrer MS, Al-Jarrah A, Eilts BE, Paccamonti DL and Devireddy RV. 2003. Cryopreservation of canine spermatozoa: Theoretical prediction of optimal cooling rates in the presence and absence of cryoprotective agents. Cryobiology 47: 109-124.

Thirumala S, Huang C, Dong Q, Tiersch TR, Devireddy RV. 2005. A theoretically estimated optimal cooling rate for the cryopreservation of sperm cells from a live-bearing fish, the green swordtail, *Xiphophorus helleri*. Theriogenology 63:2395-2415.

Thirumala S, Devireddy RV. 2005. A simplified procedure to determine the optimal rate of freezing biological systems. Amer Soc Mech Eng J Biomech Eng 127:295-300.

Toner M. 1993. Nucleation of ice crystals in biological cells. In Steponkus PL, editor. Advances in Low Temperature Biology. Vol. 2, JAI Press. pp. 1-52.

Trump BF, Goldblatt PJ, Griffin CC, Waravdekar VS, Stowell RE. 1964. Effects of freezing and thawing on the ultrastructure of mouse parenchymal cells. Lab Invest 13:967-1002.

Tulandi T, Gosden R. (eds) 2004. Preservation of Fertility. Taylor and Francis, London UK.

Van Duijn C. 1960. Mensuration of the heads of bull spermatozoa. Mikroskopie 14:265-276.

Van Duijn C, Van Voorst C. 1971. Precision measurements of dimensions, refractive index

and mass of bull spermatozoa in the living state. *Mikroskopie* 27:142-167.

Van Wagenen G, Simpson ME. Embryology of the Ovary and Testis, *Homo sapiens and Macca mulatta*. New Haven: Yale University Press; 1973: 88–160.

Vincent C, Johnson MH. 1992. Cooling, cryoprotectants, and the cytoskeleton of the mammalian oocyte. *Oxford Rev Reprod Biol* 14:73-100.

Visconti PE, Galantino-Homer H, Ning XP, Moore GD, Valenzuela JP, Jorgez CJ, Alvarez JG, Kopf GS. 1999. Cholesterol efflux-mediated signal transduction in mammalian sperm. *J Biol Chem* 274 3235-3242.

Vishwanath R and Shannon P. 2000. Storage of bovine semen in liquid and frozen state. *Anim Reprod Sci* 62:23-53.

Watson PF. 1981. The effects of cold shock on sperm cell membranes. In Morris GJ, Clarke A, editors. *Effects of Low Temperature on Biological Membranes*. Academic Press, London, UK. pp. 189-218.

Watson PF, Kunze E, Cramer P, Hammerstedt RH. 1992. A comparison of critical osmolarity and hydraulic conductivity and its activation energy in fowl and bull spermatozoa. *J Androl* 13:131-138.

Watson PF. 1995. Recent developments and concepts in the cryopreservation of spermatozoa and the assessment of their post-thawing function. *Reprod Fert Dev* 7: 871-891.

Willoughby CE, Mazur P, Peter AT, Critser JK. 1996. Osmotic tolerance limits and properties of murine spermatozoa. *Biol Reprod* 55: 715–727.

White IG. 1993. Lipids and calcium uptake of sperm in relation to cold shock and preservation: a review. *Reprod Fert Develop* 5:639-658.

Woelders H. 1997. Fundamentals and recent development in cryopreservation of bull and boar semen. *Vet Quart* 19:135–138.

Woelders H, Matthijs A, Engel B. 1997. Effects of trehalose and sucrose, osmolality of the freezing medium, and cooling rate on viability and intactness of bull sperm after freezing and thawing. *Cryobiology* 35:93-105.

Woelders H, Malva AP. 1998. How important is the cooling rate in cryopreservation of (bull) semen, and what is its relation to thawing rate and glycerol concentration. *Reprod Dom Anim* 33:299–305.

Wolfe J, Bryant G. 2001. Thermodynamic and mechanical effects, *International Journal of Refrigeration. Cellular cryobiology* 24(5): 438-450.

Wilmot I, Polge C, Rowson LE. 1975. The effect on cow embryos of cooling to 20, 0 and –196 °C. *J Reprod Fert* 45:409-411.

Yin H, Wang X, Kim SS, Chen H, Tan SL, Gosden RG. 2003. Transplantation of intact rat gonads using vascular anastomosis: Effects of cryopreservation, ischaemia and genotype. *Hum Reprod* 18:1165-1172.

Younis AI, Toner M, Albertini DF, Biggers JD. 1996. Cryobiology of non-human primate oocytes. *Hum Reprod* 11:156–165.

Zenzes MT, Bielecki R, Casper RF, Leibo SP. 2001. Effects of chilling to 0°C on the morphology of meiotic spindles in human metaphase II oocytes. *Fert Steril* 75: 769–777.

Vita

Guanglei Li is from a small village, Hepu in Hubei province of China. She first went to the Baihe Wan Elementary school and then studied in ShuangfengAo Junior School and No. One Middle school of Luotian County. She got her Bachelor's degree of Engineering from the University of Science and Technology of China. From August 2004, she has been studying in Louisiana State University and will get her Master of Science in Mechanical Engineering in December 2005. She will study for her Ph.D. after graduation.